Cellular aging impedes stress-activation of a crucial JDP-Hsp70 protein disaggregase

Short title: Collapse of siDAP in cellular aging

Authors: Yasith Mathangasinghe[1]†, Niels Alberts[1,2]†, Carlos J. Rosado[3], Dezerae Cox[4], Natalie L. Payne[1], Angelique R. Ormsby[4], Keziban Merve Alp[5], Roman Sakson[6], Sanjeev Uthishtran[7], Thomas Ruppert[8], Senthil Arumugam[7,9,10], Danny M. Hatters[4], Harm H. Kampinga[2] and Nadinath B. Nillegoda[1,11]*

Affiliations

[1]Australian Regenerative Medicine Institute, Monash University, Clayton, Victoria, Australia.
[2]Department of Biomedical Sciences of Cells & Systems, University Medical Center Groningen (UMCG) and University of Groningen (RuG), Groningen, The Netherlands.
[3]Department of Diabetes, Central Clinical School, Monash University, Melbourne, Victoria, Australia.
[4]Department of Biochemistry and Pharmacology, Bio21 Molecular Science and Biotechnology Institute, The University of Melbourne, Melbourne, Victoria, Australia.
[5]Max Delbrück Center for Molecular Medicine in the Helmholtz Association, Berlin, Germany.
[6]Leibniz-Institut für Analytische Wissenschaften-ISAS-e.V., Dortmund, Germany.
[7]Monash Biomedicine Discovery Institute, Monash University, Melbourne, Victoria, Australia.
[8]Core facility for Mass Spectrometry and Proteomics, Zentrum für Molekulare Biologie der Universität Heidelberg, Heidelberg, Germany.
[9]European Molecular Biological Laboratory Australia (EMBL Australia), Monash University, Melbourne, Victoria, Australia
[10]Australian Research Council Centre of Excellence for Advanced Molecular Imaging, Monash University, Clayton, Victoria, Australia
[11]Centre for Dementia and Brain Repair at the Australian Regenerative Medicine Institute, Monash University, Melbourne, Victoria, Australia

† These authors contributed equally to this work

*Corresponding author. Email: nadinath.nillegoda@monash.edu

Abstract
The breakdown of protein homeostasis manifests itself in inappropriate protein aggregation, which can lead to cell death resulting in disease and aging. To resolve aggregates, organisms rely on protein disaggregases. How these disaggregases are regulated in mammals is poorly understood. We report the identification of a protein quality control (PQC) pathway dedicated to boosting protein disaggregation activity in human cells recovering from heat stress. This pathway, termed the stress-induced protein disaggregase activation pathway (siDAP), selectively induces a ternary DNAJA1+DNAJB1-Hsp70 protein disaggregase. Hsp70 disaggregase functions sequentially with AAA ATPase VCP to resolve different populations of aggregates in temporally distinct aggregate clearance phases in repairing cells. siDAP targets aggregates containing immobile tightly packed misfolded proteins that are different from stress-induced phase-separating biomolecular condensates. Strikingly, the assembly of this disaggregase is compromised in cells undergoing replicative aging. However, these cells still retain a fully functional heat shock response, making siDAP one of the first PQC pathways to collapse in aging cells.

Keywords
Protein disaggregation, protein aggregation, regulation, siDAP, hyperthermia, fever, heat shock, cell stress, amyloids, replicative aging, senescence, Hsp70, J-domain protein, VCP, UPS, DNAJA1, DNAJB1, protein quality control pathway.

Introduction
Proteins can inappropriately aggregate in cells when protein homeostasis collapses. Breakdown of protein homeostasis could result from numerous extrinsic and intrinsic factors, including exposure to proteotoxic stresses such as heat shock (HS), metabolic load, chronic expression of misfolded proteins known to cause conformational diseases, and aging (*1*). Healthy cells deploy a surveillance system that integrates stress signals from protein quality control (PQC) pathways and regulates the flux from different aspects of protein biogenesis (e.g. protein synthesis, folding, transport, and degradation) to counteract conditions leading to protein homeostasis collapse, and prevent the accumulation of potentially toxic misfolded/aggregated proteins that could trigger premature cell death (*2, 3*). Mechanisms that facilitate protein disaggregation (Figure 1A) form an integral component of this surveillance system (*4*). Previous studies show that the disruption of protein disaggregation function significantly decreases the fitness and lifespan of prokaryotes and lower eukaryotes after HS (*5-8*). The cell machinery that performs aggregate solubilization is well understood in unicellular organisms (e.g., bacteria and fungi) (*9*), where AAA+ ATPases of the Hsp100 class of chaperones (e.g., bacterial ClpB; yeast Hsp104) use a threading mechanism to untangle and release aggregate-trapped polypeptides (*9, 10*).

Metazoans lack cytosolic/nuclear Hsp100 disaggregases and instead appear to have evolved aggregate solubilization machines based on Hsp70 (*11*). This is supported by several *in vitro* studies showing the disassembly of artificially formed protein aggregates by biochemically reconstituted Hsp70-J-domain protein (JDP) disaggregases (*12-15*). Mechanistic work indicates that specific JDPs belonging to classes A (DNAJA) and B (DNAJB) assemble scaffolds that recognize protein aggregates and then direct Hsp70 into a ternary complex to form these disaggregases (*13, 16*). Class A and class B JDPs carry an N-terminal J-domain (the highly conserved signature domain of all JDPs) vital for the interaction of Hsp70 and the assembly of JDP scaffolds (*13*). The J-domain is linked to the C-terminal substrate-binding domains (CTDs) through a flexible G/F-rich region. Class A members such as DNAJA1 and DNAJA2 possess an additional zinc finger-like subdomain (ZFLR) integrated into CTD-I, making class A JDPs distinct from class B members (*e.g.,* DNAJB1 and DNAJB4) (Figure S1A) (*17*). The correct dimer-dimer

pairing between the two classes of JDPs is mediated by an intricate selection strategy (*14*). *In vitro* studies show that efficient targeting of heat-induced amorphous aggregates requires Hsp70 disaggregases comprised of mixed class JDP scaffolds (*7, 13, 14*). This unique structural feature is not required for other Hsp70 functions such as protein (re)folding or substrate holding (*12-14, 18*). Biochemical studies suggest that these JDP scaffolds could facilitate simultaneous recruitment of multiple Hsp70 molecules to complete the assembly of the disaggregase (*4, 16*). Clustered binding of Hsp70 molecules, potentially to the same aggregated polypeptide, has been proposed to decrease entropy and increase the extraction forces required for aggregate disassembly (*16, 19, 20*). Furthermore, mixed-class JDP scaffolds could presumably facilitate increased sampling of aggregate surfaces by bringing together distinct substrate binding modules (*4, 13*).

However, *ex vivo* and/or *in vivo* supporting evidence for protein disaggregation activity in multicellular organisms is largely limited to observational data showing clearance of aggregates formed by model proteins in cells (*7, 21*), correlations made between heat-induced aggregate clearance and thermotolerance (*7, 22*), and large-scale proteomics studies that monitored proteome solubility dynamics after proteotoxic stress insults (*23, 24*). Direct visualization of functional Hsp70 disaggregases in living cells has not been possible due to the unavailability of methods that specifically track Hsp70 disaggregases over other Hsp70 chaperone machines (*e.g.,* foldases). Therefore, it has remained unknown how these disaggregases are assembled and regulated in multicellular organisms, and how this crucial activity affects protein homeostasis maintenance, stress tolerance, aging, and disease. Using a new approach that involves an advanced protein-protein interaction assay, we identified an Hsp70 disaggregase comprising DNAJA1 and DNAJB1, which is selectively induced in human cells recovering from heat stress through a PQC pathway termed siDAP. The aggregates targeted by this disaggregase contain immobile tightly packed misfolded proteins that are different from biomolecular condensates containing heat denatured proteins in nucleoli and cytosol (*e.g.,* stress granules (SGs)). The heat shock response (HSR), an evolutionarily conserved transcriptional program that is activated by proteotoxic stresses (*25, 26*), is essential for the synthesis of components of the disaggregase and helps modulate the time of activation of this machine during stress recovery. The activated DNAJA1+DNAJB1-Hsp70 disaggregase operates sequentially with AAA ATPase VCP, another protein aggregate solubilizing machine in human cells. However, the function of this disaggregase cannot be compensated for by boosting VCP. Furthermore, siDAP is important for cellular fitness after heat stress. Finally, we show that siDAP-mediated assembly of DNAJA1+DNAJB1-Hsp70 disaggregase is severely hampered in cells that undergo replicative aging, which could trigger the aggregation of pathological proteins.

Results

Multiple mixed-class JDP scaffolds of the Hsp70 disaggregase exist in human cells.

First, we tested the ability of eight human Hsp70 disaggregase configurations reconstituted with different homo or hetero JDP scaffolds to solubilize and reactivate thermally aggregated luciferase from *Photinus pyralis, in vitro.* The Hsp110 cochaperone, which functions primarily as a nucleotide exchange factor (NEF) for Hsp70, was added to reactions to power protein disaggregation efficiency (*27*). The JDPs tested include two members of class A (DNAJA1 and DNAJA2) and class B (DNAJB1 and DNAJB4). A synergistic increase in disaggregation and refolding of aggregated luciferase was observed in all reactions that could form mixed-class JDP scaffolds *in vitro* (Figure 1B), consistent with previous findings (*13*).

Next, we used an antibody-based protein-protein interaction technique called the *in situ* proximity ligation assay (PLA) (*28*) to trace the assembly of Hsp70 disaggregases in human cells. In previous

studies, we have shown that PLA, which has high specificity and sensitivity, can be used successfully to visualize transiently formed chaperone assemblies in various cell types (*14, 29*). We therefore hypothesized that this technique could capture the assembly of mixed-class JDP scaffolds specific to the highly active Hsp70 disaggregases after triggering proteome folding stresses in cells (Figure 1C). After signal amplification, the PLA-based disaggregase tracing assay (PLA^{DT}) detected all four mixed-class JDP scaffolds in unstressed (U) HeLa cells. The captured JDP assemblies appeared as fluorescent puncta (yellow, false-colored; left, Figure 1D), whereas controls consisting of only one of the JDP-specific primary antibodies did not generate fluorescent puncta (Figure S1B). The specificity of the interaction was confirmed by disrupting the formation of JDP scaffolds via depleting JDP members using RNAi, which decreased the PLA^{DT} signal in cells (Figure S1C and D). In essence, HeLa cells appeared to be competent in forming all four *in vitro* characterized mixed-class JDP scaffolds of the Hsp70 disaggregase.

Heat shock triggers induction of the DNAJA1+DNAJB1-Hsp70 disaggregase

Next, we examined whether JDP scaffold levels changed in cells after applying a protein aggregation stress through a brief heat shock (HS) (Figure S1E). HS led to a large and transient increase in the DNAJA1+DNAJB1 scaffold compared to other JDP complexes (Figure 1D; Figure S1F) peaking around 6h after recovery from the treatment (Figure 1D). However, strikingly, this assembly occurred hours after the time point at which most protein aggregates are expected to form (*30-33*). In fact, the peak assembly of this JDP scaffold coincided with the maximum expression of the disaggregase components (at protein level) in HeLa cells (Figure S1G). Consequently, we observed an increase in the interaction between Hsp70 and the two JDPs on a very similar time scale (Figure 1E), indicating the formation of the complete disaggregase. Disassembly of the disaggregase to base level (unstressed) occurred at 24h post-HS (Figure 1D, E and F), independent of the JDP protein levels (Figure S1G).

The observed proximity signals capture direct protein interactions during assembly of the Hsp70 disaggregase machine

One of the caveats of PLA is that signal amplification could also occur when the targeted proteins are not directly interacting, but in close proximity (approximately 10-30 nm apart). We used complex-forming defective mutants of Hsp70 and JDP to demonstrate that the PLA^{DT} signals captured during disaggregase assembly occurred as a result of direct interactions between machine components. The formation of mixed-class JDP scaffolds is mainly driven by intermolecular electrostatic interactions between the J-domain and the CTD (Figure S1A) of opposite class members (*13, 14*). Our previous biochemical work characterized a scaffold forming defective mutant of DNAJB1 that carries a triple amino acid charge reversion (D4R, E69R, and E70R denoted $DNAJB1^{RRR}$) along helices 1 and 4 of the J-domain. This mutant cannot interact with partnering class A JDP to support efficient Hsp70-mediated solubilization of heat-induced aggregates, *in vitro* (*13*). However, $DNAJB1^{RRR}$ could assist other functions of Hsp70 *in vitro* (*e.g.,* refolding of heat-denatured luciferase) (*13*) and in cells (*e.g.,* entry and exit from nucleoli, (Figure S2A) shown to be associated with refolding of heat-denatured proteins (*30, 31, 33*)). We then evaluated the ability of HA-tagged $DNAJB1^{RRR}$ to form JDP scaffolds in cells and observed a decrease in the PLA^{DT} signal under unstressed and HS conditions that indicated $DNAJB1^{RRR}$ complexed poorly with endogenous DNAJA1 and DNAJA2 compared to wild-type DNAJB1 (Figure S2B). Similarly, a Hsp70-binding deficient mutant of DNAJB1 (with a disrupted HPD motif; $DNAJB1^{H32Q}$) (*34*) also showed a decrease in PLA^{DT} signal for its interaction with endogenous Hsp70 (Figure S2C). Together, these findings support the conclusion that the PLA^{DT} signals generated during disaggregase assembly resulted from direct interactions between machine components.

Stress-induced Hsp70 disaggregase hinges on a set of specific partner JDPs in cells

To investigate whether the JDP^A-JDP^B scaffold of this disaggregase is interchangeable with other class A and B members (as observed in biochemically reconstituted systems, Figure 1B), we systematically knocked down DNAJA1 and DNAJB1 in HeLa cells using RNAi and sought induction of alternative JDP scaffolds to support disaggregase assembly. As expected, depletion of DNAJA1 or DNAJB1 decreased the assembly of the DNAJA1+DNAJB1 scaffold during stress recovery. However, knocking down DNAJA1 or DNAJB1 did not result in the unpaired JDP partner forming complexes with DNAJA2 or DNAJB4 during stress recovery, respectively (Figure S2D). Thus, regardless of the presence of potential JDP partners in mutual subcellular locations (Figure S3), the heat-induced Hsp70 disaggregase appears to be cogged to function primarily with DNAJA1 and DNAJB1. The findings also suggest that there is tight regulation of JDP partnering in cells. Due to this high specificity, DNAJA1+DNAJB1 scaffold formation is used henceforth as a readout to monitor stress-induced dynamics of the DNAJA1+DNAJB1-Hsp70 disaggregase in cells.

Newly synthesized JDPs assemble Hsp70 disaggregase after heat shock

Before HS, DNAJA1 was widely distributed in the cytosol and to a lesser extent in the nucleus, but excluded from the nucleoli (Figure S3A). In contrast, DNAJB1 was mainly localized in the nucleus (apart from the nucleoli) with very low protein levels in the cytosol (Figure S3C). Immediately after HS, DNAJA1 and DNAJB1 rapidly relocalized to nucleoli, and then proceeded to redistribute back to the unstressed locations upon recovery before 6 hours (Figure S3A and C). A similar HS-induced nucleoli distribution pattern was observed for Hsp70 (Figure S3E), consistent with previous reports (*30, 33, 35*). However, the paralogs of the two JDPs, DNAJA2 and DNAJB4, did not enrich in nucleoli after HS (Figure S3B and D). Treatment of cells with the translational inhibitor cycloheximide (CHX) immediately after HS did not block DNAJA1 and DNAJB1 relocalization into nucleoli or their subsequent distribution to the original cell compartments (DNAJA1: Figure S4A and B; DNAJB1: Figure S4C and D). These stress-induced movements of pre-HS synthesized (co)chaperones coincide with Hsp70-mediated refolding and extraction of heat-denatured proteins from nucleoli immediately after HS (*30, 31, 33*). We observed that DNAJA1 and DNAJB1 molecules synthesized before HS, although released from the nucleoli at 6h post-HS, were not prompting an increase in JDP scaffold levels in the nucleus/cytosol (Figure S5). This suggests that predominantly newly synthesized DNAJA1 and DNAJB1 molecules drive the assemblage of the DNAJA1+DNAJB1-Hsp70 disaggregase in cells after HS. In essence, this implies that pre- and post-HS synthesized DNAJA1 and DNAJB1 molecules can assemble spatially and temporally separated Hsp70 chaperone machines to repair proteins in different cell compartments during mammalian stress recovery. This outlines a new strategy employed by Hsp70-JDP systems to efficiently organize different chaperone machines that cater to various cell needs on a priority basis (*e.g.,* rapid recovery of proteins associated with nucleoli functions crucial for immediate stress adaptation (*36-39*) *vs.* subsequent removal of the remaining aggregated protein junk) under challenging growth conditions.

The heat shock response schedules induction of Hsp70 disaggregase during stress recovery

Our initial findings showed that the DNAJA1+DNAJB1-Hsp70 disaggregase is assembled with newly synthesized machine components after heat stress. qRT PCR measurements showed that DNAJA1 and DNAJB1 mRNA levels were rapidly induced during HS (Figure S6A). This resulted in an increase in the production of the two JDPs, as shown by mass spectrometry-based multiple reaction monitoring (MRM) (Figure S6B). In particular, the maximum induction of DNAJB1 at 6h after HS coincided with the highest level of DNAJA1+DNAJB1 scaffold formation and

consequently the peak assembly of Hsp70 disaggregase (Figure 1D-F). Based on these observations, we hypothesized that the HSR, which induces the heat shock protein genes to cope with cellular proteotoxic stresses, may play a crucial regulatory role in the assembly of this disaggregase (Figure 1G) (*40*). HSF-1 transcription factor is the master regulator of the HSR and drives chaperone expression by binding to heat shock elements (HSE) in promoter regions of specific chaperones (*25, 41, 42*). RNAi knock down of HSF-1 resulted in blocking the synthesis of new DNAJA1 and DNAJB1 molecules after HS (left, Figure 1H), which inhibited the subsequent formation of the JDP scaffold of the Hsp70 disaggregase (right, Figure 1H). In contrast, depletion of HSF-1 did not hinder the nucleolar entry and exit of pre-existing (*i.e.* made before HS) JDPs (Figure S7A-C). This is consistent with what we found after CHX treatment (Figure S4) and the findings reconfirmed that newly synthesized JDPs were employed primarily to form this protein disaggregase. Collectively, our findings highlight the emergence of an HSF-1-dependent stress-induced PQC pathway, which selectively increases the assembly of DNAJA1+DNAJB1-Hsp70 disaggregase in human cells. We henceforth name this stress pathway siDAP.

Other chaperone cofactors that participate in modulating siDAP

By facilitating the dissociation of ADP from Hsp70, NEFs promote the rebinding of ATP and the interconversion of Hsp70 to an open conformation to engage new substrates (*43*). Previous *in vitro* studies have shown that Hsp110-type NEFs accelerate protein disaggregation activity by resetting and/or removing unproductive machine assemblies on aggregates (*16, 27*). We hypothesized that NEF activity might particularly influence the disassembly dynamics of the DNAJA1+DNAJB1-Hsp70 disaggregase. To test this, we depleted members of three different families of NEFs (BAG1, HSPBP1, HSPH1-3) using RNAi and evaluated both induction and attenuation of Hsp70 disaggregase assembly during stress recovery. A considerable delay in disassembly of the disaggregase was observed when all three Hsp110s (HSPH1-3) were simultaneously knocked down, suggesting that the paralogs function redundantly to support siDAP in HeLa cells. On the contrary, the depletion of BAG1 or HSPBP1 did not have an effect (Figure S8) consistent with the *in vitro* findings (*44*).

Activation of siDAP is essential for resolving heat-induced protein aggregates in cells

To assess the functional consequences of activating siDAP, we monitored the fate of heat-induced protein aggregates in human cells (HeLa and HEK 293). To trace heat-induced aggregates of endogenous proteins in bulk, a catalytically inactive yeast Hsp104 tagged with GFP (E285Q, E687Q Double Walker B; Hsp104^{DWB}-GFP) was used (Figure 2A) (*45*). Unstressed HeLa cells (U) ectopically expressing Hsp104^{DWB}-GFP showed a diffuse GFP fluorescent signal (cyan) indicating that protein aggregates were largely absent. Immediately after HS (0h), fluorescent puncta emerged, indicating the presence of aggregates. Upon full induction of the Hsp70 disaggregase at 6h after HS, the frequency of Hsp104^{DWB}-GFP decorated puncta (aggregates) began to decrease, and their disappearance coincided with the disassembly of the disaggregase (Figure 2B; Figure S9; Figure S10B for 12h recovery time point). It should be noted that we did not observe Hsp104^{DWB}-GFP puncta decorating nucleoli, where many heat-denatured proteins accumulate immediately after HS and recover rapidly, that is, within the initial hours after HS (*30, 31, 33*).

To directly assess the significance of siDAP-induced disaggregation activity on aggregate solubilization, we employed two approaches. First, we blocked siDAP activation by depleting HSF-1. This resulted in complete abrogation of aggregate solubilization in HS-recovering cells (Figure S9A). Second, we used VER-155008, a specific adenosine-derived small molecule inhibitor of Hsp70 (*46*). Adding VER-155008 to DNAJA1+DNAJB1-Hsp70 disaggregase

significantly inhibited the solubilization of heat-induced luciferase aggregates, *in vitro* (Figure 2C). Next, VER-155008 was added to cells 5h after HS to exclude its effects on, for example, nucleoli protein recovery by Hsp70, which occurs immediately after HS (*31, 33*), and instead, block DNAJA1+DNAJB1-Hsp70 disaggregase activity at its peak. Compared to control cells treated with DMSO, cells treated with VER-155008 showed considerable defects in the removal of heat-induced Hsp104^{DWB}-GFP positive aggregates (Figure 2D, Figure S9B and C). Blocking Hsp70 activity by VER-155008 also caused DNAJA1+DNAJB1 scaffolds to persist up to 24h after HS, presumably due to their continuous association with the aggregates (Figure 2D). Next, we tested whether the assembled JDP scaffolds could support the re-initiation of protein disaggregation upon removal of the Hsp70 inhibitor. The washing of VER-155008 by a change in culture medium 12h after HS resulted in the resumption of aggregate solubilization and subsequent disassembly of JDP scaffolds (Figure S10A-C). Together, these findings corroborate that siDAP-induced DNAJA1+DNAJB1-Hsp70 disaggregase activity is vital for removing a specific fraction of (*e.g.,* non-nucleolar-associated) heat-induced aggregated proteins in recovering human cells.

Efficient targeting of heat-induced aggregates in cells requires DNAJA1+DNAJB1 scaffolds

We have previously shown that scaffolds containing class A and B JDPs are required, along with Hsp70, to efficiently solubilize amorphous aggregates *in vitro* (*13*). However, biochemical studies show that Hsp70 disaggregases can form with DNAJA or DNAJB alone. These single JDP-type containing machine configurations have been reported to show varying degrees of activity with different substrates, *in vitro* (Figure 1B) (*14, 44, 47-49*). To analyze whether single JDP type containing Hsp70 disaggregases could support siDAP, we again used the complex-forming defective mutant of DNAJB1. Consistent with previous observations (*13*), the ability of DNAJB1^{RRR} to cooperate with DNAJA1 and synergize luciferase disaggregation was strongly compromised compared to the wild-type protein, *in vitro* (Figure 2E). Accordingly, ectopically expressed wild-type DNAJB1, but not DNAJB1^{RRR}, was able to solubilize heat-induced Hsp104^{DWB}-GFP positive aggregates in *DNAJB1* knocked-out HEK 293 cells recovering from HS (Figure 2F-J; Figure S11A and B). DNAJB1$^{H32Q, D34N}$ (DNAJB1^{QPN}), which cannot cooperate with Hsp70, readily complexed with endogenous DNAJA1 after HS (Figure 2J). However, these JDP scaffolds could not form active disaggregases due to the inability of DNAJB1 to recruit Hsp70, which prevented aggregate resolution in recovering cells (Figure 2J). Next, we asked whether DNAJB1 activity can be restored in *DNAJB1* knocked-out cells by overexpressing another JDP. However, ectopically expressing DNAJA1, DNAJA2, or DNAJB4 in these cells could not fully resolve heat-induced Hsp104^{DWB}-GFP positive aggregates (Figure S11C). Together, these findings demonstrate that i) the interaction between DNAJA1 and DNAJB1 is crucial to drive efficient protein disaggregation in human cells recovering from HS and ii) other class A or class B JDPs, even when overexpressed, cannot (fully) replace the function of DNAJB1. Overall, the observations indicate that single JDP-containing disaggregases are ineffective in supporting siDAP. It should be noted that the rapid decrease in Hsp104^{DWB}-GFP positive aggregates observed at 6h after HS in *DNAJB1* knocked-out cells overexpressing DNAJB1 (Figure 2H) compared to the much slower degree of aggregate resolution observed in wild-type cells (Figure S11A) could be explained by the rapid assembly of DNAJA1+DNAJB1-Hsp70 disaggregase within 1h after HS (Figure S11D). From this, we conclude that DNAJB1 is a 'bottleneck' component of this assemblage, and its levels play a central role in modulating both the efficacy and the timing of induction of the DNAJA1+DNAJB1-Hsp70 disaggregase in cells recovering from heat stress.

The fate of the disaggregated proteins

Following solubilization of Hsp104^{DWB}-GFP positive aggregates, the released non-native proteins could be directed toward refolding, degradation, or re-aggregation. Recovery of aggregated

proteins through Hsp100-based disaggregation activity is vital for the thermoresistance and survival of bacteria and yeast after heat stress (*50-52*). Protein repair through this process has been proposed to greatly reduce protein resynthesis requirements during stress recovery, which arguably decreases the demand for cellular resources (*32, 53*). To test whether siDAP-induced DNAJA1+DNAJB1-Hsp70 disaggregase activity leads to the recovery of some proteins from heat-induced aggregates, we applied a simple two-phase fractionation approach coupled to a proteomic workflow conceptually described in Figure S12A (*23*). Data were agnostically clustered into four different response patterns by k-means clustering. The proteins in cluster (iii) showed a pattern of aggregation and recovery that was consistent with them being substrates for this disaggregase activity. Specifically, they appeared to show impaired solubility recovery after treatment with VER-155008 between 6 and 12 hours (Figure S12B and C). Two proteins in cluster (iii) that were further studied included: Heterogeneous nuclear ribonucleoprotein K (HNRNPK; solubility profile in Figure 3A) and Adenosylhomocysteinase (AHCY; solubility profile in Figure 3B). HNRNPK is involved in the processing and transport of mRNA, and AHCY plays a crucial role in cellular methyl homeostasis by removing excess *S*-adenosylhomocysteine. Immunocytochemical analysis of the aggregation and disaggregation patterns of these proteins after HS showed that both HNRNPK and AHCY remained considerably aggregated (appearance of punctated fluorescent signal *vs.* diffuse signal) at 6h after HS in HeLa cells. However, with the induction of Hsp70 disaggregase, the aggregated proteins were completely solubilized and precisely localized back to their original cell compartments at the recovery time point of 12h (Figure 3C and D). Blocking the activity of Hsp70 disaggregase with VER-155008 prevented the resolubilization of aggregated HNRNPK and AHCY (Figure 3C and D; Figure S12D). More directly, knocking down DNAJA1 or DNAJB1 also resulted in a similar inhibition of the resolution of HNRNPK aggregates (Figure 3E), again demonstrating that cooperation between the two JDPs is essential for the efficient disaggregation of these heat-aggregated endogenous substrates. Furthermore, the data strengthen previous findings showing that alternative JDP scaffolds are ineffective in supporting this activity in cells.

Although the above data suggest that a set of heat-aggregated endogenous substrates is recovered by siDAP (relocalization of the disaggregated substrates to their original cell compartments tentatively imply that the recovered proteins are refolded), we also found that a cooperation between this pathway and protein degradation is needed for the efficient removal of heat-induced aggregated proteins in cells. Inhibition of protein degradation (at 5h post-HS) using the 26S proteasome inhibitor bortezomib (*54*) concomitant to activation of the DNAJA1+DNAJB1-Hsp70 disaggregase resulted in defective clearance of $Hsp104^{DWB}$-GFP positive heat-aggregated proteins compared to control cells treated with DMSO (Figure S13A). As a consequence, the disassembly of Hsp70 disaggregase was prolonged in HeLa cells (Figure S13B). The decreased efficiency in aggregate solubilization could arise from increased (re)aggregation events triggered by defective protein degradation (*55*) and/or other impairments in protein homeostasis (*56*) that could overwhelm protein disaggregation function. Taken together, these results show an important cooperation between siDAP and UPS to remove a subset of heat-damaged protein junk as part of a healthy balance between protein repair and disposal during the stress recovery process.

Protein aggregates distinct from stress granules are targeted by siDAP-induced disaggregase

In part, due to spatial and temporal differences, the siDAP-induced DNAJA1+DNAJB1-Hsp70 disaggregase appears to be not involved in targeting substrates that accumulate in biomolecular condensates such as nucleoli after HS. However, HS also induces proteins to denature and form or associate with phase separated biomolecular condensates such as SGs in the cytosol (*30-33, 57-60*). T cell-restricted intracellular antigen-1 (TIA-1) is a protein that accumulates in cytosolic SGs

after heat stress in mammalian cells (*57, 61, 62*). TIA-1 shares a similarity to HNRNPK in that both proteins bind to RNA. Upon HS, SGs decorated with TIA-1 appeared in the cytosol of HeLa cells (Figure 3F). These SGs were spatially distinct from HNRNPK-containing aggregates. During stress recovery, the TIA-1 SGs disassembled relatively rapidly after HS (as observed with proteins accumulating in nucleoli) whilst HNRNPK containing aggregates recovered more slowly consistent with the latter being a siDAP substrate. To directly test whether Hsp70-mediated disaggregation activity is involved in TIA-1-containing SG recovery in the cytosol, we disrupted multiple Hsp70-JDP chaperone machines, including the DNAJA1+DNAJB1-Hsp70 disaggregase. We observed that these particular SGs did not rely on HSF-1-mediated HSR and the essential components of the siDAP machinery for disassembly (Figure 3F; Figure S14; Figure S15). A closer inspection revealed that the inclusions of TIA-1 and HNRNPK show markedly different solubility properties. Fluorescence recovery after photobleaching (FRAP) analysis showed an extremely low level of fluorescent signal recovery after photobleaching in heat-induced GFP-tagged HNRNPK aggregates. This indicates that the misfolded HNRNPK was almost completely immobile in these aggregates due to tight packing (Figure S16). In contrast, TIA-1 in SGs shows high mobility (*57, 63*). These findings suggest that DNAJA1+DNAJB1-Hsp70 disaggregase works to disassemble tightly packed solid-like amorphous aggregates that persist beyond the initial stress recovery stage, which resolves phase separated proteins in SGs and nucleoli.

Hsp70 disaggregase operates within a network of aggregate solubilizing machines that target different populations of heat-induced aggregates

To this point, our analysis revealed that siDAP is not responsible for disassembling all heat-induced protein inclusions. This inferred that perhaps there is redundancy in protein disaggregation function in cells and that a combined action of multiple protein disaggregating systems is needed to effectively target different types of aggregates and recover from proteotoxic stresses. Recent findings reveal that there are other molecular machines in mammals that can resolve specific types of aggregated proteins. For example, AAA ATPase VCP (p97) was recently shown to target and disassemble polyubiquitinated amyloid aggregates (*64, 65*). We hypothesized that VCP might also be processing some of the heat-induced aggregates in human cells. Following HS, we observed the generation of a population of aggregates that were 1% NP-40 insoluble and Ub positive (Ub+). These aggregates were largely removed before peak activation of siDAP (Figure S17A). To test whether VCP targets these Ub+ aggregates, we knocked down the AAA ATPase using RNAi. The knocked-down cells showed a considerable delay in the clearance of heat-induced Ub+ aggregates (Figure 4A), thus confirming our prediction. Cells depleted of VCP also showed a delay in TIA-1 SG disassembly, but the condensates resolved completely within 24h after HS (Figure S17B). This result is consistent with the role of VCP in promoting the disassembly of various SGs, possibly by targeting ubiquitinated component(s) in phase-separated condensates (*66*). Surprisingly, knocking down VCP also delayed the solubilization of siDAP-targeted HNRNPK and Hsp104^{DWB}-GFP positive and aggregates (Figure S17B and C) that generally do not have a Ub+ signature (Figure S18A). In line, the disassembly of the Hsp70 disaggregase complex was also delayed upon VCP knockdown (Figure 18B). To test whether disrupting VCP function directly affected the action of DNAJA1+DNAJB1-Hsp70 disaggregase, we treated cells with the VCP inhibitor NMS-873 (*67*) at 0h or 5h after HS. Adding NMS-873 at 0h post-HS triggered the same phenotype as that of knocking down VCP. However, blocking the VCP function using a low (1 μM) or high (10 μM) dosage of NMS-873 5h after HS, *i.e.* after clearing of heat-induced Ub+ aggregates, did not affect Hsp104^{DWB}-GFP positive aggregate solubilization mediated by siDAP-induced Hsp70 disaggregase (Figure 4B; Figure S18C). Consequently, in this condition, the Hsp70 disaggregase disassembled back to basal levels at 24h post-HS (Figure 4C). This indicates that the two systems are functionally divided and non-redundant. These experiments also rule out the possibility that

VCP and siDAP-induced Hsp70 disaggregase form an Hsp100-Hsp70 bichaperone-like disaggregase system to target tightly packed aggregates during the latter stages of stress recovery. We infer from the data that a fraction of heat-induced aggregate load needs to be cleared first by VCP-dependent actions before siDAP can become effective during stress recovery.

Next, we examined whether DAXX, a polyD/E protein recently shown to possess protein disaggregation activity *in vitro* (*68*), functions together with the other disaggregase systems in heat-shocked cells. Interestingly, depletion of DAXX also prolonged the resolution of heat-induced HNRNPK aggregates, but did not significantly affect solubilization of TIA-1 SGs (Figure S19A). Furthermore, we observed a considerable delay in the disassembly of DNAJA1+DNAJB1 scaffold in these cells (Figure S19B). However, this delay was largely due to down-regulation of HSF-1 activity, resulting in decreased Hsp70 induction after HS (*69*) (Figure S19C). Consequently, we detected a reduced loading of Hsp70 onto DNAJA1 and DNAJB1 that led to defective disaggregase assembly (Figure S19D), thus explaining the observed aggregate persistence phenotype.

Importantly, increasing the levels of both VCP and DAXX did not affect the assembly and disassembly dynamics of the Hsp70 disaggregase during stress recovery (Figure S20), which is in stark contrast to the overexpression of yeast Hsp104 disaggregase that attenuated downstream siDAP activity (see below section on siDAP exerts a tailor-made response to heat stress damage). These observations suggest that the function of Hsp70 disaggregase cannot be compensated by stimulating other endogenous disaggregase systems in human cells. The findings also provide information on the mechanisms by which these disaggregase systems cooperate in the clearance of aggregated proteins. In general, the findings show that an integrated aggregate removal system with more than one type of disaggregase works to target different populations of heat-induced aggregates/SGs in cells.

Activation of siDAP is important for cellular fitness after heat stress

Next, we evaluated the impact of activating siDAP on the fitness of human cells recovering from heat stress. Cell survival after HS was monitored using a highly sensitive lactate dehydrogenase (LDH)-Glo-based cytotoxicity assay. The assay detects the release of LDH from damaged or dying cells and generates a proportional bioluminescence signal through a cascade of enzyme reactions (Figure 5A) that were quantified at different time points during cell recovery. To block siDAP activity, we again added VER-155008 (at 2.5 after HS) and started measuring cell cytotoxicity 3h after HS (Figure S21A). At this time point, rapid recovery of heat-denatured proteins from nucleoli (*i.e.* immediately after HS) was completed (*30*). The inactivation of siDAP led to a considerable increase in heat toxicity in HeLa cells compared to the control treated with DMSO (Figure 5A). These findings are consistent with the role of protein disaggregation in promoting cell thermoresistance.

In fact, we found that human cells can tune the activation of siDAP according to the level of protein damage sustained after HS. We observed that siDAP responding to even relatively small temperature increases (37 °C to 39 °C) typically observed with mild to moderate fever (Figure 5B) (*70*), revealing that this pathway could act under physiologically relevant circumstances. By increasing the temperature by another 3 °C (37 °C to 42 °C), mimicking high fever (*70*), we not only detected a greater level of induction (>2 fold), but also prolonged activation of Hsp70 disaggregase in cells (Figure 5B). This infers that there is flexibility in the response of this pathway and that the strength of the response could be adjusted proportionately to the intensity of damage

caused by the stress insult.

To provide further support, we used yeast Hsp104 disaggregase to manipulate the aggregate load and show that the response of siDAP is sensitive to the degree of protein aggregation in heat-shocked cells. Cross-species cooperation between metazoan Hsp70 and yeast Hsp104 has previously been reported to enhance overall cellular disaggregation capacity (*71*). We hypothesized that by expressing wild-type Hsp104, we could artificially boost disaggregation immediately after heat insult and quickly resolve the resulting aggregates to increase cell repair. By combining yeast Hsp104 disaggregase with the human Hsp70 system, we were able to demonstrate the establishment of a potent bichaperone disaggregase system, *in vitro* (Figure S21B). Consistently, we observed that heat aggregated proteins that generally rely on siDAP (*e.g.* HNRNPK) are rapidly solubilized before the 6h recovery time point in Hsp104-GFP-expressing cells (Figure S21C). As a consequence of the rapid removal of aggregates, we detected a considerable decrease in the induction of Hsp70 disaggregase during recovery from HS (Figure S21D). This indicates that the siDAP-induced assembly of DNAJA1+DNAJB1 scaffold is sensitive to the protein aggregate levels in the cell and that the formation of DNAJA1+DNAJB1-Hsp70 disaggregase is not stochastic. In contrast, despite the rapid decrease in aggregate levels (and the need to assemble disaggregases), the HSR-mediated induction of DNAJA1 and DNAJB1 proteins remained intact (Figure S21D). This is not surprising, because HSR activation via HSF-1 does not depend on post-damage repair but rather on the level of damage to the cells (*72*). The observed redundancy with Hsp104 activity further confirms that the DNAJA1+DNAJB1-Hsp70 machine functions as a protein disaggregase in human cells.

siDAP collapses during replicative cellular aging

Cellular aging is intimately linked to a collapse in protein homeostasis (*73, 74*), but the underlining mechanisms are largely unknown. Chronological aging in some multicellular organisms results in cells losing the ability to induce stress responses, such as the HSF-1 dependent HRS, to up-regulate components of PQC machines (*e.g.* Hsp70-based) vital for counteracting proteotoxic stresses (*75-77*). However, this phenomenon is context dependent, can vary from cell type to cell type due to differences in the organization of PQC networks and sensitivity for detecting mistakes, and remains ambiguous in mammals (*78, 79*). To understand how protein disaggregation activity is affected during chronological aging, we analyzed six lines of primary dermal fibroblasts derived from humans with ages ranging from 21 to 75 years. The upper limit of the chosen range encompasses the average human life expectancy of 72.6 years (based on global populations for 2019, United Nations). We did not observe a substantial chronological age-driven variation in the inducibility of Hsp70s and JDPs (at protein level) after HS, consistent with previous reports (*78, 79*). Moreover, siDAP was fully active in all fibroblast lines tested (Figure 6A; Figure S22A and B). Similar to immortalized HeLa cells, primary dermal fibroblasts only induced the DNAJA1+DNAJB1 JDP scaffold after HS (Figure S22C). From these data, it appears that chronological age-associated cellular alterations (*e.g.,* DNA methylation-based epigenetic changes) that remain preserved in e*x vivo* cultured human fibroblasts (*80*) do not have a modulatory effect on siDAP. However, this could vary according to cell type and human subjects.

Next, we evaluated whether replicative aging, which results in cell senescence and loss of tissue resistance to disease-causing stresses (*81*), has any effect on activating siDAP. We subjected three of the human dermal fibroblast lines (derived from 21-, 55-, and 75-year-old donors) to replicative aging by *ex vivo* passaging (P) of cells up to 18 times (Figure 6B). The cell senescence state was quantitatively and qualitatively confirmed using cell lysate-based SPiDER-βGal and direct cell staining methods that measure increases in the specific β-galactosidase activity, respectively

(Figure 6C; Figure S22D and E). Cells in P 12 and P 18 showed a significant increase in senescence specific β-galactosidase activity (both in lysates and individually stained cells) independent of the chronological age of the donor. Interestingly, these cells undergoing replicative aging showed a complete absence of the siDAP-mediated induction of Hsp70 disaggregase after HS compared to cells at P 3 or 6 (Figure 6D; Figure S22A-C). Importantly, immunoblot analysis showed that the defect in disaggregase assembly in cells at P 12 (and P 18) was not caused by a deficiency in the induction of disaggregase components through impaired HSR (Figure 6D), which occurs during prolonged cellular senescence (*79, 82*). These findings argue that an important replicative aging-specific facet(s) modulates siDAP and controls the assembly of DNAJA1+DNAJB1-Hsp70 disaggregase. Similar to siDAP inhibited HeLa cells (with VER-155008) (Figure 2D), the siDAP defective P 12 dermal fibroblasts showed an inability to resolve heat-induced protein aggregates (Figure S23A and B) and displayed increased cytotoxicity after HS (Figure 6E). We noted that P 12 cells contained protein aggregates even under unstressed conditions (Figure S23B), a hallmark of aging cells.

Appearance of intracellular fiber-like amyloid protein aggregates are intrinsically linked to age-associated neurodegeneration (*e.g.* in Huntington's disease) (*83*). First, we explored whether this type of pathological protein aggregates are affected by activating siDAP. For this analysis, we used GFP tagged Huntingtin protein (Htt) exon 1 containing an expanded polyglutamine sequence (polyQ) (Figure S24A). These cytotoxic aggregates could form independently of proteotoxic stresses, such as heat. PolyQ aggregation was induced in unstressed HeLa cells (cyan foci, Figure S24B) by overexpressing Htt exon-1 carrying varying lengths of sequential glutamine stretches (HttQ46-mEmGFP and HttQ119-GFP; HttQ23-mEmGFP, non-aggregating control). siDAP was activated by HS (Figure S24B) and CHX was added 5h after HS to prevent aggregation of newly synthesized HttpolyQ molecules. CHX addition at 5h after HS had minimal effects on the induction of DNAJA1+DNAJB1-Hsp70 disaggregase. We observed the solubilization of preexisting HttQ46-GFP aggregates (disappearance of fluorescent puncta and appearance of a diffuse signal 12h after HS) with induction of the disaggregase (Figure S24B). Adding the Hsp70 inhibitor with CHX 5h after HS (Figure S24C) or knocking down DNAJA1 and DNAJB1 using RNAi (Figure S24D), completely abrogated amyloid solubilization. Together, these results indicate that DNAJA1+DNAJB1-Hsp70 disaggregase also has the ability to target amyloid aggregates in cells. Interestingly, the omission of CHX treatment from the experimental regime prevented the previously observed decrease in the steady-state level of HttQ46-GFP aggregates (Figure S24E) despite the induction of Hsp70 disaggregase. Given the highly aggregate-prone nature of HttpolyQ species, we presume that the aggregation rate of newly synthesized HttQ46-GFP monomers was faster than the disaggregation rate of the DNAJA1+DNAJB1-Hsp70 machine. In contrast, the amyloids formed by Htt exon-1 with a longer Q stretch (HttQ119-GFP) were completely resistant to the action of Hsp70 disaggregase even after blocking the aggregation of newly synthesized proteins using CHX (Figure S24B and E). These observations highlight important functional boundaries associated with the inherent capacity of siDAP to modulate amyloid load in cells. Next, we assessed how these pathological aggregates are affected in dermal fibroblasts undergoing replicative aging. Interestingly, unlike in HeLa cells (Figure S24), Htt46Q-GFP was largely soluble with only a mild aggregation phenotype in unstressed dermal fibroblasts at P 6 and P 12 (Figure 6F). Upon HS, soluble Htt46Q-GFP quickly formed into prominent aggregates (punctated cyan fluorescent signal, 6h after HS) in P 6 and P 12 cells. However, these heat-induced polyQ aggregates were only solubilized in P 6 fibroblasts that could still activate siDAP (Figure 6D and F). In essence, siDAP, when induced, could dissolve amyloid-type aggregates formed by pathological proteins and the early inactivation of this pathway could enhance such aggregation events. Overall, our findings suggest that siDAP is one of the first PQC

pathways to malfunction in cells that undergo replicative aging and may have important implications for aging, tissue regeneration, and age-related diseases associated with protein aggregation in humans.

Discussion

In this study, we identified a novel, dedicated PQC pathway termed siDAP, which accelerates protein disaggregation function in human cells recovering from HS. siDAP selectively increases the levels of DNAJA1+DNAJB1-Hsp70 disaggregase (Figure 7). The DNAJA1+DNAJB1-Hsp70 disaggregase is modulated to function during proteotoxic stress recovery as part of an apparatus that clears aggregates. We identified two major disaggregase systems made up of VCP and Hsp70 that operate in two distinct aggregate/SG resolving phases in human cells (Figure 7). The initial phase (phase 1) is predominated by the VCP disaggregase activity, which facilitates the disassembly of Ub+ aggregates and SGs to rapidly decrease the total load of cellular aggregates (Figure 7). Phase 2 depends on the completion of phase 1, but does not require VCP. Phase 2 is initiated by siDAP activation, which triggers massive assembly of DNAJA1+DNAJB1-Hsp70 disaggregase to effectively "mop up" solid-like tightly packed aggregates that escape phase 1 clearance. This function cannot be substituted for by VCP even when overexpressed, thus highlighting differences in substrate preference and non-overlapping roles of the disaggregase systems. Overall, our data demonstrate that at least two protein disaggregation systems have evolved to optimally divide labor by systematically targeting different types of aggregates/condensates to support cells recovering from heat stress-triggered proteostatic imbalance.

There are fundamental differences between VCP and Hsp70 protein disaggregation systems in how they work and respond to stress. The activation of DNAJA1+DNAJB1-Hsp70 disaggregase in part is based on HSF-1-mediated HSR, which produces the required disaggregase machine components. On the contrary, cellular VCP levels are not modulated by proteotoxic stresses (*84*) and remain unchanged after HS (Figure 4A). VCP largely depends on a Ub signal to recognize its aggregates and SG components, but could also function independently of Ub to disassemble some protein complexes (*85*). In contrast, Hsp70 disaggregases use specific JDP scaffolds to target aggregated substrates. In terms of disaggregase action, VCP employs an Hsp104-like mechanism of protein extraction (*86, 87*). This mechanism is entirely different from that of Hsp70-based disaggregases that appear to rely on entopic pulling to generate the necessary forces to untangle and release trapped polypeptides, and dismantle aggregates (*11, 16*). Finally, after extraction of trapped polypeptides, Hsp70 disaggregase disassembles. In contrast, VCP, after assembly, functions as a stable dodecamer (*88*) (Figure 7). In terms of the fate of disaggregated polypeptides, there is likely a culmination of protein recovery and degradation during both phases (Figure 7) (*86, 89-91*). How triage decisions are made to repair or degrade a disaggregated protein remains unclear.

There is some evidence to suggest that cellular surveillance systems that usually keep protein aggregation in check deteriorate during aging (*1, 74, 92*), and thereby presumably drive the characteristic appearance of resilient aggregates in old cells (*93*). However, the age-related breakdown of the PQC pathways and the ensuing physiological consequences are poorly understood in mammals. Our findings show that, remarkably, the ability to stress induce the DNAJA1+DNAJB1-Hsp70 disaggregase through siDAP dwindles even before human cells that undergo replicative aging lose their ability to trigger HSR (Figure 6D), which has often been considered to precede the collapse of proteostasis in cells during late senescence (*93*). Mechanistically, the breakdown of this pathway stems from the inability of aging cells to

effectively assemble the DNAJA1+DNAJB1 JDP scaffold of Hsp70 disaggregase, and not the synthesis of machine components. Considerable effort is now being put towards understanding the molecular basis of selective JDP scaffold formation and how this process collapses during replicative aging. In general, these findings add another important dimension to our current understanding of the cellular mechanisms of aging, where protein aggregation is often considered a major attribute.

The health implications related to the inactivation of this pathway could be significant. In humans, the elevation of body temperature is an integrated response to a variety of infective, inflammatory, neoplastic, and immune-mediated insults. These stimuli alter the set point of the hypothalamic thermoregulation center, which, in turn, activates neuroendocrine responses that result in hyperthermia (*94*). Additionally, hyperthermic stress could also result from heat stroke. Such temperature elevations, if not controlled, could cause protein misfolding/aggregation, leading to a breakdown of protein homeostasis and premature death of cells. This could potentially trigger detrimental dysregulations in various body organs (*94, 95*) resulting in increased morbidity and mortality (*94, 96, 97*). Protein disaggregation function appears to be selected by evolution to be optimally active, for example via siDAP, under such conditions to solubilize and detoxify aggregated proteins, support cell survival, and limit tissue damage. However, tissues highly vulnerable to senescence could display reduced resistance to proteotoxic stress due to the collapse of siDAP, and when challenged, they may likely become pathological, as observed in our proof-of-principle experiments with Huntington's disease-associated polyQ aggregates (Figure 6F). In essence, the findings show how changes in the efficacy of a specific PQC activity could be linked to a disease condition during cellular aging. On the contrary, pharmacological blocking of this pathway in specific disease conditions such as cancer may provide therapeutically beneficial outcomes. Brief hyperthermic treatments have been shown to enhance the cytotoxic properties of many chemotherapeutic agents (*98*) such as bortezomib (*99*). Our findings provide a new underlying mechanism, in addition to the processes currently debated (*55, 99-101*), to explain the increased gain of cytotoxicity and thermal sensitization observed when proteasome inhibition (with bortezomib or its derivatives) is combined with HS in anticancer studies (*55, 99-101*). Overall, this PQC pathway offers a new target to find therapeutically valuable ways to fight against several major diseases in humans that have limited or no treatments.

In summary, the presence of different configurations of Hsp70-based disaggregase in human cells provides flexible target selectivity, allowing the possibility of additional diversification of the protein disaggregation function. siDAP is specifically geared toward activating one of such disaggregases to detoxify stress-induced protein aggregates that otherwise perturb recovery leading to decreased cellular fitness and even cell death, with a fundamental impact on human health.

References

1. C. L. Klaips, G. G. Jayaraj, F. U. Hartl, Pathways of cellular proteostasis in aging and disease. *J. Cell Biol.* **217**, 51-63 (2018).
2. J. Labbadia, R. I. Morimoto, The biology of proteostasis in aging and disease. *Annu. Rev. Biochem.* **84**, 435-464 (2015).
3. M. E. Rebeaud, S. Mallik, P. Goloubinoff, D. S. Tawfik, On the evolution of chaperones and cochaperones and the expansion of proteomes across the Tree of Life. *Proc. Natl. Acad. Sci. U. S. A.* **118**, (2021).
4. N. B. Nillegoda, A. S. Wentink, B. Bukau, Protein disaggregation in multicellular organisms. *Trends Biochem. Sci.* **43**, 285-300 (2018).

5. Y. Sanchez, S. L. Lindquist, HSP104 required for induced thermotolerance. *Science* **248**, 1112-1115 (1990).
6. S.-W. Hong, E. Vierling, Mutants of Arabidopsis thaliana defective in the acquisition of tolerance to high temperature stress. *Proc. Natl. Acad. Sci. U. S. A.* **97**, 4392-4397 (2000).
7. J. Kirstein *et al.*, In vivo properties of the disaggregase function of J-proteins and Hsc70 in Caenorhabditis elegans stress and aging. *Aging Cell* **16**, 1414-1424 (2017).
8. C. Squires, S. Pedersen, B. Ross, C. Squires, ClpB is the Escherichia coli heat shock protein F84. 1. *J. Bacteriol.* **173**, 4254-4262 (1991).
9. J. Shorter, D. R. Southworth, Spiraling in control: structures and mechanisms of the Hsp104 disaggregase. *Cold Spring Harb. Perspect. Biol.* **11**, a034033 (2019).
10. T. Haslberger *et al.*, Protein disaggregation by the AAA+ chaperone ClpB involves partial threading of looped polypeptide segments. *Nat. Rev. Mol. Cell Biol* **15**, 641-650 (2008).
11. N. B. Nillegoda, B. Bukau, Metazoan Hsp70-based protein disaggregases: emergence and mechanisms. *Frontiers in molecular biosciences* **2**, 57 (2015).
12. H. Yoo, J. A. Bard, E. V. Pilipenko, D. A. Drummond, Chaperones directly and efficiently disperse stress-triggered biomolecular condensates. *Mol. Cell* **82**, 741-755. e711 (2022).
13. N. B. Nillegoda *et al.*, Crucial HSP70 co-chaperone complex unlocks metazoan protein disaggregation. *Nature* **524**, 247-251 (2015).
14. N. B. Nillegoda *et al.*, Evolution of an intricate J-protein network driving protein disaggregation in eukaryotes. *Elife* **6**, e24560 (2017).
15. C. C. Gonçalves, I. Sharon, T. M. Schmeing, C. H. Ramos, J. C. Young, The chaperone HSPB1 prepares protein aggregates for resolubilization by HSP70. *Sci. Rep.* **11**, 1-16 (2021).
16. A. S. Wentink *et al.*, Molecular dissection of amyloid disaggregation by human HSP70. *Nature* **587**, 483-488 (2020).
17. R. Zhang, D. Malinverni, D. M. Cyr, P. De Los Rios, N. B. Nillegoda, J-domain protein chaperone circuits in proteostasis and disease. *Trends Cell Biol.*, (2022).
18. J. M. Nunes, M. Mayer-Hartl, F. U. Hartl, D. J. Müller, Action of the Hsp70 chaperone system observed with single proteins. *Nature communications* **6**, 1-9 (2015).
19. P. Goloubinoff, P. De Los Rios, The mechanism of Hsp70 chaperones:(entropic) pulling the models together. *Trends Biochem. Sci.* **32**, 372-380 (2007).
20. P. De Los Rios, A. Ben-Zvi, O. Slutsky, A. Azem, P. Goloubinoff, Hsp70 chaperones accelerate protein translocation and the unfolding of stable protein aggregates by entropic pulling. *Proc. Natl. Acad. Sci. U. S. A.* **103**, 6166-6171 (2006).
21. R. Gupta *et al.*, Firefly luciferase mutants as sensors of proteome stress. *Nature methods* **8**, 879-884 (2011).
22. H. H. Kampinga, Thermotolerance in mammalian cells. Protein denaturation and aggregation, and stress proteins. *J. Cell Sci.* **104**, 11-17 (1993).
23. X. Sui *et al.*, Widespread remodeling of proteome solubility in response to different protein homeostasis stresses. *Proc. Natl. Acad. Sci. U. S. A.* **117**, 2422-2431 (2020).
24. T. A. Määttä *et al.*, Aggregation and disaggregation features of the human proteome. *Mol. Syst. Biol.* **16**, e9500 (2020).
25. S. Lindquist, The heat-shock response. *Annu. Rev. Biochem.* **55**, 1151-1191 (1986).
26. K. Richter, M. Haslbeck, J. Buchner, The heat shock response: life on the verge of death. *Mol. Cell* **40**, 253-266 (2010).
27. H. Rampelt *et al.*, Metazoan Hsp70 machines use Hsp110 to power protein disaggregation. *EMBO J.* **31**, 4221-4235 (2012).

28. O. Söderberg *et al.*, Direct observation of individual endogenous protein complexes in situ by proximity ligation. *Nat. Methods* **3**, 995-1000 (2006).
29. N. Alberts, Y. Mathangasinghe, N. B. Nillegoda, In Situ Monitoring of Transiently Formed Molecular Chaperone Assemblies in Bacteria, Yeast, and Human Cells. *JoVE*, e60172 (2019).
30. E. A. Nollen *et al.*, Dynamic changes in the localization of thermally unfolded nuclear proteins associated with chaperone-dependent protection. *Proc. Natl. Acad. Sci. U. S. A.* **98**, 12038-12043 (2001).
31. M. Azkanaz *et al.*, Protein quality control in the nucleolus safeguards recovery of epigenetic regulators after heat shock. *Elife* **8**, e45205 (2019).
32. E. W. Wallace *et al.*, Reversible, specific, active aggregates of endogenous proteins assemble upon heat stress. *Cell* **162**, 1286-1298 (2015).
33. F. Frottin *et al.*, The nucleolus functions as a phase-separated protein quality control compartment. *Science* **365**, 342-347 (2019).
34. A. A. Michels, B. Kanon, O. Bensaude, H. H. Kampinga, Heat shock protein (Hsp) 40 mutants inhibit Hsp70 in mammalian cells. *J. Biol. Chem.* **274**, 36757-36763 (1999).
35. K. Ohtsuka, H. Nakamura, C. Sato, Intracellular distribution of 73 000 and 72 000 dalton heat shock proteins in HeLa cells. *Int. J. Hyperthermia* **2**, 267-275 (1986).
36. K. Ninomiya *et al.*, Lnc RNA-dependent nuclear stress bodies promote intron retention through SR protein phosphorylation. *The EMBO journal* **39**, e102729 (2020).
37. J. Chen, L. A. Stark, Insights into the relationship between nucleolar stress and the NF-κB pathway. *Trends Genet.* **35**, 768-780 (2019).
38. D. L. Lafontaine, J. A. Riback, R. Bascetin, C. P. Brangwynne, The nucleolus as a multiphase liquid condensate. *Nature Reviews Molecular Cell Biology* **22**, 165-182 (2021).
39. M. C. Lafita-Navarro, M. Conacci-Sorrell, in *Semin. Cell Dev. Biol.* (Elsevier, 2022).
40. R. I. Morimoto, Regulation of the heat shock transcriptional response: cross talk between a family of heat shock factors, molecular chaperones, and negative regulators. *Genes Dev.* **12**, 3788-3796 (1998).
41. R. M. Vabulas, S. Raychaudhuri, M. Hayer-Hartl, F. U. Hartl, Protein folding in the cytoplasm and the heat shock response. *Cold Spring Harb. Perspect. Biol.* **2**, a004390 (2010).
42. K. A. Morano, C. M. Grant, W. S. Moye-Rowley, The response to heat shock and oxidative stress in Saccharomyces cerevisiae. *Genetics* **190**, 1157-1195 (2012).
43. R. Rosenzweig, N. B. Nillegoda, M. P. Mayer, B. Bukau, The Hsp70 chaperone network. *Nat. Rev. Mol. Cell Biol* **20**, 665-680 (2019).
44. X. Gao *et al.*, Human Hsp70 disaggregase reverses Parkinson's-linked α-synuclein amyloid fibrils. *Mol. Cell* **59**, 781-793 (2015).
45. A. M. Rogers, M. J. Egan, Autophagy machinery promotes the chaperone-mediated formation and compartmentalization of protein aggregates during appressorium development by the rice blast fungus. *Mol. Biol. Cell* **31**, 2298-2305 (2020).
46. R. Schlecht *et al.*, Functional analysis of Hsp70 inhibitors. *PLoS One* **8**, e78443 (2013).
47. J. Shorter, The mammalian disaggregase machinery: Hsp110 synergizes with Hsp70 and Hsp40 to catalyze protein disaggregation and reactivation in a cell-free system. *PLoS One* **6**, e26319 (2011).
48. A. Scior *et al.*, Complete suppression of Htt fibrilization and disaggregation of Htt fibrils by a trimeric chaperone complex. *EMBO J.* **37**, 282-299 (2018).

49. E. Nachman *et al.*, Disassembly of Tau fibrils by the human Hsp70 disaggregation machinery generates small seeding-competent species. *J. Biol. Chem.* **295**, 9676-9690 (2020).
50. J. Weibezahn *et al.*, Thermotolerance requires refolding of aggregated proteins by substrate translocation through the central pore of ClpB. *Cell* **119**, 653-665 (2004).
51. D. A. Parsell, A. S. Kowal, M. A. Singer, S. Lindquist, Protein disaggregation mediated by heat-shock protein Hspl04. *Nature* **372**, 475-478 (1994).
52. J. R. Glover, S. Lindquist, Hsp104, Hsp70, and Hsp40: a novel chaperone system that rescues previously aggregated proteins. *Cell* **94**, 73-82 (1998).
53. Y. Mathangasinghe, B. Fauvet, S. M. Jane, P. Goloubinoff, N. B. Nillegoda, The Hsp70 chaperone system: distinct roles in erythrocyte formation and maintenance. *Haematologica* **106**, 1519 (2021).
54. A. L. Goldberg, Development of proteasome inhibitors as research tools and cancer drugs. *J. Cell Biol.* **199**, 583-588 (2012).
55. Z. Sha, A. L. Goldberg, Multiple myeloma cells are exceptionally sensitive to heat shock, which overwhelms their proteostasis network and induces apoptosis. *Proc. Natl. Acad. Sci. U. S. A.* **117**, 21588-21597 (2020).
56. A. Franz, L. Ackermann, T. Hoppe, Create and preserve: proteostasis in development and aging is governed by Cdc48/p97/VCP. *Biochimica et Biophysica Acta (BBA)-Molecular Cell Research* **1843**, 205-215 (2014).
57. I. R. Mackenzie *et al.*, TIA1 mutations in amyotrophic lateral sclerosis and frontotemporal dementia promote phase separation and alter stress granule dynamics. *Neuron* **95**, 808-816. e809 (2017).
58. M. D. Figley, G. Bieri, R.-M. Kolaitis, J. P. Taylor, A. D. Gitler, Profilin 1 associates with stress granules and ALS-linked mutations alter stress granule dynamics. *J. Neurosci.* **34**, 8083-8097 (2014).
59. J. E. Shattuck, K. R. Paul, S. M. Cascarina, E. D. Ross, The prion-like protein kinase Sky1 is required for efficient stress granule disassembly. *Nat. Commun.* **10**, 1-11 (2019).
60. H. Glauninger, C. J. W. Hickernell, J. A. Bard, D. A. Drummond, Stressful steps: Progress and challenges in understanding stress-induced mRNA condensation and accumulation in stress granules. *Mol. Cell*, (2022).
61. J. B. Rayman, K. A. Karl, E. R. Kandel, TIA-1 self-multimerization, phase separation, and recruitment into stress granules are dynamically regulated by Zn2+. *Cell Rep.* **22**, 59-71 (2018).
62. N. Gilks *et al.*, Stress granule assembly is mediated by prion-like aggregation of TIA-1. *Mol. Biol. Cell* **15**, 5383-5398 (2004).
63. N. Kedersha *et al.*, Dynamic shuttling of TIA-1 accompanies the recruitment of mRNA to mammalian stress granules. *The Journal of cell biology* **151**, 1257-1268 (2000).
64. N. F. Darwich *et al.*, Autosomal dominant VCP hypomorph mutation impairs disaggregation of PHF-tau. *Science* **370**, eaay8826 (2020).
65. I. Saha *et al.*, The AAA+ chaperone VCP disaggregates Tau fibrils and generates aggregate seeds. *BioRxiv*, (2022).
66. J. R. Buchan, R.-M. Kolaitis, J. P. Taylor, R. Parker, Eukaryotic stress granules are cleared by autophagy and Cdc48/VCP function. *Cell* **153**, 1461-1474 (2013).
67. P. Polucci *et al.*, Alkylsulfanyl-1, 2, 4-triazoles, a new class of allosteric valosine containing protein inhibitors. Synthesis and structure–activity relationships. *J. Med. Chem.* **56**, 437-450 (2013).
68. L. Huang *et al.*, DAXX represents a new type of protein-folding enabler. *Nature* **597**, 132-137 (2021).

69. F. Boellmann *et al.*, DAXX interacts with heat shock factor 1 during stress activation and enhances its transcriptional activity. *Proceedings of the National Academy of Sciences* **101**, 4100-4105 (2004).
70. B. D. Schmitt, Fever phobia: misconceptions of parents about fevers. *Am. J. Dis. Child.* **134**, 176-181 (1980).
71. S. H. Satyal *et al.*, Polyglutamine aggregates alter protein folding homeostasis in Caenorhabditis elegans. *Proc. Natl. Acad. Sci. U. S. A.* **97**, 5750-5755 (2000).
72. X. Zheng *et al.*, Dynamic control of Hsf1 during heat shock by a chaperone switch and phosphorylation. *elife* **5**, e18638 (2016).
73. M. S. Hipp, P. Kasturi, F. U. Hartl, The proteostasis network and its decline in ageing. *Nat. Rev. Mol. Cell Biol* **20**, 421-435 (2019).
74. S. K. Calderwood, A. Murshid, T. Prince, The shock of aging: molecular chaperones and the heat shock response in longevity and aging–a mini-review. *Gerontology* **55**, 550-558 (2009).
75. J. Labbadia, R. I. Morimoto, Repression of the heat shock response is a programmed event at the onset of reproduction. *Mol. Cell* **59**, 639-650 (2015).
76. D. David *et al.*, Widespread protein aggregation as an inherent part of aging in. *C. elegans. PLoS Biol.* **8**, (2010).
77. G. E. Janssens, L. M. Veenhoff, Evidence for the hallmarks of human aging in replicatively aging yeast. *Microb. Cell* **3**, 263 (2016).
78. R. Ambra *et al.*, Characterization of the hsp70 response in lymphoblasts from aged and centenarian subjects and differential effects of in vitro zinc supplementation. *Exp. Gerontol.* **39**, 1475-1484 (2004).
79. A. Gutsmann-Conrad, A. R. Heydari, S. You, A. Richardson, The Expression of Heat Shock Protein 70 Decreases with Cellular Senescencein Vitroand in Cells Derived from Young and Old Human Subjects. *Exp. Cell Res.* **241**, 404-413 (1998).
80. C. J. Huh *et al.*, Maintenance of age in human neurons generated by microRNA-based neuronal conversion of fibroblasts. *Elife* **5**, e18648 (2016).
81. B. G. Childs, M. Durik, D. J. Baker, J. M. Van Deursen, Cellular senescence in aging and age-related disease: from mechanisms to therapy. *Nat. Med.* **21**, 1424-1435 (2015).
82. M. Fumagalli, F. Rossiello, C. Mondello, F. d'Adda di Fagagna, Stable cellular senescence is associated with persistent DDR activation. *PLoS One* **9**, e110969 (2014).
83. H. H. Kampinga, S. Bergink, Heat shock proteins as potential targets for protective strategies in neurodegeneration. *Lancet Neurol.* **15**, 748-759 (2016).
84. T. Wang *et al.*, Pathogenic mutations in the valosin-containing protein/p97 (VCP) N-domain inhibit the SUMOylation of VCP and lead to impaired stress response. *J. Biol. Chem.* **291**, 14373-14384 (2016).
85. M. Weith *et al.*, Ubiquitin-independent disassembly by a p97 AAA-ATPase complex drives PP1 holoenzyme formation. *Mol. Cell* **72**, 766-777. e766 (2018).
86. N. Tolay, A. Buchberger, Role of the Ubiquitin System in Stress Granule Metabolism. *Int. J. Mol. Sci.* **23**, 3624 (2022).
87. J. van den Boom, H. Meyer, VCP/p97-mediated unfolding as a principle in protein homeostasis and signaling. *Mol. Cell* **69**, 182-194 (2018).
88. G. Yu *et al.*, Cryo-electron microscopy structures of VCP/p97 reveal a new mechanism of oligomerization regulation. *Iscience* **24**, 103310 (2021).
89. A. Turakhiya *et al.*, ZFAND1 recruits p97 and the 26S proteasome to promote the clearance of arsenite-induced stress granules. *Mol. Cell* **70**, 906-919. e907 (2018).
90. B. A. Maxwell *et al.*, Ubiquitination is essential for recovery of cellular activities after heat shock. *Science* **372**, eabc3593 (2021).

91. Y. Gwon *et al.*, Ubiquitination of G3BP1 mediates stress granule disassembly in a context-specific manner. *Science* **372**, eabf6548 (2021).
92. R. Higuchi-Sanabria, P. A. Frankino, J. W. Paul III, S. U. Tronnes, A. Dillin, A futile battle? Protein quality control and the stress of aging. *Dev. Cell* **44**, 139-163 (2018).
93. J. Labbadia, R. I. Morimoto, Proteostasis and longevity: when does aging really begin? *F1000Prime Rep.* **6**, (2014).
94. A. Bouchama, J. P. Knochel, Heat stroke. *N. Engl. J. Med.* **346**, 1978-1988 (2002).
95. B. Szczesny *et al.*, Time-dependent and organ-specific changes in mitochondrial function, mitochondrial DNA integrity, oxidative stress and mononuclear cell infiltration in a mouse model of burn injury. *PLoS One* **10**, e0143730 (2015).
96. Y. Launey, N. Nesseler, Y. Mallédant, P. Seguin, Clinical review: Fever in septic ICU patients-friend or foe? *Critical Care* **15**, 1-7 (2011).
97. A. Guihur *et al.*, Moderate fever cycles as a potential mechanism to protect the respiratory system in COVID-19 patients. *Front. Med.* **7**, 583 (2020).
98. H. H. Kampinga, Cell biological effects of hyperthermia alone or combined with radiation or drugs: a short introduction to newcomers in the field. *Int. J. Hyperthermia* **22**, 191-196 (2006).
99. V. Milani *et al.*, Combination of hyperthermia and bortezomib results in additive killing in mantle cell lymphoma cells. *Int. J. Hyperthermia* **25**, 262-272 (2009).
100. F. Chen, R. Rezavi, C.-C. Wang, L. E. Harrison, Proteasome inhibition potentiates the cytotoxic effects of hyperthermia in HT-29 colon cancer cells through inhibition of heat shock protein 27. *Oncology* **73**, 98-103 (2007).
101. H. Miki *et al.*, Effective impairment of myeloma cells and their progenitors by hyperthermia. *Oncotarget* **9**, 10307 (2018).
102. J. Anckar, L. Sistonen, in *Molecular Aspects of the Stress Response: Chaperones, Membranes and Networks*. (Springer, New York, 2007), vol. 594, pp. 78-88.

Acknowledgements
We thank Paolo D. L. Rios, Ph.D., and Joachim Berger, Ph.D., for scientific discussions and critical reading of the manuscript. Special acknowledgements go to Oleksandr Chernyavskiy, Ph.D. (Monash Micro Imaging Facility) and Tim E. Powers, Ph.D. (Monash eResearch Center) for assistance with microscopy and statistical analysis. Peck S. Tan, Ph.D., Sophie Kopetschke, and Jeanette F. Brunsting for experimental/technical support. Some figures were created with BioRender.com.

Funding
National Health and Medical Research Council of Australia Investigator Grant APP1197021 to NBN, APP1161803, and APP1154352 to DMH.
Recruitment Grant from Monash University Faculty of Medicine Nursing and Health Sciences with funding from the State Government of Victoria and the Australian Government to NBN.
Yulgilbar Foundation, Australia to NBN
Australian Research Council of Australia Grant DP170103093 to DMH.
Deutsche Forschungsgemeinschaft Project ID FOR2509 P05, Bundesministerium für Bildung und Forschung (BMBF), Ministerium für Kultur und Wissenschaft des Landes Nordrhein-Westfalen (MKW), Regierender Bürgermeister von Berlin to TR.
We thank Merck PTY LTD Australia for its concessional product pricing for the work.

Authors' contributions
Conceptualization: NBN

Methodology: YM, NA, DC, CJR, RS, KMA and NBN
Software development: SU and SA
Investigation: YM, NA, CJR, DC, NLP, ARO, RS, KMA, and NBN
Formal analysis: YM, NA, CJR, DC, RS, KMA, SU, TR, SA, DMH, HHK and NBN
Original draft writing: NBN
Editing: YM, NA, CJR, DC, RS, KMA, SU, TR, SA, DMH, HHK and NBN
Reviewing: YM, NA, DMH, HHK and NBN

Competing interests

The authors declare that they have no competing interests.

Figures

Figure 1. The DNAJA1+DNAJB1-Hsp70 chaperone machine forms the primary heat-induced disaggregase in human cells. (**A**) Diagram illustrating the function of protein disaggregation in cells. (**B**) All reactions containing mixed-class JDP scaffolds show increased protein disaggregation/refolding activity, *in vitro*. Top: Luciferase disaggregation/refolding assay. Heat denaturation triggers misfolding and aggregation of luciferase. Bottom: Disaggregation/refolding efficiencies by different JDP scaffolds containing Hsp70 disaggregases, *in vitro* (n = 3, data are mean + / - s.e.m., * adjusted p-value < 0.05, ** adjusted p-value < 0.01, one-way ANOVA Tukey post hoc test). Hsp110 functions as a NEF. (**C**) Top: Hsp70-JDP and JDP-JDP interactions during the assembly of Hsp70 disaggregase. Bottom: Tracking Hsp70 disaggregases in cells using *in situ* proximity ligation assay (PLA^{DT}). Captured protein-protein interactions generate fluorescent puncta (yellow) after signal amplification by rolling circle PCR. Fluorescently labeled oligonucleotides hybridize with an amplified DNA bundle to enhance the proximity signal. (**D**) Detection of multiple JDP^{A}-JDP^{B} scaffolds of Hsp70 disaggregase in unstressed (U) HeLa cells using PLA^{DT}. Upon heat shock (HS, red), cells show selective induction of the DNAJA1+DNAJB1 scaffold (PLA^{DT} fluorescent signal, yellow). Nuclei stained with DAPI (magenta). HS was performed at 43 ° C for 1h; Stress recovery at 37 ° C for 0h, 6h and 24h. Scale bar 20 µm (n = 3). Images are maximum intensity projections (all channels). (**E**) PLA^{DT}-based detection of DNAJA1+Hsp70 and DNAJB1+Hsp70 interactions during the formation of DNAJA1+DNAJB1-Hsp70 disaggregase. The Hsp70 antibody used in PLA^{DT} recognizes both constitutively expressed Hsc70 and the stress-induced Hsp70 paralog. Scale bar 20 µm (n = 3). (**F**) Quantification of PLA^{DT} signal from (D) and (E) (data are mean +/- s.e.m.). (**G**) HS-activated HSF-1 binds to consensus heat shock elements (HSE) in the promoter regions of the target genes (*102*). (**H**) Inhibition of DNAJA1 and DNAJB1 protein synthesis after HS through HSF-1 depletion blocks Hsp70 disaggregase assembly. Left: Immunoblots show HSF-1 knockdown by RNAi and inhibition of JDP synthesis after HS. GAPDH, loading control. Right: PLA^{DT} shows a decreased assembly of Hsp70 disaggregase in HSF-1-depleted cells. The non-targeting control siRNA (siScrambled) is used as the control for RNAi. Scale bar 20 µm (n = 3).

Figure 2. Solubilization of heat-induced protein aggregates requires induction of DNAJA1+DNAJB1-Hsp70 disaggregase. (**A**) Decoration of heat-induced aggregates by yeast $HSP104^{DWB}$-GFP. The Hsp70-JDP chaperone system facilitates the loading of $HSP104^{DWB}$-GFP onto the aggregate surface. (**B-D**) DNAJA1+DNAJB1-Hsp70 disaggregase drives the solubilization of heat induced aggregates. (**B**) Top: HS triggered the formation and solubilization of $Hsp104^{DWB}$-GFP positive aggregates (cyan; punctated fluorescent signal pointed by white arrows) in HeLa cells. U denotes unstressed cells. Heat shock (HS) in red. Scale bar 20 µm (n = 3). Bottom: Visualization of assembly and disassembly of Hsp70 disaggregase through the formation of the JDP scaffold (PLA^{DT}; yellow) in HeLa cells recovering from heat shock (HS).

Nuclei in magenta. Scale bar 20 µm (n = 3). (**C**) Inhibition of disaggregation/refolding of preformed luciferase aggregates by the Hsp70 inhibitor VER-155008, *in vitro* (n = 3, data are mean +/- s.e.m. ** adjusted p < 0.01, one-way ANOVA Tukey post hoc test). (**D**) As in (B), inhibition of Hsp70 disaggregase function with VER-155008 blocks the resolution of heat-induced aggregates in cells. The inhibitor was added to cells 5h after HS. Scale bar 20 µm (n = 3). DMSO in (B), vehicle control for VER-155008 in (D). (**E-H**) DNAJA1+DNAJB1 scaffold formation is required to efficiently target heat-induced aggregates. (**E**) The reaction containing mixed-class complex forming defective mutant DNAJB1^{RRR} (RRR denotes D4R+E69R+E70R) shows decreased disaggregation of heat-induced luciferase aggregates, *in vitro* (n = 3, data are mean +/- s.e.m. ** adjusted p-value < 0.01, one-way ANOVA Tukey post hoc test). (**F**) Immunoblot showing expression levels of wild-type DNAJB1-HA, DNAJB1^{RRR}-HA and Hsp70-binding defective DNAJB1^{QPN}-HA (H32Q+D34N) mutant in *DNAJB1* knocked out (KO) HEK 293 cells. (**G-J**) Defective assembly of DNAJA1+DNAJB1-Hsp70 disaggregase results in persistence of heat-induced aggregates in cells. As in (B), Visualization of (dis)assembly dynamics of DNAJA1+DNAJB1-Hsp70 disaggregase by PLA^{DT} (yellow) and solubilization of Hsp104^{DWB}-GFP positive heat-induced aggregates during HS recovery in *DNAJB1* KO HEK 293 cells ectopically expressing (**G**) empty vector (control), (**H**) wild-type DNAJB1-HA, (**I**) DNAJB1^{RRR}-HA, and (**J**) DNAJB1^{QPN}-HA. U denotes unstressed cells. Scale bar 20 µm (n = 3).

Figure 3. Aggregates distinct from stress granules are targeted by siDAP-induced disaggregase.
(**A-D**) Recovery of heat aggregated HNRNPK and AHCY (SAHH) requires the induction of Hsp70 disaggregase through siDAP. (**A**) Solubility profile of HNRNPK: Graphs show representative traces for ΔpSup in the presence of DMSO (left panel) or VER-155008 (center panel), and the corresponding ΔΔpSup (right panel) (n = 3). (**B**) As in (A), for AHCY (n = 3). (**C**) Hsp70-based disaggregation of heat aggregated HNRNPK in HeLa cells visualized using immunocytochemistry (HNRNPK, cyan; DAPI stained nuclei, magenta). siDAP induced Hsp70 disaggregase is inhibited with VER-155008 added 5h after HS. Cycloheximide (CHX) was added to inhibit protein synthesis at 5h after HS. White arrows indicate heat-aggregated HNRNPK. Aggregate solubilization is indicated by the disappearance of the punctated fluorescence signal and the appearance of a diffused signal. DMSO, vehicle control for VER-155008. Heat shock (HS) in red. U denotes unstressed cells. Scale bar 20 µm (n = 3). (**D**) As in (C), for AHCY (n = 3). (**E**) Disruption of JDP scaffold formation prevents solubilization of heat-aggregated HNRNPK. Left: Immunoblot showing JDP knockdown efficiencies in HeLa cells. Right: Persistence of heat aggregated HNRNPK in DNAJA1 and DNAJB1 depleted HeLa cells. The non-targeting control siRNA (siScrambled) is used as the control for RNAi. Scale bar 20 µm (n = 3). (**F**) Stress-induced Hsp70 disaggregase targets different aggregate types in cells. Top: Hsp70-depended solubilization of HNRNPK aggregates (cyan) *vs* TIA-1-GFP containing SGs (yellow) in HeLa cells recovering from heat stress. The addition of VER-155008 at 0h after HS blocks resolution of HNRNPK aggregates, but not TIA-1 SGs. The inset depicts zoomed-out cells. Scale bar 20 µm. Below: Quantification of TIA-1 SGs and HNRNPK aggregates (n = 3, data are mean +/- s.e.m. * adjusted p-value < 0.05, one-way ANOVA LSD post hoc test).

Figure 4. A dual disaggregase system operates in cells recovering from heat stress. (**A**) The disaggregase activity exerted by VCP facilitates rapid resolution of heat-induced ubiquitin (Ub) positive protein aggregates. 1% NP-40 insoluble aggregates were isolated at indicated time points during heat stress recovery using a two-phase fractionation approach and probed with antibody against ubiquitin (n = 3). Immunoblots show depletion of VCP delays the disaggregation and clearance of Ub-positive protein aggregates in HeLa cells. VCP protein levels show knockdown

efficiency. GAPDH, loading control. (**B**) Blocking VCP disaggregase activity with inhibitor NMS-873 (1 μM. low dosage) after 5h post-HS does not inhibit the resolution of Hsp104^{DWB}-GFP positive aggregates by Hsp70 disaggregase. On the contrary, the addition of NMS-873 at 0h post-HS results in a phenotype similar to the depletion of VCP. DMSO, vehicle control for the inhibitor (n = 2). Nuclei stained with DAPI (magenta). (**C**) Disassembly of Hsp70 disaggregase is delayed in HeLa cells treated with NMS-873 at 0h post-HS, but not at 5h post-HS (PLA^{DT} signal, yellow). Nuclei stained with DAPI (magenta). Heat shock (HS) in red. U denotes unstressed cells. Scale bar 20 μm (n = 2).

Figure 5. siDAP exerts a tailor-made response to gain thermoresistance in human cells. (**A**) Top: Simplified scheme of Ultra-Glo rLuciferase-based cytotoxicity assay. Leaked LDH is detected as a readout for damaged or dying cells. Bottom: Disruption of siDAP activity decreases cell fitness after HS. Cytotoxicity level in unstressed (blue) and HS recovering HeLa cells (red) with and without VER-155008 treatment. DMSO, vehicle control for the inhibitor. Error bars depicted as s.e.m. (n = 3). (**B**) Top: Cells tune the activation of siDAP according to the level of protein damage sustained after HS. Heat stress at 39 ˚C *vs* 42 ˚C for 2h mimics mild-moderate and high fever, respectively. The nuclei stained with DAPI (magenta). Scale bar 20 μm (n = 3). Bottom: Quantification of PLA^{DT} signals (data are mean +/- s.e.m.).

Figure 6. Collapse of siDAP during replicative cellular aging. (**A**) Chronological age has no effect on siDAP activation in human cells. Top: The PLA^{DT} signal (yellow) shows the induction of DNAJA1+DNAJB1-Hsp70 disaggregase in heat-stressed primary human dermal fibroblasts derived from 21-year-old (21-y), 55-y and 75-y human subjects. Nuclei stained with DAPI (magenta). U denotes unstressed cells. Heat shock (HS) in red. Scale bar 20 μm (n = 3). Bottom: Analysis of the induction of disaggregase machine components using immunoblotting. **(B)** Experimental scheme showing replicative aging of human dermal fibroblasts. P denotes cell passage. (**C**) Cells at P = 12 and 18 show a considerable increase in the marker of senescence. Cellular senescence correlates to increased levels of senescence specific β-galactosidase activity in replicating fibroblasts. (**D**) siDAP-induced assembly of Hsp70 disaggregase collapses in cells undergoing replicative aging. Top: level of induction of Hsp70 disaggregase after HS in human dermal fibroblasts at P = 6, 12 and 18 using PLA^{DT}. Scale bar 20 μm (n = 3). Bottom: Immunoblot analysis of the induction of components of the disaggregase machine after HS (n = 3). (**E**) Cells defective in activating siDAP due to aging (replicative) show reduced cellular fitness after HS. Level of cytotoxicity measured with Ultra-Glo rLuciferase-based cytotoxicity assay in unstressed (blue) and HS recovering (red) human dermal fibroblasts at P 6 and P 12. P 12 cells have lost the ability to activate siDAP. Error bars depicted as s.e.m. (n = 3). (**F**) Human dermal fibroblasts at P 12 lose the ability to solubilize Htt46Q-GFP aggregates (cyan) by activating siDAP. Note the cell morphological changes as a result of replicative aging and HS. Scale bar 20 μm (n = 3).

Figure 7. A two-phased model for protein aggregate solubilization in proteotoxic stress recovering cells. Two primary disaggregases based on VCP and Hsp70 operate in temporally separated aggregate/SG resolving phases in human cells. Phase 1 is predominated by the activity of the VCP disaggregase, which facilitates the disassembly of the Ub+ aggregates and SGs to rapidly decrease the overall load of cellular aggregates. Phase 2 of aggregate solubilization is initiated by activation of siDAP, which induces massive assembly of DNAJA1+DNAJB1-Hsp70 disaggregase to effectively "mop up" relatively denser cytotoxic aggregates that escape phase 1 clearance. The HSF-1 mediated heat shock response facilitates the synthesis of disaggregase machine components, and plays a crucial role in regulating the activation of siDAP in phase 2. siDAP boosts the selective assembly of the DNAJA1+DNAJB1 scaffold to recruit Hsp70 during

disaggregase formation. Once the disaggregase is formed, pulling forces (black arrows) are generated to disassemble the aggregates. This mechanism is distinct from VCP, which exists as a dodecamer, and extracts trapped polypeptides using an Hsp104-like mechanism. The disaggregated non-native proteins can be repaired or degraded to support cell viability and recovery. The selective assembly of the DNAJA1+DNAJB1 scaffold is disrupted in cells undergoing replicative aging, which triggers aggregate persistence and reduced cellular fitness.

Figure S1. Assembly of Hsp70 disaggregase monitored by PLA^{DT} after heat shock. (**A**) Left: Domain architectures of class A (green) and class B (blue) JDPs (depicted as monomers). JD, J-domain; CTD, C-terminal domain; ZFLR, Zink finger like region; DD, dimerization domain. HPD (His-Pro-Asp) motif vital for binding and inducing ATP hydrolysis in Hsp70. Right: Mixed-class JDP^{A}-JDP^{B} complexation is driven by intermolecular interactions between JD and CTD (*13*). (**B**) Technical controls of PLA^{DT} for antibody specificity. PLA^{DT} was performed in HeLa cells with single primary antibodies only. Signal amplification (yellow) was not observed in any of the controls. DAPI (magenta) staining indicates nuclei. Scale bar 20 µm (n = 2). (**C**) Immunoblot (IB) showing RNAi knockdown efficiencies for DNAJA1, DNAJA2, DNAJB1, DNAJB4 in HeLa cells. GAPDH, loading control. (**D**) RNAi knockdown-based controls of PLA^{DT} for antibody and complexation specificity. RNAi knockdown of single JDPs decreased JDP^{A}-JDP^{B} and JDP$^{A/B}$-Hsp70 complex formation (yellow puncta) in HeLa cells. The non-targeting control siRNA (siScrambled) is used as the control for RNAi. Scale bar 10 µm (n = 2). (**E**) Top: The graphs show the temperature changes observed in two HS regimes (at 42 ˚C 2h in an incubator *vs.* 43 ˚C 1h in a water bath) used in the study. Bottom: Induction of the DNAJA1+DNAJB1 scaffold (PLA^{DT} signal, yellow) after applying the two HS regimes to HeLa cells. Nuclei stained with DAPI (magenta). HS indicated in red. Unstressed cells indicated as U. Scale bar 20 µm (n = 3). (**F**) Formation of intraclass JDP scaffolds between DNAJA1 and DNAJA2 and DNAJB1 and DNAJB4 in HeLa cells during HS recovery. (**G**) Immunoblots showing changes in steady-state protein levels of DNAJA1, DNAJA2, DNAJB1, DNAJB4 and Hsp70 after HS in HeLa cells.

Figure S2. PLA^{DT} signals capture direct interactions between disaggregase machine components during assembly. (**A**) DNAJB1^{RRR} can support chaperoning function(s) in nucleoli similar to wild-type DNAJB1. The immunocytochemical signal from the HA tag (yellow) shows that both DNAJB1-HA and the JDP scaffold forming defective mutant DNAJB1^{RRR}-HA rapidly localize into the nucleoli of HeLa cells immediately after heat shock (HS), and relocate out of the nucleoli before 6h post-HS. RRR denotes the D4R + E69R + E70R mutations in DNAJB1. Unstressed cells are denoted as U. Nuclei stained with DAPI (magenta). The nucleoli are unstained by DAPI and appear as dark spots in the nucleus. Line scans across the nucleoli are indicated in white. Corresponding line scan plots are shown on the right. **(B)** The PLA^{DT} signal captures the direct interaction between DNAJA1 and DNAJB1 during the formation of the JDP scaffold. A decreased PLA^{DT} signal (yellow) is observed for the interaction between the JDP scaffold forming defective mutant DNAJB1^{RRR}-HA and endogenous DNAJA1 or DNAJA2. Nuclei stained with DAPI (magenta). Scale bar 20 µm (n = 2). Immunoblot shows expression levels of mutant and wild type DNAJB1. (**C**) As in (B), a similar decrease in the PLA^{DT} signal is observed for the interaction between Hsp70 binding defective mutant V5-DNAJB1^{H32Q} and endogenous Hsp70. Scale bar 20 µm (n = 2). Immunoblot shows expression levels of mutant and wild type DNAJB1. **(D)** As in (B), depleting either DNAJA1 or DNAJB1 via RNAi does not result in unpaired JDPs forming alternative scaffolds with DNAJA2 or DNAJB4. Left: Levels of DNAJA1+DNAJB1 and DNAJA2+DNAJB1 scaffolds in DNAJA1 depleted HeLa cells. Right: Levels of DNAJA1+DNAJB1 and DNAJA1+DNAJB4 scaffolds in DNAJB1 depleted HeLa cells. The non-

targeting control siRNA (siScrambled) is used as the control for RNAi. Scale bar 20 µm (n = 3). Corresponding immunoblots show JDP knockdown efficiencies. GAPDH, loading control.

Figure S3. DNAJA1, DNAJB1, and Hsp70 localize to nucleoli immediately after heat shock. (**A**) DNAJA1 rapidly localizes into nucleoli immediately after heat shock (HS, red), and relocates out of nucleoli before 6h post-HS. Subcellular location of DNAJA1 in unstressed (U) and heat shocked (HS) HeLa cells monitored by immunocytochemistry (yellow). Nuclei stained with DAPI (magenta). The nucleoli are unstained by DAPI and appear as dark spots in the nucleus. Line scans across the nucleoli are indicated in white. Corresponding line scan plots are shown on the right. Scale bar 10 µm (n = 3). (**B**-**E**), As in (A), (**B**) DNAJA2, (**C**) DNAJB1, (**D**) DNAJB4 and (**E**) Hsp70. DNAJB1 and Hsp70, but not DNAJA2 and DNAJB4, show nucleoli localization dynamics similar to DNAJA1.

Figure S4. Pre-HS synthesized DNAJA1 and DNAJB1 shuttle to nucleoli immediately after heat stress. (**A**) The DNAJA1 molecules rapidly localize into nucleoli immediately after heat shock (HS, red), and relocate out of the nucleoli before 6h post-HS. DMSO added at 0h post-HS as vehicle control. Subcellular location of DNAJA1 in unstressed (U) and heat shocked (HS) HeLa cells monitored by immunocytochemistry (yellow). Nuclei stained with DAPI (magenta). The nucleoli are unstained by DAPI and appear as dark spots in the nucleus. Line scans across the nucleoli are indicated in white. Corresponding line scan plots are shown on the right. Scale bar 10 µm (n = 3). (**B**), As in (A), except cycloheximide (CHX) was added to inhibit protein synthesis 0h after HS. The DNAJA1 molecules synthesized before heat stress show similar dynamics in terms of nucleolar entry and exiting. Scale bar 10 µm (n = 3). (**C**), As in (A), DNAJB1 molecules rapidly locate into nucleoli immediately after HS, and relocate out of nucleoli before 6h post-HS. Scale bar 10 µm (n = 3). (**D**), As in (C), CHX was added at 0h post-HS. DNAJB1 molecules synthesized before HS showed similar dynamics in terms of nucleolar shuttling. Scale bar 10 µm (n = 3).

Figure S5. DNAJA1 and DNAJB1 molecules synthesized before HS are not involved in Hsp70 disaggregase formation. Left: Cycloheximide (CHX) is added to HeLa cells to block the induction of DNAJA1 and DNAJB1 at specific time points during recovery from heat stress. DNAJA1 and DNAJB1 induction after heat stress is shown by immunoblotting. GAPDH, loading control. DMSO, vehicle control for CHX (n = 2). Right: The newly synthesized DNAJA1 and DNAJB1 molecules are used to assemble the DNAJA1+DNAJB1 scaffold of Hsp70 disaggregase after heat shock (HS, red). The addition of CHX at 0h after HS, which blocks the synthesis of new DNAJA1 and DNAJB1 molecules, completely blocks the assembly of the JDP scaffold (PLA^{DT} signal, yellow). Treatment of cells with CHX at 2.5h post-HS does not prevent the synthesis of new DNAJA1 and DNAJB1 molecules, and assembly of the JDP scaffold. Nuclei stained with DAPI (magenta). DMSO, vehicle control for CHX. Scale bar 20 µm (n = 3).

Figure S6. Transcription and translation of DNAJA1+DNAJB1-Hsp70 disaggregase machine components after heat shock. (**A**) Induction of DNAJA1 and DNAJB1 mRNA measured by qRT-PCR ($\log_2$ fold (-ΔCt; relative to GAPDH mRNA) in HeLa cells recovering from HS. s.e.m. calculated from ΔCt value per experiment. Error bars reflect mean +/- s.e.m. (n = 3). (**B**) HS triggered increase in DNAJA1 and DNAJB1 protein levels in recovering HeLa cells measured through multiple reaction monitoring (MRM) mass spectrometry (normalized to tubulin alpha-1A and unstressed JDP levels). Error bars reflect fold change +/- s.e. of regression (n = 4).

Figure S7. The localization of DNAJA1 and DNAJB1 into nucleoli immediately after heat shock occurs independent of the heat shock response. (**A**) Inactivation of the heat shock

response through depletion of the HSF-1 transcription factor in HeLa cells. Cellular HSF-1 levels after RNAi knockdown are shown by immunoblot. GAPDH, loading control. The non-targeting control siRNA (siScrambled) is used as the control for RNAi. (**B**) In HSF-1 depleted Hela cells, DNAJA1 molecules synthesized prior to heat stress rapidly localize into nucleoli immediately after heat shock (HS, red), and relocate out of nucleoli before 6h post-HS. Subcellular localization of DNAJA1 in unstressed (U) and heat shocked (HS) HeLa cells monitored by immunocytochemistry (yellow). Nuclei stained with DAPI (magenta). The nucleoli are unstained by DAPI and appear as dark spots in the nucleus. Line scans across the nucleoli are indicated in white. Corresponding line scan plots are shown on the right. Scale bar 10 µm (n = 3). (**C**), As in (B), DNAJB1 molecules synthesized prior to HS rapidly locate into nucleoli immediately after HS, and relocates out of nucleoli before 6h post-HS in HSF-1 depleted HeLa cells. Scale bar 10 µm (n = 3).

Figure S8. Hsp110-type nucleotide exchange factors (NEF) modulate the disassembly of DNAJA1+DNAJB1-Hsp70 disaggregase. The Hsp110 chaperone family of NEFs functions redundantly to facilitate the dissociation of ADP from Hsp70 and stimulate the disaggregation activity. (**A**) Mini RNAi screen targeting NEFs from Hsp110 (HSPH1, HSPH2, and HSPH3), Bag (BAG-1), and HSPB1 (HSPB-1) families in HeLa cells. Single NEF depletions do not affect the assembly or disassembly of DNAJA1+DNAJB1-Hsp70 disaggregase (PLA^{DT} signal, yellow) during heat stress recovery (HS, red). Triple knockdown of the Hsp110s, which removes functional redundancy, results in delayed disassembly of the Hsp70 disaggregase. The non-targeting control siRNA (siScrambled) and depletion of HSF-1 are used as controls for RNAi. Nuclei stained with DAPI (magenta). Scale bar 20 µm (n = 3). (**B**) Quantification of the PLA^{DT} signals from (A). Data are mean +/- s.e.m.

Figure S9. Disaggregation of heat-induced $Hsp104^{DWB}$-GFP positive aggregates requires an intact heat shock response and Hsp70 disaggregase activity. (**A**) Disruption of the heat shock response by depleting HSF-1 blocks solubilization of heat-induced $Hsp104^{DWB}$-GFP (cyan) positive aggregates in recovering HeLa cells. Aggregated proteins are visualized as punctated fluorescence signals and indicated by white arrows. Nuclei stained with DAPI (magenta). Line scans across the nucleoli are indicated in white. Corresponding line scan plots are shown on the right. Scale bar 10 µm (n = 3). (**B**) Inhibition of Hsp70 disaggregase function with VER-155008 blocks resolution of heat-induced aggregates in cells. The inhibitor was added to cells 5h after HS. Scale bar 10 µm (n = 3). DMSO, vehicle control for VER-155008. (**C**) Quantification of $Hsp104^{DWB}$-GFP positive aggregate levels in HeLa cells during HS recovery. Data are mean +/- s.e.m.

Figure S10. Disaggregation of heat-induced aggregates re-initiates after washing off VER-155008. (**A**) VER-155008 wash-off experimental setup. (**B**) Washing off VER-155008 by cell culture medium change at 12h post-HS results in the resumption of $Hsp104^{DWB}$-GFP (cyan) positive aggregate solubilization by Hsp70 disaggregase in HeLa cells recovering from heat stress. VER-155008 was added to cells at 5h post-HS. DMSO, vehicle control for VER-155008. Nuclei stained with DAPI (magenta). Aggregates are indicated by white arrows. Scale bar 20 µm (n = 3). (**C**) The assembled DNAJA1+DNAJB1 scaffolds (PLA^{DT} signal, yellow) support the resumption of protein disaggregation after washing off the Hsp70 inhibitor. VER-155008 washed off HeLa cells show efficient disassembly of the disaggregase at 24h after HS compared to control with the inhibitor. DMSO, vehicle control for VER-155008. Nuclei stained with DAPI (magenta). Scale bar 20 µm. (n = 3).

Figure S11. Cooperation between DNAJB1 and DNAJA1 is crucial for efficient Hsp70

disaggregase function in cells. (**A**) Top: Visualization of the (dis)assembly dynamics of DNAJA1+DNAJB1-Hsp70 disaggregase (PLA^{DT} signal, yellow) in HEK 293 cells recovering from heat shock (HS, red). Below: Solubilization of heat-induced $Hsp104^{DWB}$-GFP (cyan) positive aggregates in HEK 293 cells recovering from heat stress. The nuclei stained with DAPI (magenta). Aggregated proteins are indicated by white arrows. Heat shock (HS) in red. Scale bar 20 µm (n = 3). (**B**) Quantification of cells with heat-induced $Hsp104^{DWB}$-GFP positive aggregates in wild-type *vs DNAJB1* KO HEK 293 cells expressing DNAJB1, $DNAJB1^{RRR}$ and $DNAJB1^{QPN}$ tagged with HA. (**C**) The role of DNAJB1 in Hsp70-mediated disaggregase function cannot be substituted for by other class A and B JDPs in stress recovering cells. Left: Overexpression levels of DNAJA1, DNAJA2, DNAJB1 and DNAJB4 tagged with V5 in *DNAJB1* KO HEK 293 cells visualized by immunoblotting. Right: Resolution of heat-induced $Hsp104^{DWB}$-GFP positive aggregates (cyan) in *DNAJB1* KO cells ectopically expressing V5-tagged DNAJA1, DNAJA2, DNAJB1 or DNAJB4. Nuclei stained with DAPI (magenta). Aggregated proteins are indicated by white arrows. Scale bar 20 µm (n = 3). (**D**) Rapid assembly of DNAJA1+DNAJB1-Hsp70 disaggregase in heat shocked *DNAJB1* KO HEK 293 cells overexpressing DNAJB1 *vs* wild-type HEK 293 cells (PLA^{DT}, yellow). Nuclei stained with DAPI (magenta). Scale bar 20 µm (n = 3).

Figure S12. Identification of aggregated proteins recovered by siDAP. (**A**) Schematic representation of the proteomics workflow used to identify aggregated proteins rescued by siDAP. The fractions were distinguished by isobaric labeling and proteins that regained solubility between 6-12h in DMSO, but not in cells treated with VER-155008 were identified and quantified by LC-MS/MS. (**B**) Ridge plot showing the distribution of solubility (pSup) for all proteins during post-HS recovery. (**C**) Proteins for which the change in relative solubility due to the VER-155008 treatment (ΔΔpSup) exceeding 0.26 in at least one time point were clustered via k-means into four patterns. Mean ΔΔpSup for all proteins in each cluster is shown, where colored bands represent ± s.d. (n = 4). (**D**) Visualization of Hsp70-based disaggregation of heat aggregated HNRNPK in HeLa cells by immunocytochemistry (HNRNPK, cyan; DAPI stained nuclei, magenta). siDAP-induced Hsp70 disaggregase was inhibited with VER-155008 +/- cycloheximide (CHX) at 5h after HS. CHX inhibits protein synthesis. The white arrows indicate HNRNPK aggregated with heat. Aggregate solubilization is indicated by the disappearance of the punctated fluorescence signal and the appearance of a diffused signal. DMSO, vehicle control for VER-155008. Heat shock (HS) in red. U denotes unstressed cells. Scale bar 20 µm (n = 3).

Figure S13. Clearance of heat-induced aggregates requires cooperation with UPS. (**A**) The resolution of heat-induced $Hsp104^{DWB}$-GFP (cyan) positive aggregates by DNAJA1+DNAJB1-Hsp70 disaggregase is delayed in HeLa cells treated with the 26S proteasome inhibitor bortezomib. Bortezomib is added to cells at 5h post-HS. DMSO, vehicle control for bortezomib. Aggregated proteins are indicated by white arrows. Nuclei stained with DAPI (magenta). Scale bar 20 µm (n = 3). (**B**) Disassembly of the DNAJA1+DNAJB1-Hsp70 disaggregase (PLA^{DT} signal, yellow) is delayed in HeLa cells after proteasome inhibition by bortezomib, indicating that efficient protein disaggregation requires cooperation with the UPS. Bortezomib is added to cells at 5h post-HS. DMSO, vehicle control for bortezomib. Nuclei stained with DAPI (magenta). Scale bar 20 µm (n = 3).

Figure S14. The resolution of TIA-1 containing stress granules occurs independent of the heat shock response. Inactivation of the heat shock response through depletion of HSF-1 does not affect the disassembly of TIA-1-GFP containing SGs (yellow). In contrast, activation of the stress signaling pathway is required to solubilize heat-induced HNRNPK aggregates (cyan). HSF-1 depletion results in inhibition of the disaggregation of HNRNPK aggregates in HeLa cells. The

inset depicts zoomed out cells. The non-targeting control siRNA (siScrambled) is used as the control for RNAi. Nuclei stained with DAPI (magenta). Scale bar 20 µm. Scale bar 20 µm. Below: Quantification of TIA-1 SGs and HNRNPK aggregates (n = 3, data are mean +/- s.e.m. * adjusted p-value < 0.05, ** adjusted p-value < 0.01, ns - not significant, one-way ANOVA LSD post hoc test).

Figure S15. TIA-1 containing stress granules disassembly is not affected in cells depleted of class A and B JDPs. Depletion of DNAJA1, DNAJA2, DNAJB1, and DNAJB4 via RNAi has no effect on the resolution of TIA-1 SGs (yellow) in heat stress recovering HeLa cells. Solubilization of heat-induced HNRNPK aggregates (cyan) requires DNAJA1 and DNAJB1. DNAJA1 and DNAJB1, but not DNAJA2 and DNAJB4 knockdown results in inhibition of HNRNPK aggregate solubilization. The inset depicts zoomed out cells. The non-targeting control siRNA (siScrambled) is used as the control for RNAi (same from Figure S14). Nuclei stained with DAPI (magenta). Scale bar 20 µm. Below: Quantification of TIA-1 SGs and HNRNPK aggregates (n = 3, data are mean +/- s.e.m. * adjusted p-value < 0.05, ** adjusted p-value < 0.01, ns - not significant, one-way ANOVA LSD post hoc test).

Figure S16. Characterization of HNRNPK aggregates formed after heat shock. Fluorescence recovery after photobleaching (FRAP) analysis of heat-induced HNRNPK-containing aggregates shows poor recovery of the fluorescent signal after photobleaching. GFP-HNRNPK was transiently expressed in HeLa cells, and FRAP was performed after heat shock. The fluorescence signal of the selected inclusions was reduced to ~50% by photobleaching with the 488-nm laser (photobleached area indicated by the white squire), and its recovery was recorded for 40 seconds. Selected images of a cell containing GFP-HNRNPK positive aggregates (green) before photobleaching and at indicated intervals after photobleaching are shown. The white arrows indicate GFP-HNRNPK aggregates. Scale bar 2 µm (n = 7).

Figure S17. siDAP-mediated protein disaggregation relies on upstream VCP activity. (**A**) Detection of heat-induced ubiquitin (Ub) positive protein aggregates. 1% NP-40 insoluble aggregates were isolated at indicated time points during heat stress recovery using a two-phase fractionation approach and probed with antibody against ubiquitin (n = 3). Immunoblots show the clearance of Ub-positive protein aggregates in HeLa cells before 6h post-HS. GAPDH, loading control. (**B**) Top: Solubilization of heat-induced HNRNPK aggregates (cyan) and TIA-1-GFP containing SGs (yellow) are affected in VCP depleted HeLa cells. The inset depicts zoomed-out cells. The non-targeting control siRNA (siScrambled) is used as the control for RNAi (same from Figure S14). Nuclei stained with DAPI (magenta). Scale bar 20 µm. Below: Quantification of TIA-1 SGs and HNRNPK aggregates (n = 3, data are mean +/- s.e.m. * adjusted p-value < 0.05, ** adjusted p-value < 0.01, ns - not significant, one-way ANOVA LSD post hoc test). (**C**) Resolution of heat-induced Hsp104^{DWB}-GFP positive aggregates (cyan; punctated fluorescent signal pointed by white arrows) is blocked in VCP-depleted HeLa cells. Scale bar 20 µm (n = 3). Nuclei stained with DAPI (magenta). Heat shock (HS) in red. U denotes unstressed cells.

Figure S18. Resolution of Hsp104^{DWB}-GFP positive aggregates in VCP inhibited cells. (**A**) Heat-induced Hsp104^{DWB}-GFP positive aggregates do not have a ubiquitin signal. Colocalization of the immunofluorescence signal from ubiquitin (Ub, yellow) and the fluorescence signal from Hsp104^{DWB}-GFP (cyan) in HeLa cells recovering from heat shock (HS) (6h post-HS). Nuclei stained with DAPI (magenta). Line scans are indicated in white. Corresponding line scan plots are shown on the right. Scale bar 10 µm (n = 3). (**B**) Disassembly of Hsp70 disaggregase is delayed in VCP knocked down HeLa cells (PLA^{DT} signal, yellow). The non-targeting control siRNA

(siScrambled) and depletion of HSF-1 are used as controls for RNAi. Nuclei stained with DAPI (magenta). Heat shock (HS) in red. U denotes unstressed cells. Scale bar 20 µm (n = 3). (**C**) Blocking VCP disaggregase activity with inhibitor NMS-873 (10 µM. high dosage) after 5h post-HS does not inhibit the resolution of Hsp104^{DWB}-GFP positive aggregates by Hsp70 disaggregase. On the contrary, the addition of NMS-873 at 0h post-HS results in a phenotype similar to the depletion of VCP. DMSO, vehicle control for the inhibitor (n = 3). Nuclei stained with DAPI (magenta).

Figure S19. Depletion of DAXX disrupts the assembly of Hsp70 disaggregase. (**A**) Top: The solubilization of heat-induced HNRNPK aggregates (cyan), but not TIA-1-GFP containing SGs (yellow), is affected in HeLa cells depleted of DAXX (via RNAi). The inset depicts zoomed-out cells. Nuclei stained with DAPI (magenta). The non-targeting control siRNA (siScrambled) is used as the control for RNAi (same from Figure S14). Scale bar 20 µm. Below: Quantification of TIA-1 SGs and HNRNPK aggregates (n = 3, data are mean +/- s.e.m. * adjusted p-value < 0.05, ns – not significant, one-way ANOVA LSD post hoc test). (**B**) The disassembly of DNAJA1+DNAJB1 scaffold of the Hsp70 disaggregase (PLA^{DT} signal, yellow) is delayed in DAXX knocked down HeLa cells recovering from heat stress. The non-targeting control siRNA (siScrambled) and depletion of HSF-1 are used as controls for RNAi. Nuclei stained with DAPI (magenta). Scale bar 20 µm (n = 3). (**C**) Immunoblot analysis shows that heat induction of Hsp70 is decreased in DAXX depleted HeLa cells (n = 3). (**D**) Hsp70 assembly with DNAJA1 and DNAJB1 is reduced in DAXX knocked down HeLa cells (PLA^{DT} signal, yellow). Nuclei stained with DAPI (magenta). Scale bar 20 µm (n = 3).

Figure S20. Cells overexpressing VCP and DAXX still require activation of Hsp70 disaggregase during heat stress recovery. The assembly and disassembly dynamics of Hsp70 disaggregase is not affected in HeLa cells overexpressing VCP and DAXX (PLA^{DT} signal, yellow; VCP-EGFP and EmGFP-DAXX signals, cyan). Nuclei stained with DAPI (magenta). Scale bar 20 µm (n = 3).

Figure S21. siDAP and cellular fitness. (**A**) Assembly of DNAJA1+DNAJB1-Hsp70 disaggregase (PLA^{DT}, yellow) in cells treated with VER-155008 at 2.5h after HS. Control, cells without HS. DMSO, vehicle control for VER-155008. The nuclei stained with DAPI (magenta). Scale bar 20 µm (n = 3). (**B**) Right: Hsp104-Hsp70 bichaperone disaggregation system. Direct interaction between Hsp104 and Hsp70 is required to a) recruit Hsp104 to aggregates and b) trigger ATP hydrolysis in the AAA+ ATPase to facilitate polypeptide unfolding and threading. After translocation, the unfolded polypeptide is released from Hsp104. The released polypeptide may spontaneously or with the help of cellular chaperones can either refold or degrade. Left: Hsp104-Hsp70 bichaperone disaggregase is more effective in solubilizing preformed luciferase aggregates compared to Hsp70 disaggregase, *in vitro* (n = 3, data are mean +/- s.e.m., **** adjusted p value < 0.0001, one-way ANOVA with Tukey post hoc test). Hsp110 functions as NEF. (**C**) Rapid solubilization of heat-induced HNRNPK aggregates (cyan, indicated by white arrows) in HeLa cells overexpressing Hsp104-GFP (yellow). GFP-only control (yellow). Nuclei stained with DAPI (magenta). Heat shock (HS) in red. Scale bar = 20 µm (n = 3). (**D**) The assembly of DNAJA1+DNAJB1-Hsp70 disaggregase (PLA^{DT} signal, yellow) is reduced in HeLa cells that overexpress wild-type Hsp104-GFP (cyan) compared to the GFP control. Nuclei stained with DAPI (magenta). Heat shock (HS) in red. Scale bar = 20 µm (n = 3). Immunoblots show the induction of DNAJA1 and DNAJB1 after HS. GAPDH, loading control.

Figure S22. siDAP activation is not affected in dermal fibroblasts obtained from young *vs*

old humans. (A) The PLA^{DT} signal (yellow) does not show any difference in the induction of the DNAJA1+DNAJB1-Hsp70 disaggregase in heat shocked primary human dermal fibroblasts derived from humans of different chronological ages (21 years of age (21y), 26y, 55y, 58y, 70y, and 75y). Cells are at P 3. Nuclei stained with DAPI (magenta). U denotes unstressed cells. Heat shock (HS) in red. Scale bar 20 µm (n = 3). (**B**) As in (A). Cells are at P 6. Scale bar 20 µm (n = 3). (**C**) The assembly dynamics of JDP scaffolds formed between members of class A (DNAJA1 and DNAJA2) and class B (DNAJB1 and DNAJB4) (PLA^{DT} signal, yellow) in human dermal fibroblasts after HS. Nuclei stained with DAPI (magenta). Scale bar 20 µm. (n = 3). P denotes the cell passage. (**D**) Human dermal fibroblasts undergoing replicative aging show increased senescence-specific β-galactosidase levels. Detection of senescence-specific β-galactosidase levels in P 6, P 12 and P 18 human dermal fibroblasts derived from 21-year-old (21y) human. DIC images show cells at P 12 and P 18 stained positive for senescence-specific β-galactosidase (white arrows). Scale bar 20 µm. (n = 4). (**E**) Quantification of senescence-specific β-galactosidase positive cells at P 6, P 12 and P 18. P denotes the cell passage. Data are mean +/- s.e.m. **** adjusted p-value < 0.0001, one-way ANOVA Tukey post hoc test).

Figure S23. Persistence of heat-induced aggregates in aged human dermal fibroblasts. (**A**) Regardless of chronological age, nonsenescent P 6 cells can efficiently solubilize heat-induced protein aggregates during recovery. Levels of $Hsp104^{DWB}$-GFP positive aggregates (cyan) in unstressed and heat-shocked P 6 dermal fibroblasts derived from 21- and 75-year-old humans. Nuclei stained with Hoechst (magenta). White arrows show aggregates. U denotes unstressed cells. Heat shock (HS) in red. Scale bar 20 µm (n = 3). ROIs depict magnified cells. (**B**) Human dermal fibroblasts undergoing replicative aging (P 12) show defects in solubilizing heat-induced protein aggregates during recovery. Note that even unstressed cells (U) show $Hsp104^{DWB}$-GFP positive aggregates. As in (A), $Hsp104^{DWB}$-GFP positive aggregates (cyan) in unstressed and heat-shocked P 12 human dermal fibroblasts (21y and 75y). Nuclei stained with Hoechst (magenta). White arrows show aggregates. Scale bar 20 µm (n = 3). ROIs depict magnified cells. P denotes the cell passage.

Figure S24. siDAP and disassembly of disease-linked amyloids. (**A**) Disassembly of polyQ amyloids by disaggregation. (**B**) Amyloid aggregates formed by HttQ46-GFP can be solubilized by inducing siDAP. Top: The PLA^{DT} signal (yellow) shows the induction of DNAJA1+DNAJB1-Hsp70 disaggregase in HeLa cells. Bottom: Solubilization of amyloids formed by HttQ-GFP variants with different lengths of glutamine stretches (HttQ23-GFP, HttQ46-GFP and HttQ119-GFP) after induction of siDAP. HttQ23-GFP, a control that does not aggregate. Punctated GFP fluorescence (cyan) indicates aggregated polyQ (white arrows). Non-aggregating or solubilized polyQ generates a diffused fluorescence signal. Nuclei stained with DAPI (magenta). Heat shock (HS) in red. (**C**) As in (B), inhibition of siDAP-induced Hsp70 disaggregase activity 5h after heat shock (HS) by adding VER-155008 blocks HttQ46-GFP amyloid disassembly. DMSO, vehicle control for the inhibitor. Cells were treated with cycloheximide (CHX) at 5h after HS to block the translation of new HttpolyQ proteins. U denotes unstressed cells. Scale bar 20 µm (n = 3). (**D**) Depletion of DNAJA1 or DNAJB1 inhibits siDAP-mediated polyQ disassembly. Top: The disassembly of HttQ46-GFP aggregates is inhibited in DNAJA1 and DNAJB1 depleted HeLa cells. Punctated GFP fluorescence (cyan) indicates aggregated HttQ46-GFP (white arrows). The solubilized HttQ46-GFP generates a diffused fluorescence signal. The non-targeting control siRNA (siScrambled) is used as the control for RNAi. Nuclei stained with DAPI (magenta). siDAP is activated by heat shock (HS) in red. Cycloheximide (CHX) was added 5 h after HS to inhibit the synthesis of new HttQ46-GFP molecules. Bottom: Immunoblot showing knockdown of DNAJA1 and DNAJB1 in HeLa cells expressing HttQ46-GFP. (**E**) Disassembly of HttQ

inclusions by siDAP-induced Hsp70 disaggregase is masked by high levels of aggregation of newly synthesized amyloidogenic proteins. Cells treated with +/- cycloheximide (CHX) with and without VER-155008. CHX was added 5h after HS to inhibit HttQ-GFP synthesis. VER-155008 was added 5h after HS to inhibit siDAP-induced Hsp70 disaggregase activity. DMSO, vehicle control for the inhibitor. GFP fluorescence (cyan) indicates the aggregated (punctated signal, indicated by white arrows) and non-aggregated (diffused signal) state of HttQ23-GFP, HttQ46-GFP, and HttQ119-GFP. HttQ23-GFP, HttQ control that does not aggregate. The nuclei stained with DAPI (magenta). Heat shock (HS) in red. Scale bar 20 µm (n = 3).

Methods

Plasmids

Exon 1 carrying C-terminally tagged HttQ25-EmGFP and HttQ46-EmGFP were generated in the mammalian expression vector pTREX (Invitrogen). pcDNA6.2EmGFP-DAXX (Addgene, catalogue number: 169726), VCP (wt)-EGFP (Addgene, catalogue number: 23971), pFRT/TO eGFP TIA1 (Addgene, catalogue number: 106094) and pCMV3-GFP-hnRNPK (LSBio, catalogue number: LS-N40093) were purchased. pcDNA5/FRT/TO HttQ119-eGFP was previously generated (Newcombe et al., 2018). pEGFP-N1 Hsp104 and pEGFP-N1 Hsp104 $^{E285Q, E687Q}$ were kind gifts from Bernd Bukau, Ph.D. (Heidelberg University). The generation of Hsp70 (HSPA8), Hsp110 (HSPH2), DNAJA1, DNAJA2, DNAJB1, DNAJB4, and mutant variants tagged with 6xHis-Smt3 in the vector pCA528 for recombinant expression and purification was previously described (Nillegoda *et al.*, 2015; Rampelt *et al.*, 2012). Standard recombinant DNA techniques described by Sambrook et al. (Green and Sambrook, 2014) combined with standard site-directed mutagenesis with Phusion Plus DNA Polymerase (Thermo Fisher Scientific) were used to generate V5-DNAJA1, V5-DNAJA2, V5-DNAJB1, V5-DNAJB4, V5-DNAJB1^{H32Q}, DNAJB1-HA, DNAJB1^{D4R,E69R,E70R}-HA, DNAJB1^{H32Q,D34N}-HA in pcDNA5/FRT/TO mammalian expression plasmid (Thermo Fisher Scientific) (Hageman and Kampinga, 2009). Gene sequences were verified by sanger sequencing.

Protein purification

Human Hsp70, Hsp110, DNAJA1, DNAJA2, DNAJB1, DNAJB4, JDP mutants and firefly luciferase were recombinantly expressed and purified as previously described (Nillegoda *et al.*, 2015; Rampelt *et al.*, 2012). Briefly, *E. coli* strains BL21 (D3E)/ pRARE carrying the corresponding expression vectors were induced for protein expression with 0.5 mM isopropyl-1-thio-D-galactopyranoside (IPTG, Sigma-Aldrich) for three hours at 30 C. Cells were lysed in 50 mM HEPES-KOH, pH 7.5, 750 mM KCl, 5 mM $MgCl_2$, protease inhibitor cocktail (Roche), 2 mM phenylmethylsulphonyl fluoride, 10% glycerol (for human JDP purifications) or 50 mM HEPES-KOH, pH 7.5, 300 mM KCl, 5 mM $MgCl_2$, protease inhibitor cocktail (Roche), 2 mM phenylmethylsulphonyl fluoride, 10% glycerol (for human Hsp70/110 purifications). After centrifugation at 30000 x g (30 min, 4 ° C) the resulting supernatants were applied to the Ni-NTA/Ni-IDA matrix and incubated for 60 min at 4 ° C. Subsequent washing steps were performed with high salt buffers (50 mM HEPES-KOH, pH 7.5, 750 and 500 mM KCl, 5 mM $MgCl_2$ and 10% glycerol or 50 mM HEPES-KOH, pH 7.5, 300 and 100 mM KCl, 5 mM $MgCl_2$ and 10% glycerol for human JDP and Hsp70/110 purifications, respectively). In the case of Hsp70/110 purification, an additional wash step was included with ATP buffer (50 mM HEPES-KOH, pH 7.5, 100 mM KCl, 5 mM $MgCl_2$, 5 mM ATP). Protein elution was performed with 300 mM imidazole in the corresponding low salt buffers. Dialysis was performed overnight at 4 ° C in the presence of 4 µg of the 6xHis tagged Ulp1 per mg of substrate protein for proteolytic cleavage of the 6xHis-Smt3 tag. The 6xHis-Smt3 tag and Ulp1 were removed by incubating the dialyzed proteins in a Ni-NTA/ Ni-IDA matrix for 60 min at 4 ° C. Pyruvate kinase was purchased from Sigma-Aldrich. Proteins were further purified using Superdex 200 (GE Healthcare).

Luciferase disaggregation assay

Luciferase disaggregation assays were performed as previously described (Nillegoda *et al.*, 2017). Briefly, 20 nM firefly luciferase was incubated at 45 ° C for 15 minutes in HKM buffer (50 mM Hepes-KOH pH 7.5, 50 mM KCl, 5 mM $MgCl_2$, 2 mM DTT, 2 mM ATP pH 7.0, 10 µM BSA) to generate thermally denatured luciferase. Protein disaggregation was initiated by adding 1 µM HSPA8, 100 nM HSPH2, 250 nM JDP/mutant variants (total) and an ATP regenerating system (3 mM phosphoenolpyruvate (PEP) and 20 ng/µl pyruvate kinase) to the preformed luciferase aggregates followed by shifting the reaction to 30 ° C. 1 µM of

recombinant yeast Hsp104 (kind gift from Yuki Oguchi, Ph.D.) was added to generate the bichaperone disaggregation system. Luciferase activity was measured at the indicated time points with a Lumat tube luminometer (Berthold Technologies) by transferring 1 µL of the sample to 100 µL of assay buffer (25 mM Glycylglycin, pH 7.4, 5 mM ATP pH 7, 100 mM KCl, 15 mM $MgCl_2$) mixed with 100 µL of 0.25 mM luciferin. The Hsp70 inhibitor VER-155008 (Sigma, SML0271) was added at a working concentration of 5 µM.

Cell culture

Human adenocarcinoma epithelial cell line HeLa (ATCC CRM-CCL-2) and human embryonic kidney HEK 293 cells (ATCC CRL-3216) were obtained from the American Type Culture Collection. HEK 293 JB1 KO cells were kindly provided by Christian Hansen, Ph.D. (Lund University). These cell lines were cultured in DMEM (Gibco, Thermo Fisher Scientific, catalogue number: 10569044) supplemented with 10% (v/v) heat inactivated fetal bovine serum (FBS: Gibco catalogue number: 10082147), 1x L-alanine-L-glutamine dipeptide (Gibco Glutamax 100x catalogue number: 35050061), 10 mM sodium pyruvate (Gibco catalogue number: 11360070) and 100 U/ml penicillin/streptomycin (Gibco 1x 104 U/ml catalogue number: 15140122) at 37 ° C in 5% CO_2. Human dermal fibroblasts were isolated and grown from 6 mm skin punch biopsies as previously described (Song et al., 2012). Dermal fibroblasts were cultured on 0.1% gelatin (Sigma catalogue number: G1890) treated wells using fibroblast media consisting of DMEM (Gibco catalogue number: 10569044), 10% FBS, 0.1 mM MEM non-essential amino acids solution (Gibco catalogue number: 11140050), 100 U/ml penicillin/streptomycin, 0.1mM 2-Mercaptoethanol, (Gibco catalogue number: 21985023). Cell passaging: 0.25 million dermal fibroblasts were seeded in a 10 cm culture plate until cell confluency reached 70%. This was defined as a passage (P), and the process was repeated to generate replicatively aged cell lines. Mycoplasma contamination of cells was tested and ruled out with the LookOut Mycoplasma Detection kit (Sigma-Aldrich; catalogue number: MP0035).

Heat shock and drug treatments

Heat shock was performed by exposing HeLa cells to 43 ° C for 1 hour in a water bath or otherwise indicated. A 42 ° C, 2 hours heat shock in an incubator was applied to HEK 293 and human dermal fibroblasts. Following heat shock, cells were returned to 37 ° C for stress recovery. Temperature measurements for heat shock conditions in the water bath and incubator were determined using a VOLTCRAFT K101 digital thermometer (Conrad). Hsp70 inhibitor VER-155008 (Sigma, catalogue number: SML0271) was used at a working concentration of 5 µM (*in vitro*) or 50 µM (in cells) or otherwise stated. Protein synthesis was inhibited by adding cycloheximide (CHX) (Sigma, catalogue number: 01810) at a final concentration of 100 µg/mL. Proteasome inhibition was achieved by adding bortezomib (Merck, catalogue number: 5043140001) at a final concentration of 10 nM. NMS-873 (Sigma, catalogue number: SML 1182) was used for VCP inhibition at a final concentration of 1 or 10 µM.

***In situ* proximity ligation assay (PLA)**

PLA was performed according to DUOLINK manufacturer's guideline for mammalian cells (Sigma-Aldrich). DNA was stained with DAPI-containing mounting medium (Sigma-Aldrich, catalogue number: DUO82040). The staining, imaging, processing, and analysis conditions were kept consistent for each experiment.

Immunocytochemistry and staining

Cells were cultured on soda lime glass diagnostic slides masked with epoxy resin (Marienfield-superior, catalogue number: 1216530) until 70-80% confluence. Cells were washed 2x with PBS, fixed with 4% paraformaldehyde in PBS for 10 minutes, and washed 2x again with PBS. Cells were permeabilized with 0.2% Triton X-100 in PBS for 10 minutes. After

permeabilization, cells were washed 2x with PBS and blocked for 10 minutes in PBS containing 0.5% bovine serum albumin and 0.15% Glycine (PBS+ buffer). Primary antibodies were diluted in PBS+ buffer and incubated for 1.5 hours at room temperature (RT) or overnight at 4 ° C. After incubation, cells were washed 4x with PBS+ buffer. Secondary antibodies were diluted in PBS+ buffer and incubated for 1.5 hours at RT, followed by 2x washes in the same buffer. DNA was stained with DAPI-containing mounting medium (Sigma-Aldrich, catalogue number: DUO82040) or Hoechst staining (Thermo Scientific, catalogue number: 62249) according to the manufacturer's guidelines.

Transfections and siRNA knockdowns

Plasmid transfections were performed according to standard protocols using Lipofectamine 2000 or 3000 (Thermo Fisher Scientific). siRNA transfections were carried out according to standard protocols using DharmaFECT one transfection reagent (Dharmacon, DHA-T-2001).

Confocal microscopy

LSM 780 and LSM 980 laser scanning confocal systems on inverted stands with diode 405 nm, argon 488 nm, and DPSS 561 nm lasers (Carl Zeiss, Germany) were used for microscopy. The images were taken with the Plan-Apochromat 40x/1.4 oil objective (Carl Zeiss) and identical acquisition settings with a pinhole of approximately 1 AU. Maximum projection images were generated from acquired z-stacks. Linear adjustments of brightness and contrast were performed to the same degree within each experiment. The DAPI, PLA^{DT}, and GFP signals were pseudo-colored in magenta, yellow, and cyan. Fluorescence intensity profile plots (line scans) were generated on the raw images using the RGB Profiler plugin in Fiji.

PLA^{DT} quantification

The PLA^{DT} signal was quantified using custom code (https://github.com/Sanudish/Punctate-Detection.git) in MATLAB R2021a using functions from the Image Processing Toolbox, and Statistics and Machine Learning Toolbox. Briefly, the brightest slice of each volume, determined by the cumulative intensity of the slice, was extracted to perform the quantification. The nuclei-stained channel of the images was first processed with a median filter followed by a maximum filter, both of which utilized a 4x4 kernel. The user input-based percentile thresholding was then applied to the processed images. The connected nuclei were then further segmented through the implementation of a Watershed transformation. To refine nuclei segmentation, user inputs for the degree of connectivity and area were utilized. The output enabled quantification of the number of cells per image. Next, for extraction of puncta, logarithmic frequency histograms of the intensity profiles were plotted to generate a normalized user input range between -1 and 1 to threshold out puncta. To improve the segmentation of the puncta from noise, area thresholding was implemented. The resulting number of puncta, and their characteristics were measured. The product of the average punctate mean intensity per cell and the number of punctate structures per cell was calculated to obtain the siDAP raw parameter. The final induction of siDAP was reported as a PLA^{DT} fold change to an unstressed condition.

Aggregate quantification

Endogenous protein aggregates and TIA-1 biomolecular condensates in HeLa cells were quantified using a Fiji macro termed AggreCount as previously described (Klickstein et al., 2020). Briefly, the aggregates were extracted by processing images with gamma enhancement, mean background reduction, and a user-based threshold. The contrast enhancement of the nuclei enabled segmentation of nuclei regions, which were then utilized to generate a composite image with the preprocessed image. The signal-enhanced composite image enables the detection of local maxima of cell regions. Implementing the watershed algorithm, a Voronoi diagram was generated and the proportion of cells with aggregates was measured. The

fold change was determined by calculating the difference of each parameter in the stress recovery conditions and the unstressed condition. When segmenting hnRNPK aggregates, the threshold diameter of inclusions was set at 1 µm to avoid intranuclear inhomogeneities being falsely detected as aggregates. The aggregates in HEK 293 cells were calculated manually as previously described (Park et al., 2017) because AggreCount segmentation was less efficient.

Fluorescence Recovery After Photobleaching

HeLa cells expressing GFP tagged hnRNPK were exposed to 43 ° C for 1 hour in a water bath and returned to 37 ° C for 1 hour. FRAP was performed on heat-induced hnRNPK aggregates using an LSM 780 laser scanning confocal system on inverted stands at 37 ° C with argon 488 nm laser (Carl Zeiss, Germany). The images were taken with the Plan-Apochromat 40x/1.4 oil objective (Carl Zeiss). Aggregates were photobleached using 100% FRAP laser power for 10 ms. Images were obtained every 500 ms to observe fluorescence recovery up to 40 s. Images were analyzed using easyFRAP (Rapsomaniki et al., 2012). Recovery curves were normalized to background fluorescence for subtracting noise, and adjacent non-bleached aggregates for fluorescence intensity fluctuations. Average and standard errors were calculated from seven individual traces.

Immunoblotting

Immunoblot analysis was performed using standard methodologies (Nillegoda *et al.*, 2017). Briefly, cells were lysed in RIPA buffer with a protease inhibitor cocktail (Roche cOmplete - EDTA free, catalogue number: 05056489001) and sonicated (3x cycles, each cycle at 5 seconds and 50% amplitude) in a Branson SFX150 Digital Sonifier (Emerson). Protein concentrations were determined using the bicinchoninic acid protein assay kit (PierceTM, BCA, catalog numbers: Reagent-A: 23228, Reagent-B: 23224). Protein samples were stabilized with 1x sample buffer and boiled for 5 minutes at 95 ° C. For SDS-PAGE, 25 µg total protein was loaded into 4% stacking gel and resolved through 12% running gel. Protein transfer to a PVDF membrane was performed using a Bio-Rad transfer tank (Mini Trans-Blot Cell). Anti-rabbit (800CW; C90220-05) and anti-mouse (680RD; C90219-05) antibodies from LI-COR Biosciences were used as secondary antibodies. The detection was carried out with an Odyssey Immunoblotting Imaging System (LI-COR).

Supernatant-pellet assay

HeLa cells were grown in 100 mm cell culture plates. Before lysis, cells were washed 1x with ice-cold PBS, scraped, and collected with 500 µl of ice-cold PBS. Cells were collected at 600 x g for 5 minutes at 4 ˚ C. Cell pellets were resuspended in lysis buffer containing 25 mM HEPES, 75 mM NaCl, 1 mM $MgCl_2$, 1% NP-40, 75 U/ml Benzonase (EMD Millipore) and Protease Inhibitors cocktail (Roche) and lysed by vortexing for 20 seconds and subsequently for 5 seconds every 10 minutes over the course of 1 hour. Protein quantification was performed using the DC-protein assay (Bio-Rad) and the samples were equalized. 10% of the total protein lysate was transferred to a fresh Eppendorf tube and boiled in Laemmli buffer (60 mM Tris pH 6.8, 2% SDS, 10% glycerol, 5% β-mercaptoethanol). From the remaining lysate, the pellet fractions were isolated by centrifuging the samples at 20,817 x g for 30 minutes at 4 ˚ C and removing the supernatant. The pellet fractions were washed and resuspended in urea buffer (8M Urea, 50 mM Tris pH 7.4, 2% SDS, 50 mM DTT). The resuspended samples were shaken at 1000 rpm in a heating block at 60 ˚ C for 1 hour and subsequently at 1000 rpm in RT, overnight, and boiled prior to SDS-PAGE.

qRT-PCR

HeLa cells were washed with ice cold PBS, scraped in TRIzol reagent (Invitrogen) and incubated at RT for 5 minutes. Chloroform was added to cell lysates, vortexed for 15 seconds and incubated for 2-3 minutes before centrifugation at 18,000 x g for 15 minutes at 4 ˚ C. The

aqueous phase was transferred to a tube without DNAase/RNAase, isopropanol was added and incubated in RT for 10 minutes. RNA was precipitated by centrifugation at 18,000 x g for 10 minutes at 4 ˚ C. The supernatants were removed, 75% ethanol was added to the pellets, and the samples were centrifugated at 18,000 x g for 5 minutes at 4 ˚C. The supernatants were removed and the pellets were resuspended in DNA/RNAase-free H_2O. DNAases were removed with the Turbo DNAase free kit (Invitrogen) according to the manufacturer's instructions. cDNA synthesis was performed using M-MLV reverse transcriptase (Invitrogen) according to the manufacturer's instructions. The primers used in the PCR step were previously described (Hageman et al., 2011).

LDH-Glo cytotoxicity assay

Heat shock-induced cytotoxicity was determined using the LDH-Glo cytotoxicity assay (Promega, catalogue number: J2380) according to the manufacturer's guidelines.

Cellular senescence detection assay

Cellular senescence was assessed using fluorescence- and immunocytochemistry-based assays. The fluorescence-based assay was performed with the Cellular Senescence Plate Assay Kit-SPiDER-βGal (Dogindo, catalogue number: 05-05) according to the manufacturer's guidelines. Fluorescence intensity was measured using a plate reader (CLARIOstar^{Plus}, BMG Labtech; Excitation: 535 nm/ emission: 580 nm). SA-β-Gal activity was normalized to cell count determined using a hemocytometer. The immunocytochemistry-based assay was performed with Senescence β-Galactosidase Staining Kit (Cell Signaling Technology, catalogue number: 9860) according to the manufacturer's guidelines. DIC images were obtained on a Leica DMi8 system using Plan-Apochromat 40x/1.4 oil objective. The percentage of cells positive with β-Galactosidase signal was quantified manually.

Multiple reaction monitoring mass spectrometry

HeLa cells were cultured in 150 mm cell culture plates until 70-80% confluence. Light samples were grown as previously described. To generate a heavy internal standard, cells were grown in arginine and lysine-depleted DMEM (Thermo Fisher Scientific) supplemented with 100 mg/L L-arginine-HCl, $^{13}C_6$, $^{15}N_4$ (Thermo Fisher Scientific) and 100 mg/L L-Lysine-2HCl $^{13}C_6$, $^{15}N_2$ (Thermo Fisher Scientific). The cells were grown in the heavy medium for 6 passages until the incorporation of heavy amino acids was at least 95%. To ensure that all proteins of interest were detectable, a heavy standard was generated from lysates of unstressed and heat shocked cells for 1 hour at 43 ˚ C. Before lysis, cells were washed with ice-cold PBS and detached by scraping with 1 ml of ice-cold PBS. Cells were pelleted at 500 x g for 5 minutes at 4 ˚ C and the supernatant was discarded. Cell pellets were snap frozen in liquid nitrogen and stored at -80 ˚ C or processed immediately. Cell pellets were resuspended in Benzonase containing urea buffer (6 M Urea, 50 mM Tris pH = 7.5, 2 mM $MgCl_2$, 50 mM DTT, 0.25 U μL^{-1} Benzonase) and lysed for 10 minutes at RT. The lysate was centrifuged at 5,000 x g for 10 minutes in RT. The supernatant was transferred to a fresh tube. Protein quantification was performed using the DC Protein Assay (Bio-Rad).

Light samples and heavy internal standards were mixed in a 1:1 (w/w) ratio and 100 µg of total protein was precipitated using a mixture of methanol and chloroform according to a published protocol (Wessel and Flügge, 1984). For in-solution digestion, precipitated protein pellets were resolved in 50 µL of urea buffer (8 M Urea, Carl Roth, 100 mM NaCl, Applichem, in 50 mM triethylammonium bicarbonate (TEAB), pH 8.5, Sigma-Aldrich). To reduce disulfide bridges, the sample was incubated with 10 mM 1,4-dithiothreitol (Sigma-Aldrich) for 30 min at RT, constantly agitated at 350 rpm. Next, alkylation was performed with 30 mM iodacetamide (Sigma-Aldrich) in 100 mM TEAB buffer for 30 min at RT in the dark. Sample predigestion was performed by adding 2.5 µg Lysyl Endopeptidase® (Wako Chemicals) and incubating for

4 hours at 28 °C and 350 rpm agitation. After diluting the urea concentration to 2 M by adding 50 mM TEAB buffer, 1 µg of trypsin (Thermo Fisher Scientific) was added and the samples were incubated for 16 hours at 28 °C and 350 rpm agitation. The digestion process was stopped by reducing pH < 2 by adding trifluoroacetic acid (TFA, Sigma-Aldrich) to a final concentration of 0.4 – 0.8% (v/v). The samples were centrifuged for 10 min at 20,000 x g in RT and the supernatant was desalted using SepPak C18 cartridges (500 mg; Waters) and the Waters Extraction Manifold. The SepPak C18 cartridges were equilibrated by adding 3 ml of 100% acetonitrile (ACN), then 3 ml of 50% ACN / 0.1% TFA and finally 3 ml of 0.1% TFA. Digested peptide samples were loaded onto SepPak cartridges and washed with 3 ml of 0.1% TFA. Finally, the samples were eluted into fresh LoBind tubes using 1 ml of 50% ACN / 0.1% TFA. The samples were dried in a vacuum centrifuge and stored at -20 ° C until LC-MRM analysis. Before LC-MRM analysis, the peptides were resolubilized in 10 µL of 20% ACN / 0.1% (v/v) TFA and incubated for 5 min in RT, then diluted 10-fold with 0.1% TFA to obtain a final concentration of 2% ACN. 5 µg of tryptic digest including a set of 11 synthetic peptides for indexed retention time scheduling (Escher et al., 2012) were analyzed per LC-MRM injection. The samples were measured in a randomized order using a nanoACQUITY UPLC System (Waters) online-coupled to an ESI-QTrap 5500 via a NanoSpray III Source (both Sciex). The UPLC was equipped with a trapping column (Waters, Symmetry C18; 2 cm length, 180 µm inner diameter, 5 µm C18 particle size, 100 Å pore size) and an analytical column (Waters, M-Class Peptide BEH C18; 25 cm length, 75 µm inner diameter, 1.7 µm C18 particle size, 130 Å pore size). The peptides were trapped for 7 min at a flow rate of 10 µL min^{-1} with 99.4% of buffer A (1% v/v ACN, 0.1% v/v FA) and 0.6% of buffer B (89.9% v/v ACN, 0.1% v/v FA) and separated at the analytical column temperature of 60°C, with a flow rate of 300 nl min^{-1} and a 37 min linear gradient of buffer B in buffer A from 3 to 37% B, followed by washing and reconditioning of the column to 3% B. Uncoated precut emitters (Silica Tip, 20 µm inner diameter, 10 µm tip inner diameter, New Objectives, Woburn, MA) were used and a voltage of approximately 2.6 kV was applied for electrospray ionization. QTrap 5500 was operated in scheduled mode at Unit resolution for Q1 and Q3 with 180 sec MRM detection window width and 2.5 sec target scan time. Peptide retention times for scheduling were previously determined using commercial synthetic peptide standards (JPT).

LC-MRM data and statistical analysis

The MRM data was first manually reviewed using Skyline 64-bit version 20.1. Data sets were imported into Skyline, and signal quality was assessed using the Peak Areas and Retention Time visualization features. We ensured via the Results Grid that all reference dot-product (rdotp) correlations for ratios of the observed transition intensities between the corresponding light and heavy precursor pairs were equal to or above 0.9. Then, all data were exported from Skyline and imported into R version 4.0.3 (2020-10-10) "Bunny-Wunnies Freak Out" for further analysis using a custom script. Briefly, all quantitative transitions were summed up across proteins, and log2 light/heavy ratios were computed to account for technical variance. In addition, all samples were normalized to their respective tubulin alpha-1A protein level to account for biological variance. Then, pairwise group comparisons were performed using linear regression models between protein ratios of different conditions and the unstressed control. The slope of the linear regression corresponded to the fold change between the respective condition and the control and was plotted together with its respective standard error.

Identification of aggregated proteins recovered by DNAJA1+DNAJB1-Hsp70 disaggregase

Briefly, HeLa cells were heat-shocked followed by sustained recovery over 12h. We chose recovery time points that encompass the evolution and resolution (i.e. 6h and 12h post-HS) of aggregates that appeared to be the main target of siDAP. To quantify cellular proteins that change solubility at different harvest time points, we used isobaric labeling (Tandem mass tag;

TMT), a method that allows for multiplexing of samples collected at different time points in a recovery course into a single experiment. The gist of TMT is that peptides are labeled with one of several distinct agents of the same mass, but cleave into distinct reporter ions during mass spectrometry fragmentation. The workflow included a parallel examination of stress recovery in which DNAJA1+DNAJB1-Hsp70 disaggregase activity was inhibited using VER-155008 to identify potential siDAP-specific substrates. The proportion of proteins in the supernatant compared to the total proteome (pSup) was normalized to solubility prior to HS (ΔpSup), and then the effect of VER-155008 was compared to the DMSO control (ΔΔpSup). As expected, we observed a significant decrease in the median pSup at 6h after HS in both DMSO and VER-155008 treated samples (Figure S12B; p value < 0.0001, paired Wilcoxon rank test) that supports aggregation throughout the proteome as a result of heat denaturation. After 12 hours of recovery, more than 75% of proteins had recovered their solubility. However, as expected, a subset of proteins recovered differently in the presence of VER-155008, as measured by ΔΔpSup. Proteins with ΔΔpSup > +/ 0.26 (determined by Gaussian thresholding at the 99th percentile of pseudo pre-HS ΔpSup, see methods) were considered to have significantly altered solubility due to the presence of VER-155008. Of these proteins, those that were less soluble in the presence of VER-155008 compared to DMSO (ΔΔpSup > 0) at at least one time point were identified as potential clients solubilized by the disaggregase machinery (a total of 51 proteins, Table S1). We then sought to describe the general behavior of ΔΔpSup among these proteins using unsupervised k-means clustering. The proteins of interest were sorted into four distinct patterns (Figure S12C); (i) those that were more soluble at 6h-HS in the presence of VER-155008 compared to the DMSO control, but whose recovery was inhibited compared to the DMSO control at the 12h timepoint, (ii) those that were less soluble at 6h post-HS in the presence of VER155008 but then recovered similarly to the DMSO control at 12h, (iii) those with no difference in solubility due to VER-155008 at 6h post-HS, but whose recovery was inhibited compared to the DMSO control at the 12h timepoint, and (iv) those that were less soluble at both 6h and 12h post-HS in the presence of VER-155008 (Table S1). Protein degradation and processes such as the recently discovered ubiquitinome reshaping during stress recovery could have in part influenced the generated patterns we observed (Maxwell *et al.*, 2021). Given that the addition of VER-155008 was at 5h post-HS, we postulated that its impact on disaggregation would be most visible at the 12h timepoint. Therefore, we considered proteins with minimal differences in solubility at 6h but inhibited recovery at 12h in the presence of VER-155008 (cluster iii) for validation. **Cell fractionation by ultracentrifugation**: HeLa cells were grown in T75 cell culture flasks (Nunc EasYFlask, catalogue number: nun156472). Before lysis, cells were washed with 1x ice-cold PBS, scraped and collected with 10 mL of ice-cold PBS. The cells were then pelleted by a mild centrifugation step at 120 x g for 6 minutes at 4 ˚ C twice and the supernatant was discarded. Cell pellets were resuspended in 500 µL of lysis buffer 1 containing 50 mM Tris-HCl pH 7.5, 150 mM NaCl, 1% (v/v) IGEPAL CA-630, 10 units/mL DNase I, 1:1,000 protease inhibitor, and Protease Inhibitors cocktail (Roche, catalogue number: 11836145001) and lysed by extrusion through a 27-gauge needle for 25 times, followed by a 31-gauge needle for 10 times. Subsequently, EDTA was added to a final concentration of 2 mM. Cell lysate was then divided into two, one for the assessment of total protein and the other pelleted at 100,000 x *g* for 20 min at 4 ° C. The resulting supernatant was the collected sample. The volume of total protein and supernatant samples was measured and resuspended in an equal volume of a lysis buffer 2 containing lysis buffer 1, 4% sodium dodecyl sulfate (SDS, Thermo Scientific, catalogue number: 28365) and 4 mM 1,4-dithiothreitol (DTT, Thermo Scientific, catalogue number: R0861). Subsequently, the samples were incubated at 95 ° C for 20 minutes. **NanoESI-LC-MS/MS**: Samples were prepared for mass spectrometry as previously detailed (Sui *et al.*, 2020). Freeze-dried peptides were resuspended in 80 µl of distilled water and quantified by the BCA assay (Thermo Fisher Scientific) according to the manufacturer's instruction. 20 µl of each sample was diluted into a final volume of 40 µl containing 100 mM TEAB and 30% (v/v) acetonitrile. The samples

were then labeled with TMT 11-plex (Thermo Scientific, catalogue number: A37725) according to the manufacturer's protocol. The samples were analyzed by nanoESI-LC-MS/MS using an Orbitrap Exploris mass spectrometer (Thermo Scientific) equipped with a nanoflow reversed-phase-HPLC (Ultimate 3000 RSLC, Dionex) fitted with an Acclaim Pepmap nano-trap column (Dionex—C18, 100 Å, 75 µm × 2 cm) and an Acclaim Pepmap RSLC analytical column (Dionex—C18, 100 Å, 75 µm × 50 cm). For each iteration of LC-MS/MS, 0.6 µg of the peptide mix was loaded onto the enrichment (trap) column at an isocratic flow of 5 µl min^{-1} of 2% ACN containing 0.1% (v/v) trifluoroacetic acid for 5 min before the enrichment column was switched in-line with the analytical column. The eluents were 0.1% (v/v) formic acid/5% DMSO (v/v) (solvent A) and 100% ACN/0.1% formic acid/5% DMSO (v/v) (v/v) (solvent B), flowed at 300 nL min^{-1} using a gradient of 3–22% B in 90 min, 22–40% B in 10 min and 40–80% B in 5 min then maintained for 5 min before re-equilibration for 8 min at 3% B prior to the next analysis. All spectra were acquired in positive ionization mode with full scan MS acquired from m/z 300-1600 in the FT mode at a mass resolving power of 120 000, after accumulating to an AGC target value of $3.00e^6$, with a maximum accumulation time of 25 ms. The RunStart EASY-IC lock internal lockmass was used. Data-dependent HCD MS/MS of charge states > 1 was performed using a 3 s scan method, at a normalized AGC target of 75%, automatic injection, a normalized collision energy of 30%, and with spectra acquired at a resolving power of 15000. Dynamic exclusion was used for 20s. **Peptide identification:** The initial analysis of raw mass spectra was carried out using MaxQuant (v 1.6.14.0) against the Swissprot Homo Sapiens database (downloaded 04/03/2020; containing 20350 entries). Searches were conducted with 20 ppm mass tolerance for MS, and 0.2 Da for MS/MS, with one missed cleavage allowed and match between runs enabled. The MS2 reporter ion was set to TMT 11-plex and isotopic distribution correction was applied according to the product data sheet. Variable modifications included methionine oxidation and N-terminal protein acetylation, while the carbamidomethylcysteine modification was fixed. The false discovery rate maximum was set to 0.005% at the peptide identification level (actual was 0.005 for each replicate) and 1% at the protein identification level. All other parameters were left as default. **Ratio correction and scaling:** Further analysis was performed with custom Python scripts. The logic was as follows. First, common contaminant proteins were removed, and quantified proteins were considered as those identified by at least one unique peptide. The ratio of abundance for each protein in the supernatant as compared to total samples (pSup) was corrected for differences in total protein amount as quantified via BCA assay described previously (Sui *et al.*, 2020). The relative change in solubility for individual proteins after heat shock (ΔpSup) was then determined by normalizing to the preheat shock value, such that a protein with no change in solubility due to heat shock would have a value of 1. The resulting data were then scaled using a p-value weighted correction (Cox et al., 2022). This correction weights the mean ratio of biological replicates (*n=4*) according to the relative confidence with which it deviates from the expected value (in this case, 1) as per equation 1:

$$R = \frac{1 - m}{-20^{p}}$$

where *m* corresponds to the mean of the ΔpSup ratios and *p* corresponds to the p-value derived from a one-sample t-test of the ratios against the expected value under a single timepoint and treatment regime. Finally, the difference in relative solubility at 6 and 12h post-heat shock between the DMSO and VER-155008 treated samples (ΔΔpSup) was calculated as $\Delta pSup_{DMSO} - \Delta pSup_{VER}$, such that no difference in relative solubility between the DMSO and VER-155008 treatments would yield a ratio of 0. **Identifying proteins of interest:** To define a ΔΔpSup at which the changes in solubility could be considered biologically relevant, we first generated a pseudo-control ΔΔpSup by subtracting per-protein randomized pre-heat shock ratios ($\Delta pSup_{R\text{-}Control}$) from the observed pre-heat shock ratios ($\Delta pSup_{Control}$). The resulting frequency histogram of pseudo-control ΔΔpSup values was then fit to a Gaussian distribution, and by calculating three times the derived variance parameter (σ) we determined the interval

encompassing 99.7% of the pseudo-control ΔΔpSup values. The boundaries of this interval (in this case ± 0.26, consistent with previous estimates of ± 0.3 applied to similar data sets (Sui *et al.*, 2020) were then used to threshold the ΔΔpSup values at each time point. Proteins that exceeded the ΔΔpSup threshold at least one time point were collected for additional analyzes. Functional overrepresentation was tested using PantherGOSlim (http://pantherdb.org), with a Bonferroni-corrected significance cutoff of $p < 0.05$ against the complete list of proteins identified. Annotated protein-protein interactions were collected from STRINGdb (Szklarczyk et al., 2019) via Cytoscape (v 3.7.2) (Shannon et al., 2003). Finally, ΔΔpSup traces over time were clustered using k-means as implemented via the scikit-learn package (Pedregosa et al., 2011).

Statistical Methods

All quantified experiments were performed at least in triplicate. Data are shown as mean ± s.e.m. and error bars indicating s.e.m. All statistical analyzes not described elsewhere were performed on RStudio (Version 1.1.447) or GraphPad Prism 8. One-way between groups analysis of variance (ANOVA) was conducted for multiple group comparisons. All analyses were considered statistically significant at $p<0.05$.

Ethics

Derivation of human dermal fibroblasts from skin punch biopsies was performed with approval from the Monash University and Monash Medical Centre Human Ethics Committees (approval number 10006A).

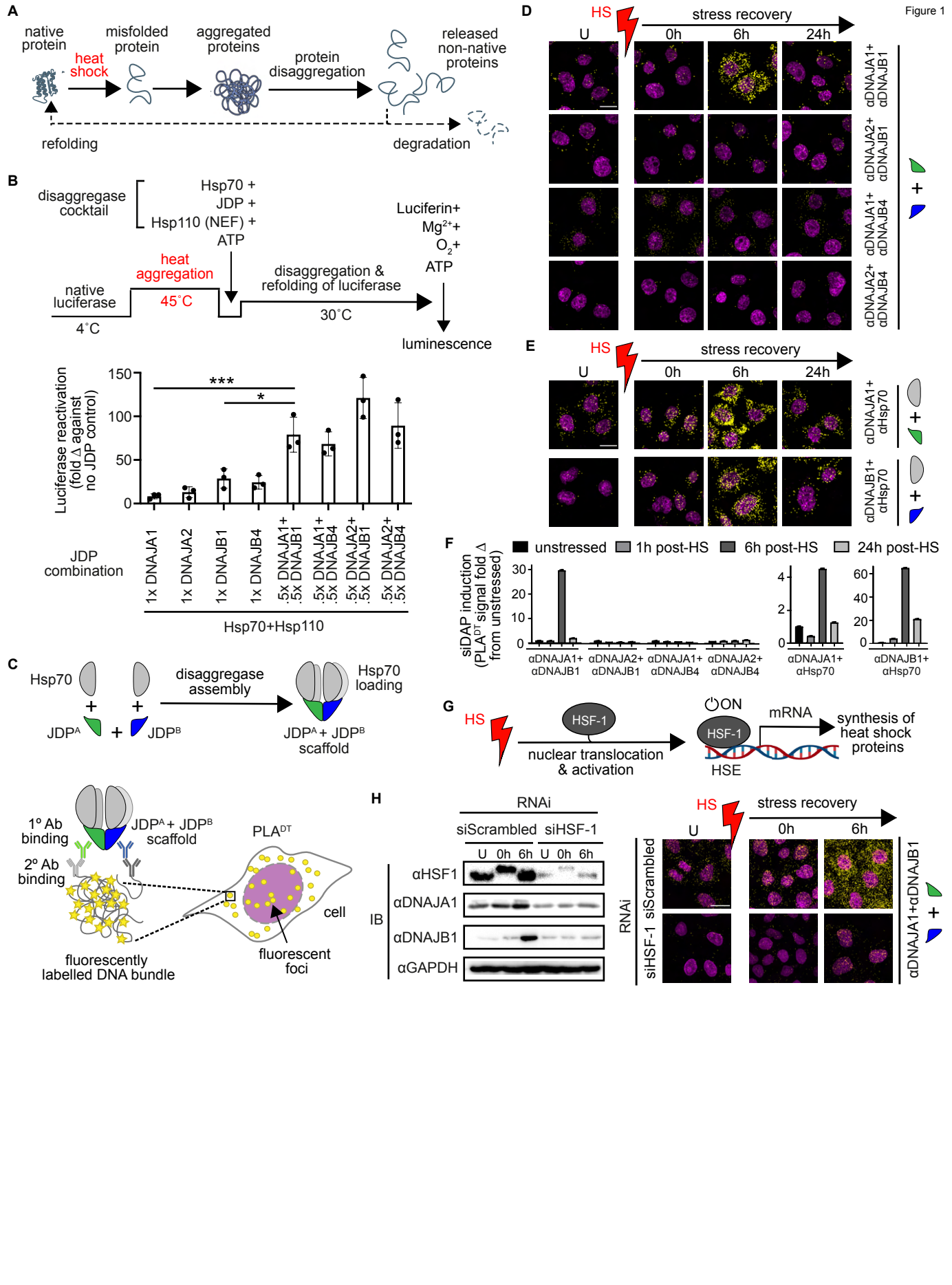
A
native protein
heat shock
misfolded protein
aggregated proteins
protein disaggregation
released non-native proteins
refolding
degradation
B
disaggregase cocktail
Hsp70 +
JDP +
Hsp110 (NEF) +
ATP
Luciferin+
Mg2+ +
O2 +
ATP
heat aggregation
45˚C
native luciferase
4˚C
disaggregation & refolding of luciferase
30˚C
luminescence
Luciferase reactivation (fold Δ against no JDP control)
150
100
50
0
***
*
JDP combination
1x DNAJA1
1x DNAJA2
1x DNAJB1
1x DNAJB4
.5x DNAJA1+ .5x DNAJB1
.5x DNAJA1+ .5x DNAJB4
.5x DNAJA2+ .5x DNAJB1
.5x DNAJA2+ .5x DNAJB4
Hsp70+Hsp110
C
Hsp70
JDPA
JDPB
disaggregase assembly
Hsp70 loading
JDPA + JDPB scaffold
1° Ab binding
2° Ab binding
JDPA + JDPB scaffold
PLADT
cell
fluorescent foci
fluorescently labelled DNA bundle
D
HS
stress recovery
U
0h
6h
24h
αDNAJA1+ αDNAJB1
αDNAJA2+ αDNAJB1
αDNAJA1+ αDNAJB4
αDNAJA2+ αDNAJB4
E
αDNAJA1+ αHsp70
αDNAJB1+ αHsp70
F
unstressed
1h post-HS
6h post-HS
24h post-HS
siDAP induction (PLADT signal fold Δ from unstressed)
αDNAJA1+ αDNAJB1
αDNAJA2+ αDNAJB1
αDNAJA1+ αDNAJB4
αDNAJA2+ αDNAJB4
αDNAJA1+ αHsp70
αDNAJB1+ αHsp70
G
HS
HSF-1
nuclear translocation & activation
ON
mRNA
synthesis of heat shock proteins
HSE
H
RNAi
siScrambled
siHSF-1
U
0h
6h
IB
αHSF1
αDNAJA1
αDNAJB1
αGAPDH
αDNAJA1+αDNAJB1

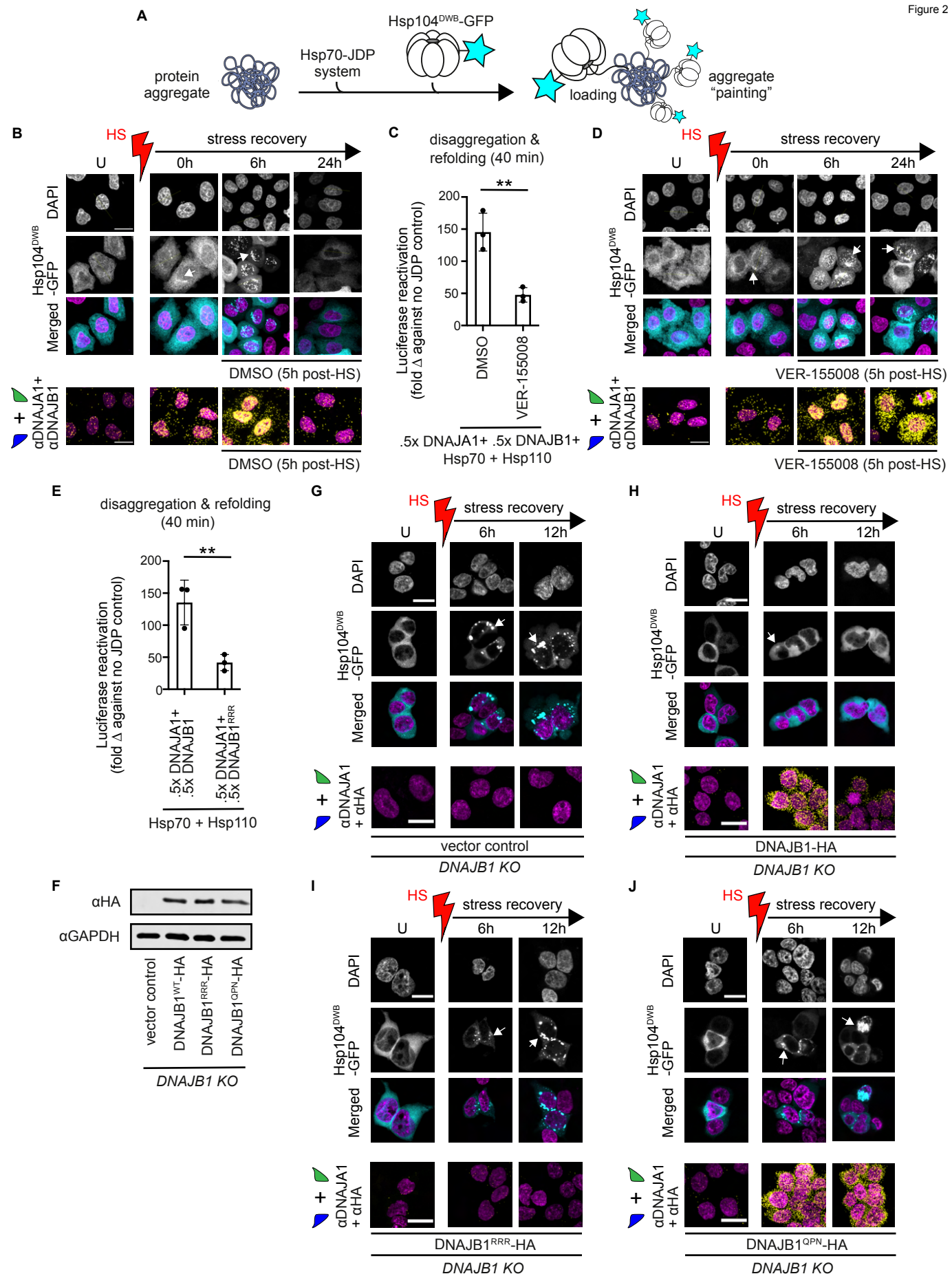
A
protein aggregate
Hsp70-JDP system
Hsp104DWB-GFP
loading
aggregate "painting"
B
HS
stress recovery
U
0h
6h
24h
DAPI
Hsp104DWB -GFP
Merged
DMSO (5h post-HS)
αDNAJA1+ αDNAJB1
DMSO (5h post-HS)
C
disaggregation & refolding (40 min)
Luciferase reactivation (fold Δ against no JDP control)
**
DMSO
VER-155008
.5x DNAJA1+ .5x DNAJB1+ Hsp70 + Hsp110
D
HS
stress recovery
U
0h
6h
24h
DAPI
Hsp104DWB -GFP
Merged
VER-155008 (5h post-HS)
αDNAJA1+ αDNAJB1
VER-155008 (5h post-HS)
E
disaggregation & refolding (40 min)
Luciferase reactivation (fold Δ against no JDP control)
**
.5x DNAJA1+ .5x DNAJB1
.5x DNAJA1+ .5x DNAJB1RRR
Hsp70 + Hsp110
F
αHA
αGAPDH
vector control
DNAJB1WT-HA
DNAJB1RRR-HA
DNAJB1QPN-HA
DNAJB1 KO
G
HS
stress recovery
U
6h
12h
DAPI
Hsp104DWB -GFP
Merged
αDNAJA1 + αHA
vector control
DNAJB1 KO
H
HS
stress recovery
U
6h
12h
DAPI
Hsp104DWB -GFP
Merged
αDNAJA1 + αHA
DNAJB1-HA
DNAJB1 KO
I
HS
stress recovery
U
6h
12h
DAPI
Hsp104DWB -GFP
Merged
αDNAJA1 + αHA
DNAJB1RRR-HA
DNAJB1 KO
J
HS
stress recovery
U
6h
12h
DAPI
Hsp104DWB -GFP
Merged
αDNAJA1 + αHA
DNAJB1QPN-HA
DNAJB1 KO

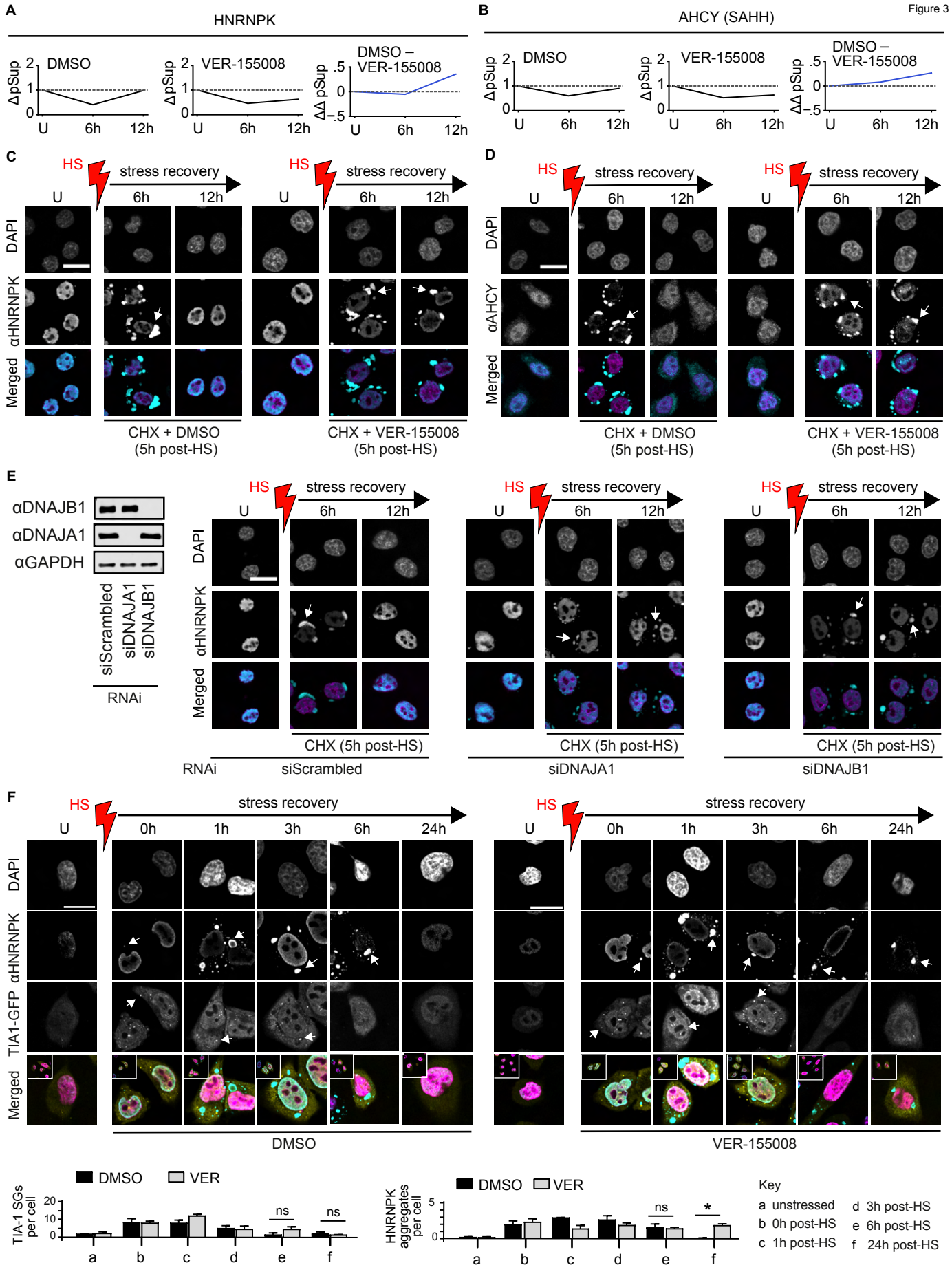
A
HNRNPK
DMSO
VER-155008
DMSO – VER-155008
ΔpSup
ΔΔ pSup
U
6h
12h
B
AHCY (SAHH)
C
HS
stress recovery
DAPI
αHNRNPK
Merged
CHX + DMSO (5h post-HS)
CHX + VER-155008 (5h post-HS)
D
αAHCY
E
αDNAJB1
αDNAJA1
αGAPDH
siScrambled
siDNAJA1
siDNAJB1
RNAi
CHX (5h post-HS)
F
0h
1h
3h
24h
TIA1-GFP
DMSO
VER-155008
TIA-1 SGs per cell
HNRNPK aggregates per cell
ns
*
Key
a unstressed
b 0h post-HS
c 1h post-HS
d 3h post-HS
e 6h post-HS
f 24h post-HS

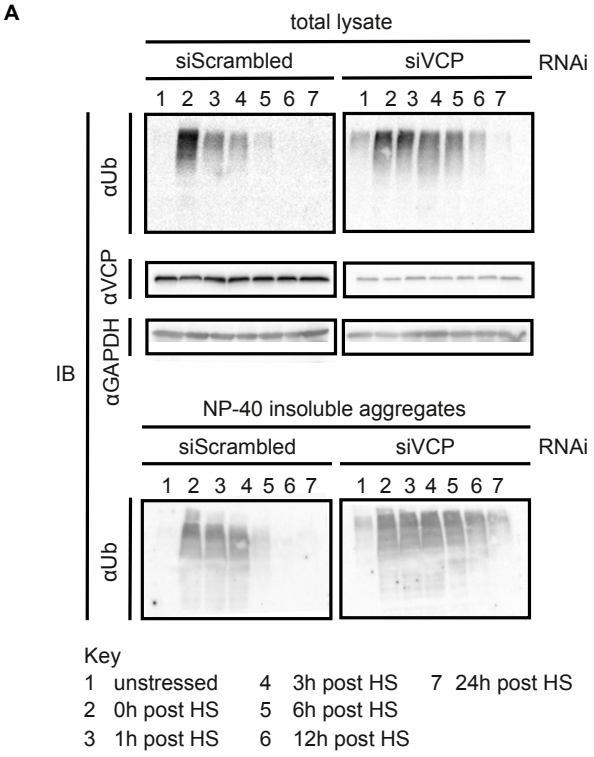
A
total lysate
siScrambled
siVCP
RNAi
1 2 3 4 5 6 7
1 2 3 4 5 6 7
αUb
αVCP
αGAPDH
IB
NP-40 insoluble aggregates
siScrambled
siVCP
RNAi
1 2 3 4 5 6 7
1 2 3 4 5 6 7
αUb
Key
1 unstressed
2 0h post HS
3 1h post HS
4 3h post HS
5 6h post HS
6 12h post HS
7 24h post HS

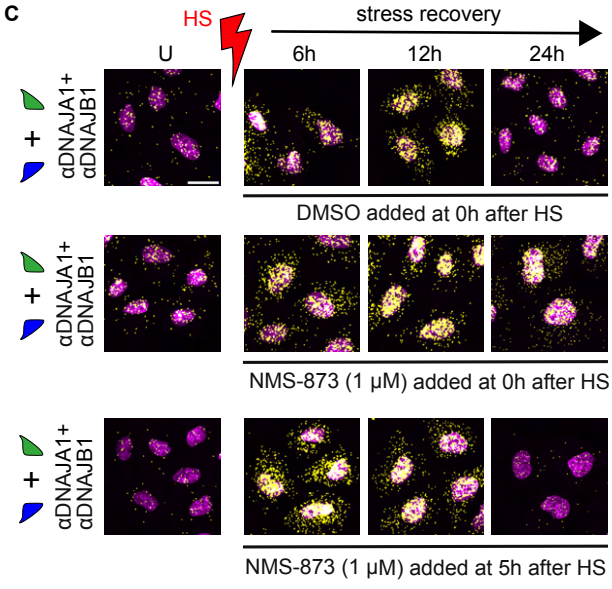
C
HS
stress recovery
U
6h
12h
24h
αDNAJA1+
αDNAJB1
DMSO added at 0h after HS
NMS-873 (1 μM) added at 0h after HS
NMS-873 (1 μM) added at 5h after HS

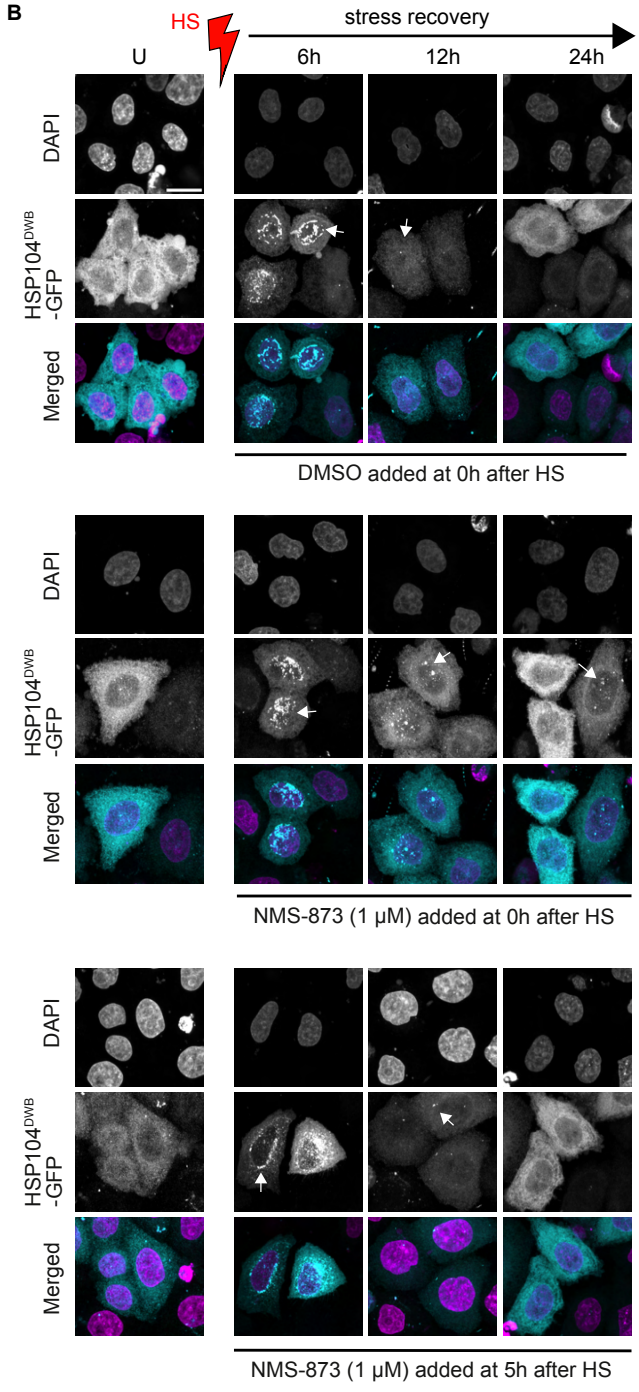
B
HS
stress recovery
U
6h
12h
24h
DAPI
HSP104DWB-GFP
Merged
DMSO added at 0h after HS
NMS-873 (1 μM) added at 0h after HS
NMS-873 (1 μM) added at 5h after HS

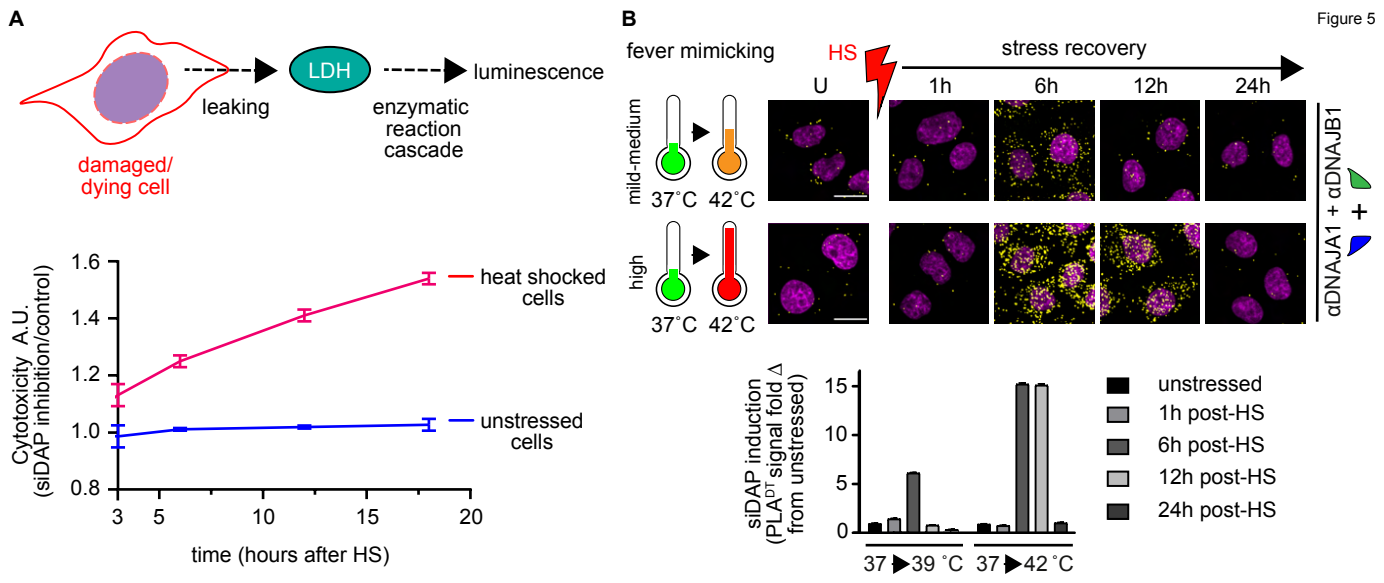
A
LDH
leaking
luminescence
enzymatic reaction cascade
damaged/ dying cell
Cytotoxicity A.U. (siDAP inhibition/control)
1.6
1.4
1.2
1.0
0.8
3
5
10
15
20
time (hours after HS)
heat shocked cells
unstressed cells
B
fever mimicking
HS
stress recovery
U
1h
6h
12h
24h
mild-medium
37˚C 42˚C
high
37˚C 42˚C
αDNAJA1 + αDNAJB1
siDAP induction (PLA^DT signal fold Δ from unstressed)
15
10
5
0
37 ▶ 39 ˚C
37 ▶ 42 ˚C
unstressed
1h post-HS
6h post-HS
12h post-HS
24h post-HS

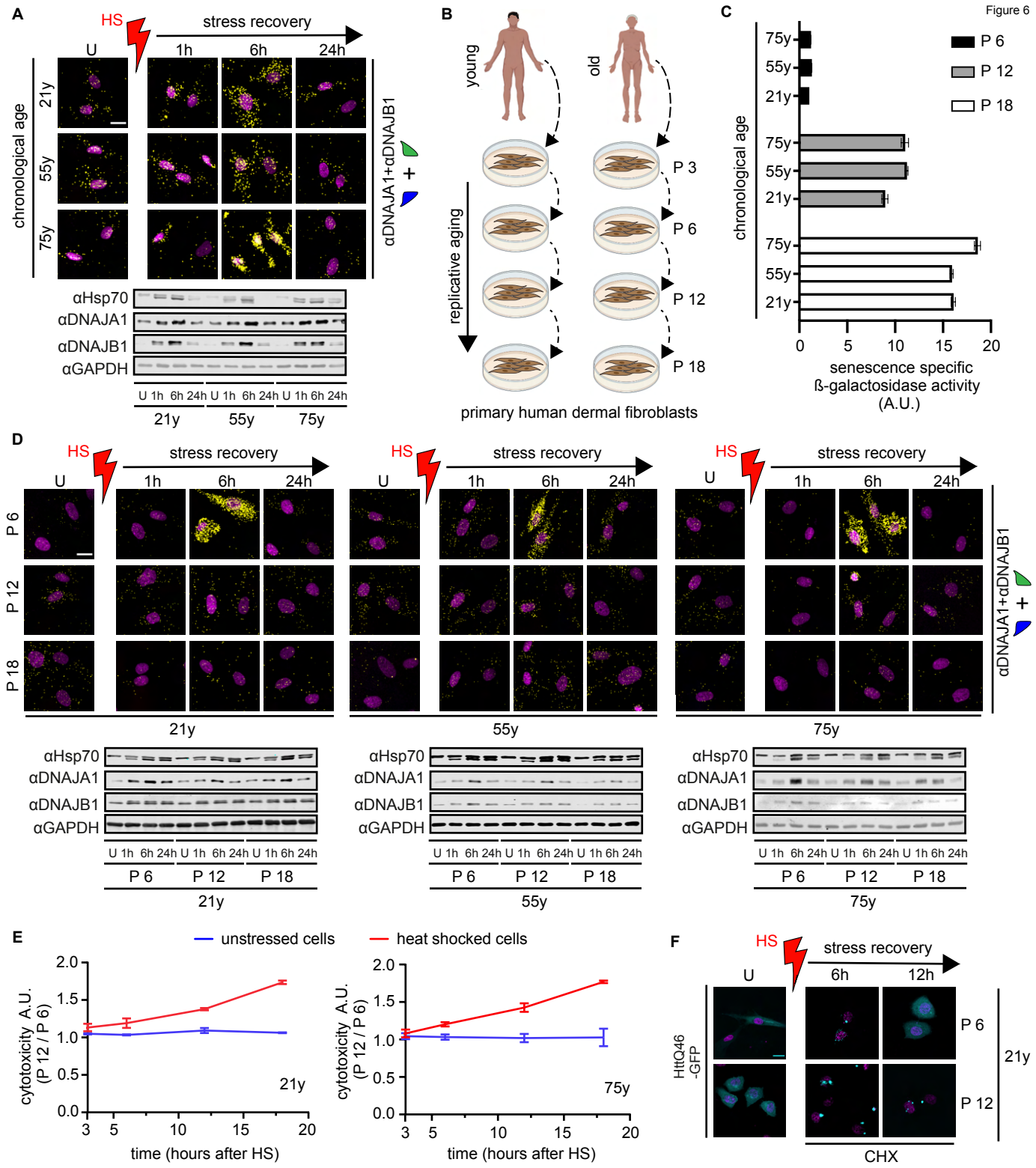
A
HS
stress recovery
U
1h
6h
24h
chronological age
21y
55y
75y
αDNAJA1+αDNAJB1
αHsp70
αDNAJA1
αDNAJB1
αGAPDH
U 1h 6h 24h U 1h 6h 24h U 1h 6h 24h
21y
55y
75y
B
young
old
P 3
P 6
P 12
P 18
replicative aging
primary human dermal fibroblasts
C
P 6
P 12
P 18
chronological age
75y
55y
21y
0
5
10
15
20
senescence specific
ß-galactosidase activity
(A.U.)
D
P 6
P 12
P 18
21y
55y
75y
αHsp70
αDNAJA1
αDNAJB1
αGAPDH
U 1h 6h 24h U 1h 6h 24h U 1h 6h 24h
P 6
P 12
P 18
E
unstressed cells
heat shocked cells
cytotoxicity A.U.
(P 12 / P 6)
2.0
1.5
1.0
0.5
0.0
3
5
10
15
20
time (hours after HS)
21y
75y
F
HS
stress recovery
U
6h
12h
HttQ46
-GFP
P 6
P 12
21y
CHX

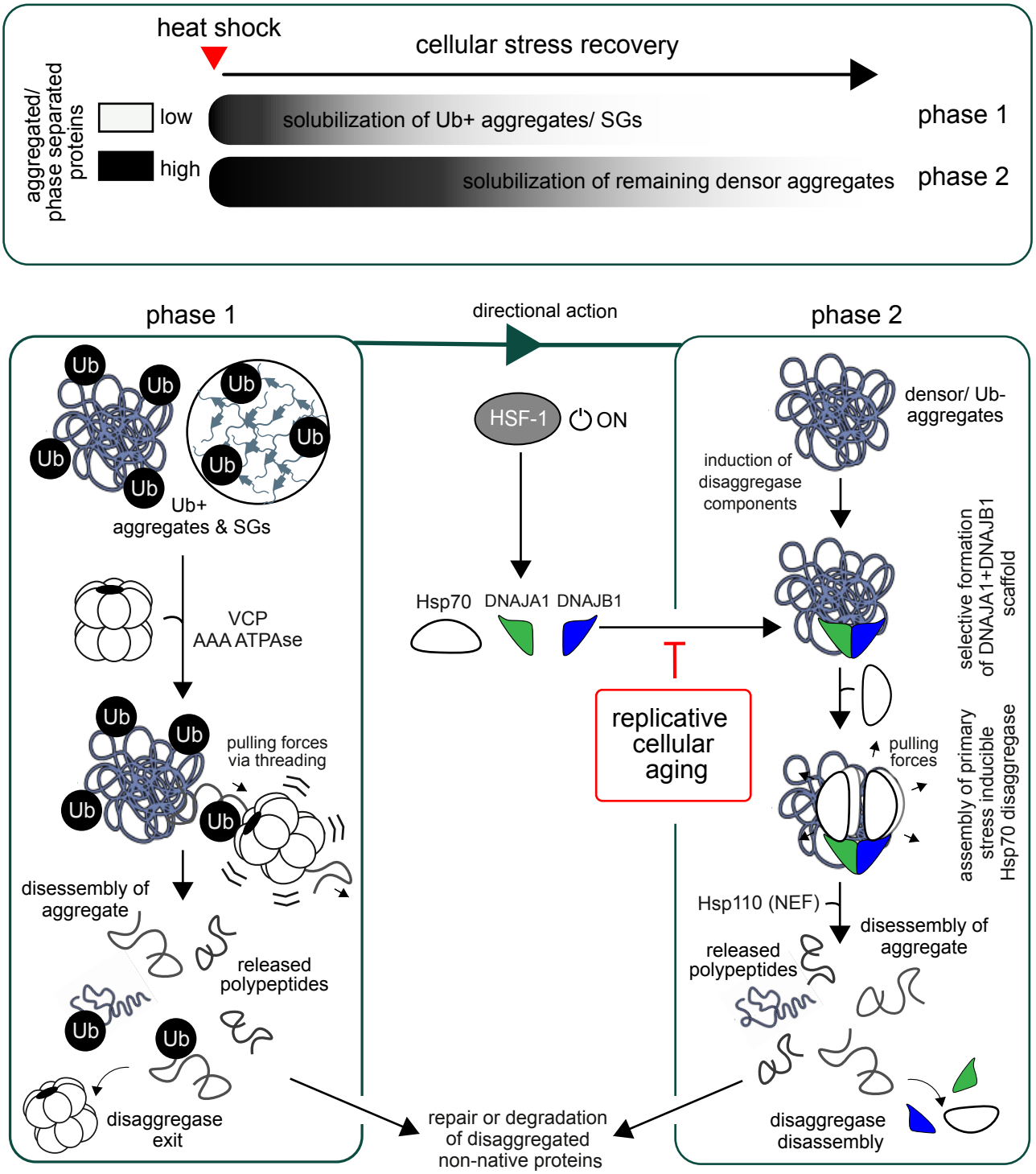
heat shock
cellular stress recovery
aggregated/ phase separated proteins
low
high
solubilization of Ub+ aggregates/ SGs
phase 1
solubilization of remaining densor aggregates
phase 2
phase 1
directional action
phase 2
Ub
Ub+ aggregates & SGs
VCP AAA ATPAse
pulling forces via threading
disessembly of aggregate
released polypeptides
disaggregase exit
predominated by VCP disaggregase activity
HSF-1
ON
Hsp70
DNAJA1
DNAJB1
replicative cellular aging
densor/ Ub-aggregates
induction of disaggregase components
selective formation of DNAJA1+DNAJB1 scaffold
pulling forces
assembly of primary stress inducible Hsp70 disaggregase
Hsp110 (NEF)
disessembly of aggregate
released polypeptides
disaggregase disassembly
repair or degradation of disaggregated non-native proteins
predominated by siDAP induced Hsp70 disaggregase activity

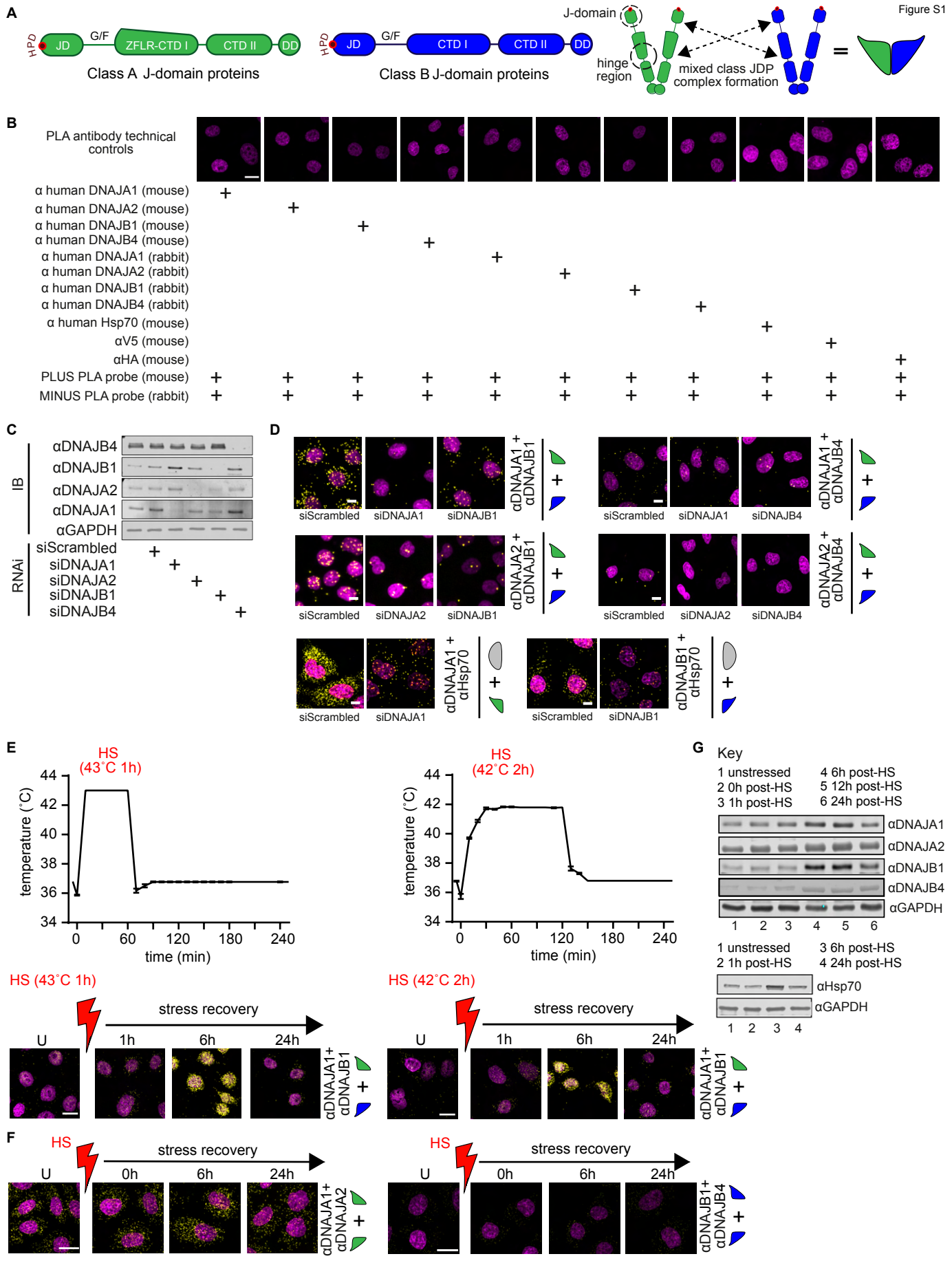
A
HPD
JD
G/F
ZFLR-CTD I
CTD II
DD
Class A J-domain proteins
HPD
JD
G/F
CTD I
CTD II
DD
Class B J-domain proteins
J-domain
hinge region
mixed class JDP complex formation
=
B
PLA antibody technical controls
α human DNAJA1 (mouse)
α human DNAJA2 (mouse)
α human DNAJB1 (mouse)
α human DNAJB4 (mouse)
α human DNAJA1 (rabbit)
α human DNAJA2 (rabbit)
α human DNAJB1 (rabbit)
α human DNAJB4 (rabbit)
α human Hsp70 (mouse)
αV5 (mouse)
αHA (mouse)
PLUS PLA probe (mouse)
MINUS PLA probe (rabbit)
C
IB
αDNAJB4
αDNAJB1
αDNAJA2
αDNAJA1
αGAPDH
RNAi
siScrambled
siDNAJA1
siDNAJA2
siDNAJB1
siDNAJB4
D
siScrambled
siDNAJA1
siDNAJB1
αDNAJA1 + αDNAJB1
siScrambled
siDNAJA1
siDNAJB4
αDNAJA1 + αDNAJB4
siScrambled
siDNAJA2
siDNAJB1
αDNAJA2 + αDNAJB1
siScrambled
siDNAJA2
siDNAJB4
αDNAJA2 + αDNAJB4
siScrambled
siDNAJA1
αDNAJA1 + αHsp70
siScrambled
siDNAJB1
αDNAJB1 + αHsp70
E
HS (43˚C 1h)
temperature (˚C)
time (min)
HS (42˚C 2h)
temperature (˚C)
time (min)
HS (43˚C 1h)
stress recovery
U
1h
6h
24h
αDNAJA1+ αDNAJB1
HS (42˚C 2h)
stress recovery
U
1h
6h
24h
αDNAJA1+ αDNAJB1
G
Key
1 unstressed
2 0h post-HS
3 1h post-HS
4 6h post-HS
5 12h post-HS
6 24h post-HS
αDNAJA1
αDNAJA2
αDNAJB1
αDNAJB4
αGAPDH
1 unstressed
2 1h post-HS
3 6h post-HS
4 24h post-HS
αHsp70
αGAPDH
F
HS
stress recovery
U
0h
6h
24h
αDNAJA1+ αDNAJA2
HS
stress recovery
U
0h
6h
24h
αDNAJB1+ αDNAJB4

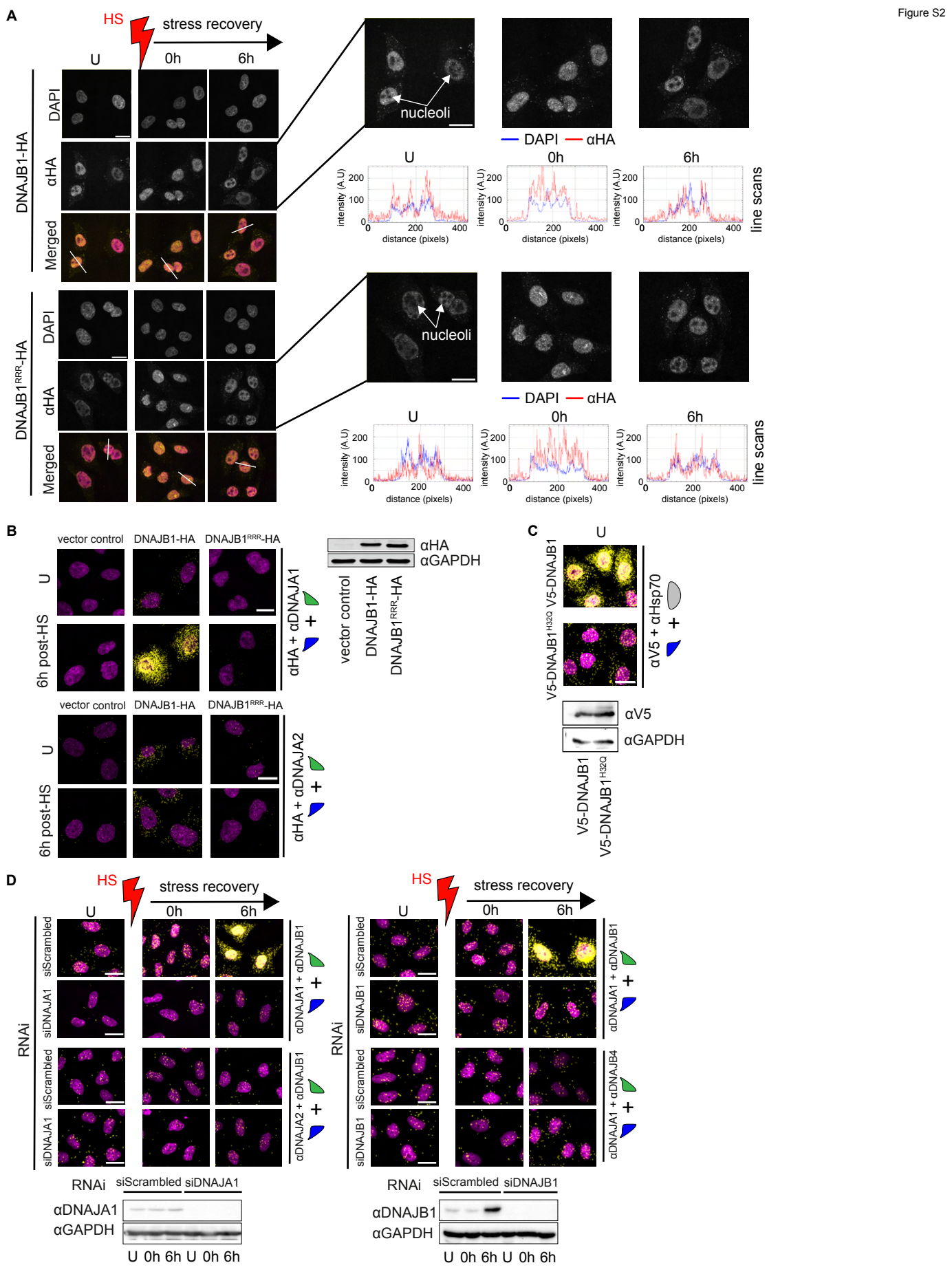
A
HS
stress recovery
U
0h
6h
DNAJB1-HA
DAPI
αHA
Merged
nucleoli
DAPI αHA
intensity (A.U)
distance (pixels)
line scans
DNAJB1RRR-HA
B
vector control
DNAJB1-HA
DNAJB1RRR-HA
U
6h post-HS
αHA + αDNAJA1
αHA + αDNAJA2
αHA
αGAPDH
C
V5-DNAJB1
V5-DNAJB1H32Q
αV5 + αHsp70
αV5
αGAPDH
D
RNAi
siScrambled
siDNAJA1
siDNAJB1
αDNAJA1 + αDNAJB1
αDNAJA2 + αDNAJB1
αDNAJA1 + αDNAJB4
αDNAJA1
αDNAJB1
αGAPDH
U 0h 6h U 0h 6h

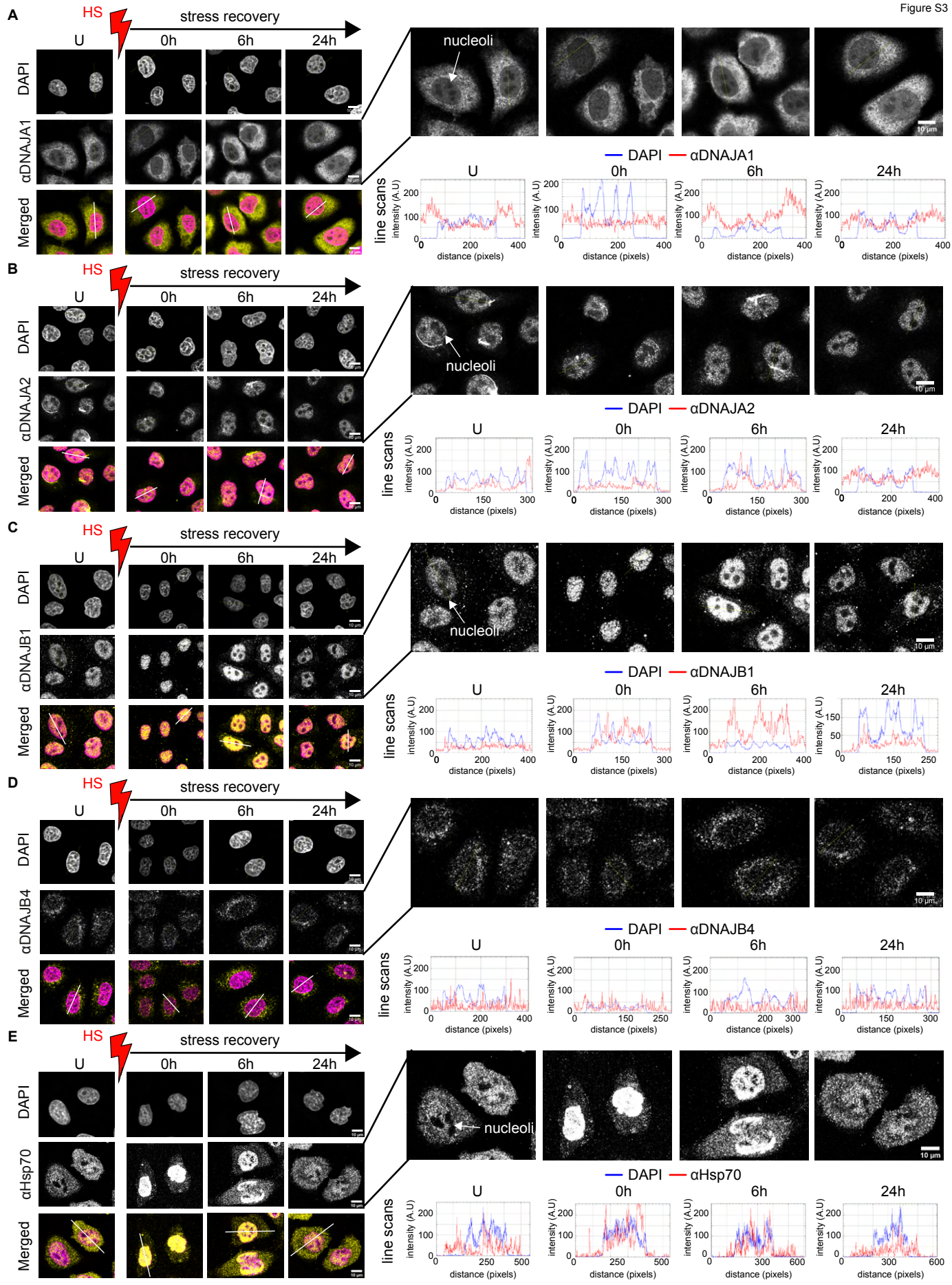
A
HS
stress recovery
U
0h
6h
24h
DAPI
αDNAJA1
Merged
nucleoli
10 µm
DAPI αDNAJA1
line scans
intensity (A.U)
distance (pixels)
B
αDNAJA2
DAPI αDNAJA2
C
αDNAJB1
DAPI αDNAJB1
D
αDNAJB4
DAPI αDNAJB4
E
αHsp70
DAPI αHsp70

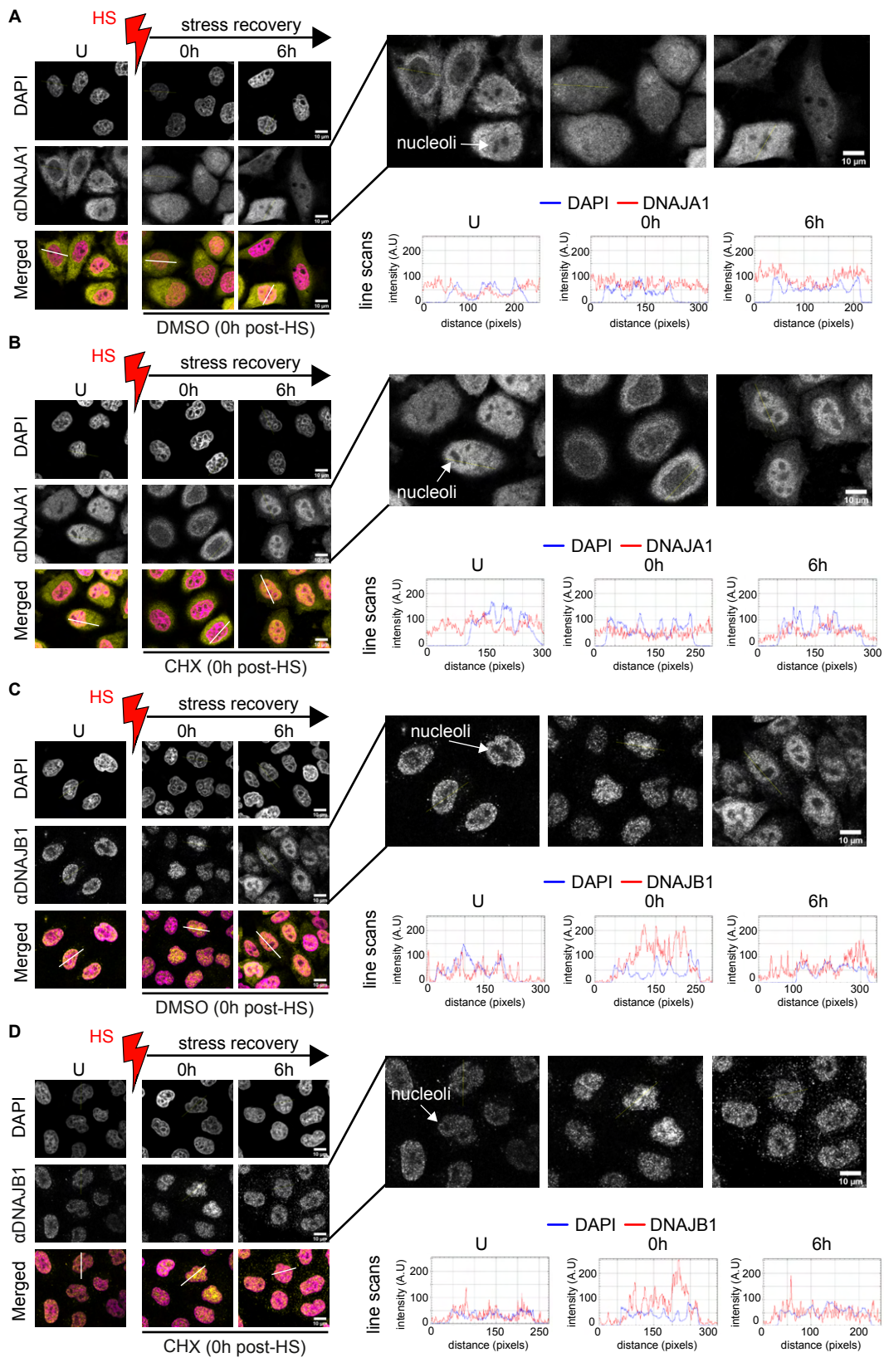
A
HS
stress recovery
U
0h
6h
DAPI
αDNAJA1
Merged
DMSO (0h post-HS)
nucleoli
10 µm
DAPI
DNAJA1
line scans
intensity (A.U)
distance (pixels)
B
CHX (0h post-HS)
C
αDNAJB1
DMSO (0h post-HS)
D
CHX (0h post-HS)

Figure S5

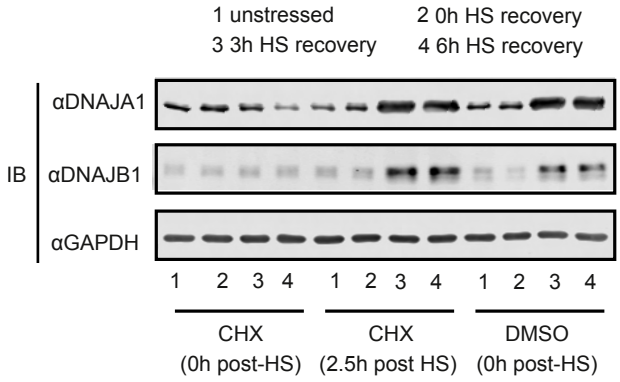
1 unstressed
2 0h HS recovery
3 3h HS recovery
4 6h HS recovery
IB
αDNAJA1
αDNAJB1
αGAPDH
1 2 3 4 1 2 3 4 1 2 3 4
CHX
(0h post-HS)
CHX
(2.5h post HS)
DMSO
(0h post-HS)

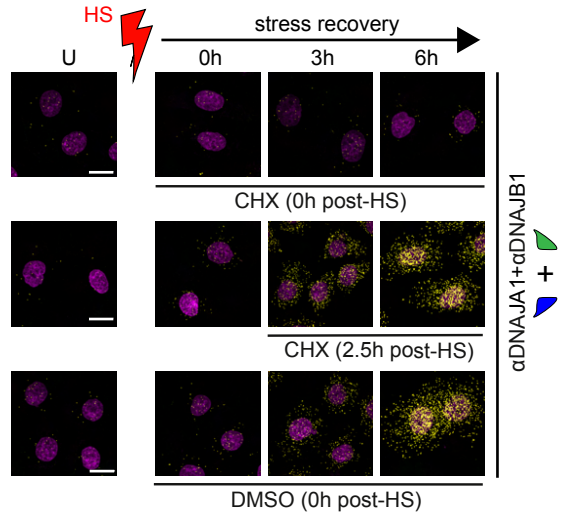
HS
stress recovery
U
0h
3h
6h
CHX (0h post-HS)
CHX (2.5h post-HS)
DMSO (0h post-HS)
αDNAJA1+αDNAJB1
+

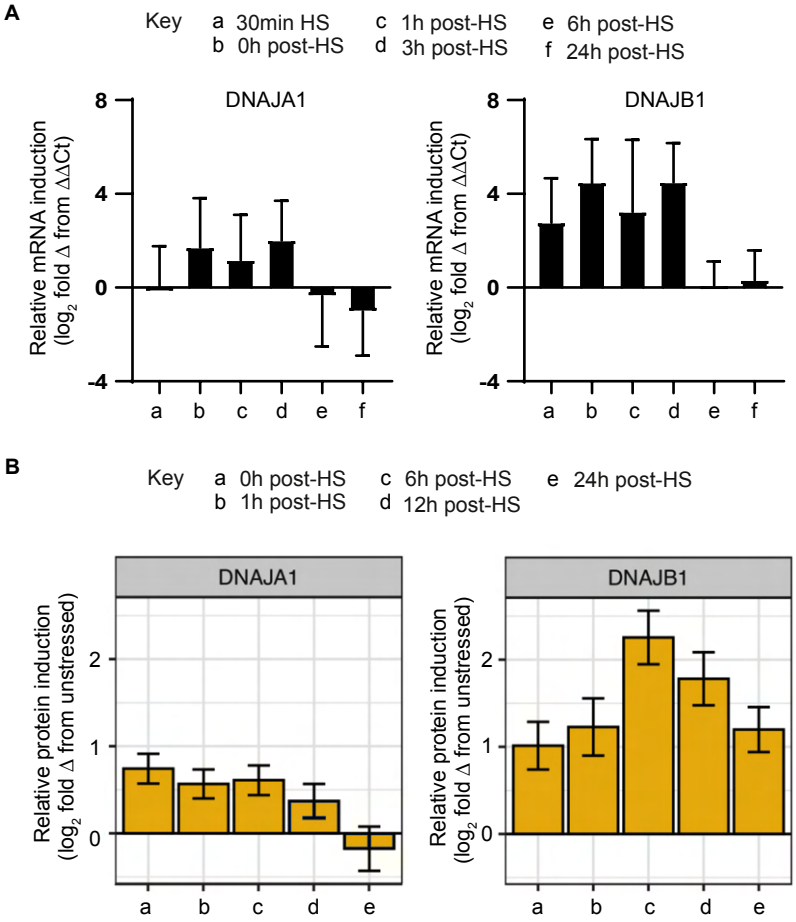
A
Key
a 30min HS
b 0h post-HS
c 1h post-HS
d 3h post-HS
e 6h post-HS
f 24h post-HS
DNAJA1
DNAJB1
Relative mRNA induction
(log2 fold Δ from ΔΔCt)
8
4
0
-4
a b c d e f
B
Key
a 0h post-HS
b 1h post-HS
c 6h post-HS
d 12h post-HS
e 24h post-HS
DNAJA1
DNAJB1
Relative protein induction
(log2 fold Δ from unstressed)
2
1
0
a b c d e

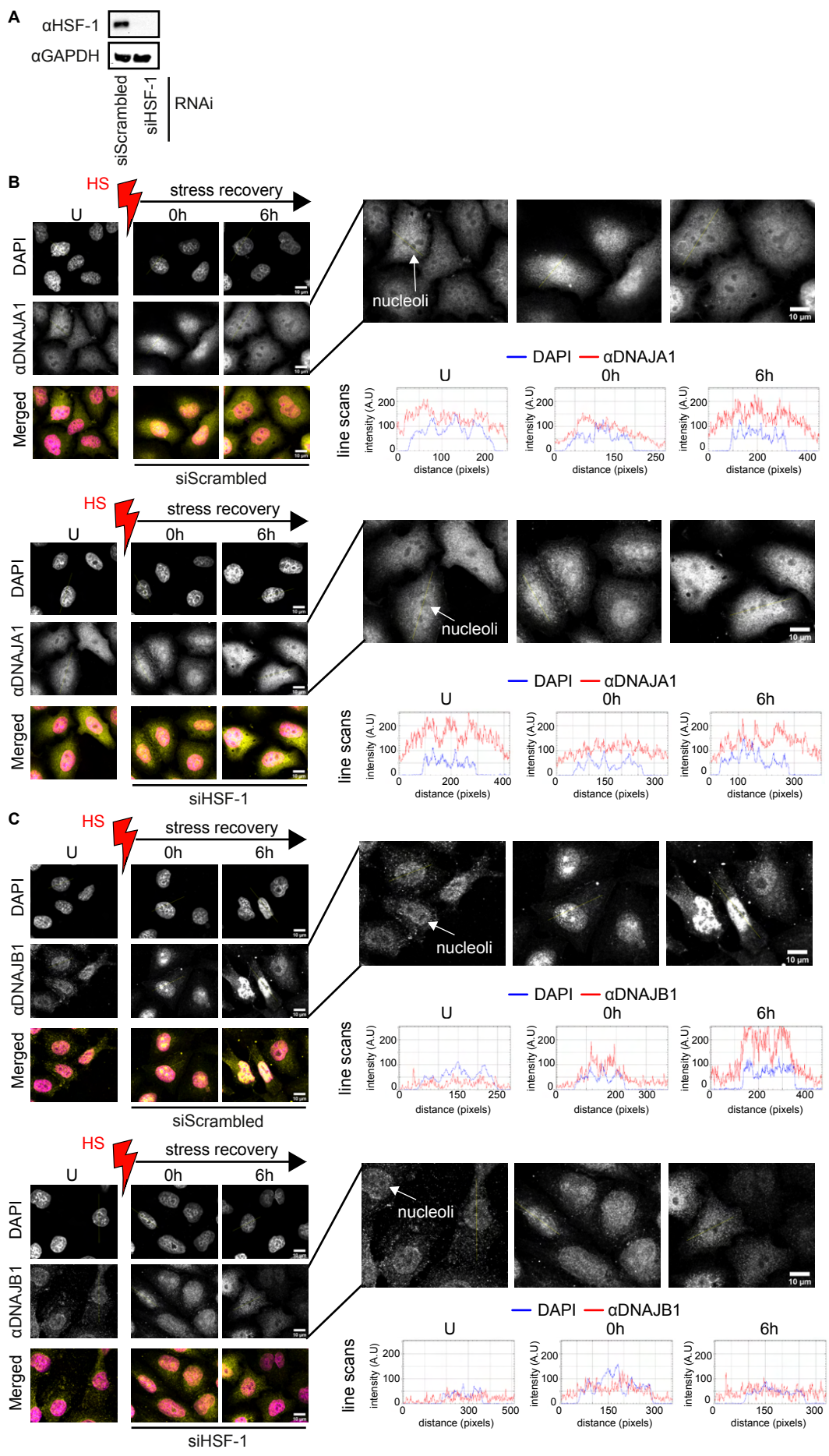
A
αHSF-1
αGAPDH
siScrambled
siHSF-1
RNAi
B
HS
stress recovery
U
0h
6h
DAPI
αDNAJA1
Merged
siScrambled
nucleoli
10 µm
DAPI αDNAJA1
line scans
intensity (A.U)
distance (pixels)
siHSF-1
C
αDNAJB1
DAPI αDNAJB1

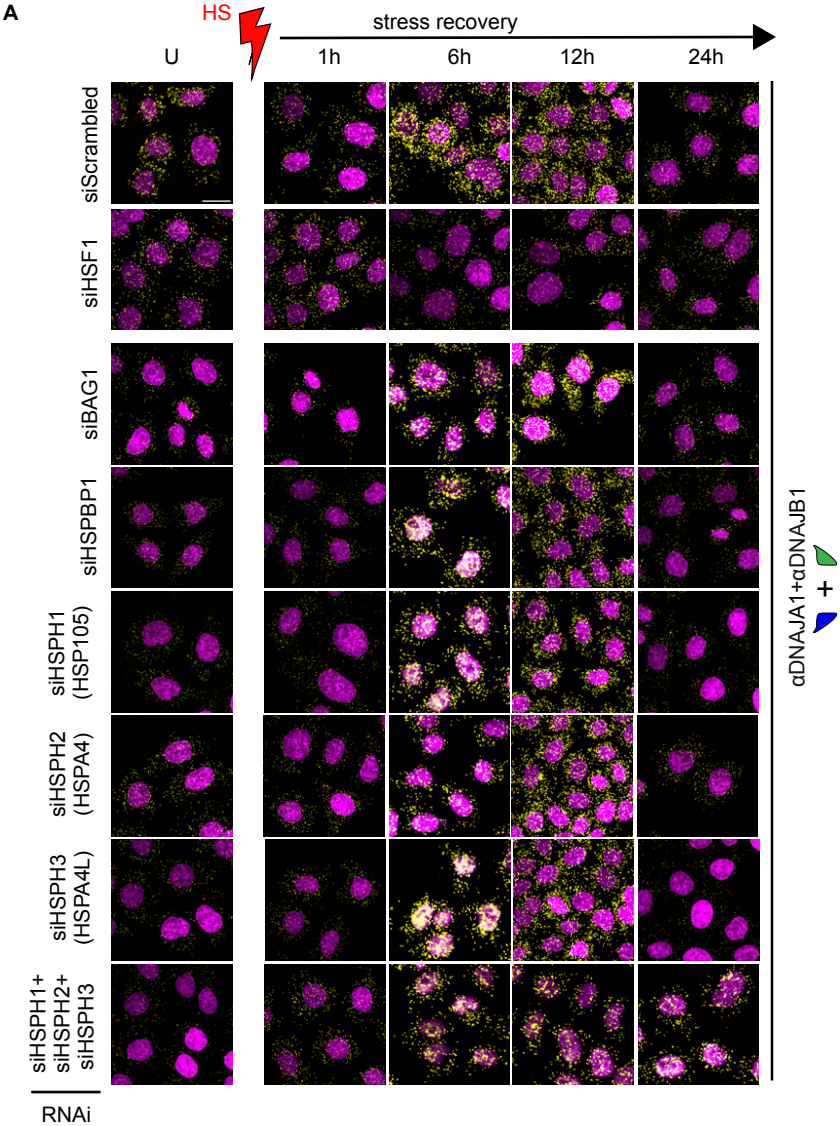
A
HS
stress recovery
U
1h
6h
12h
24h
siScrambled
siHSF1
siBAG1
siHSPBP1
siHSPH1 (HSP105)
siHSPH2 (HSPA4)
siHSPH3 (HSPA4L)
siHSPH1+ siHSPH2+ siHSPH3
RNAi
αDNAJA1+αDNAJB1
+

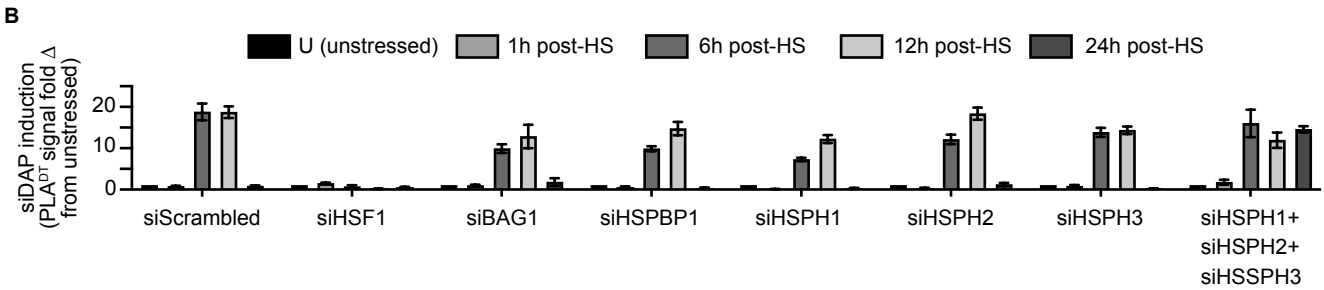
B
U (unstressed)
1h post-HS
6h post-HS
12h post-HS
24h post-HS
siDAP induction (PLA^DT signal fold Δ from unstressed)
20
10
0
siScrambled
siHSF1
siBAG1
siHSPBP1
siHSPH1
siHSPH2
siHSPH3
siHSPH1+ siHSPH2+ siHSSPH3

Figure S9

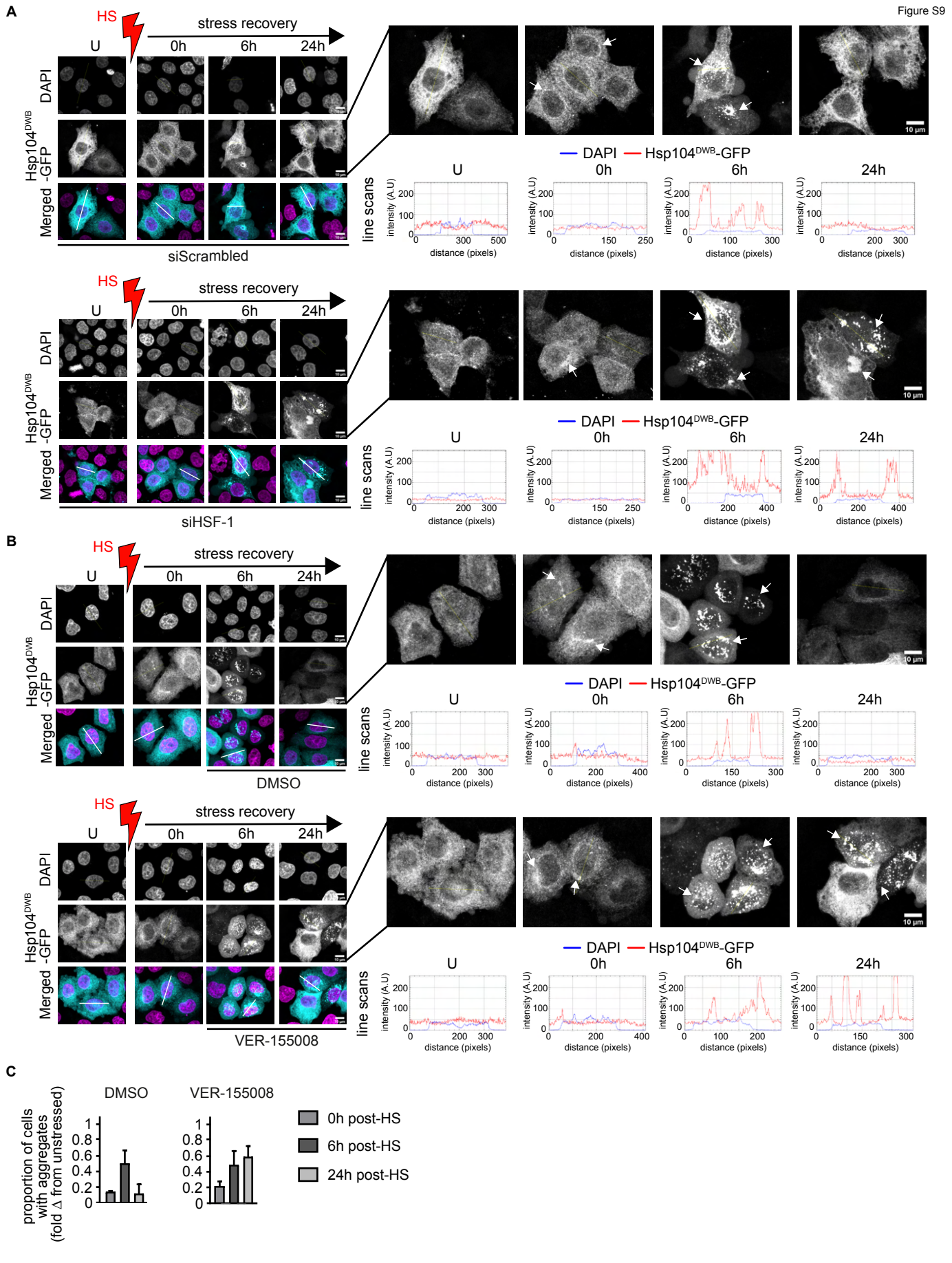
A
HS
stress recovery
U
0h
6h
24h
DAPI
Hsp104DWB -GFP
Merged
siScrambled
siHSF-1
B
DMSO
VER-155008
DAPI
Hsp104DWB-GFP
line scans
intensity (A.U)
distance (pixels)
10 µm
C
DMSO
VER-155008
proportion of cells with aggregates (fold Δ from unstressed)
0h post-HS
6h post-HS
24h post-HS

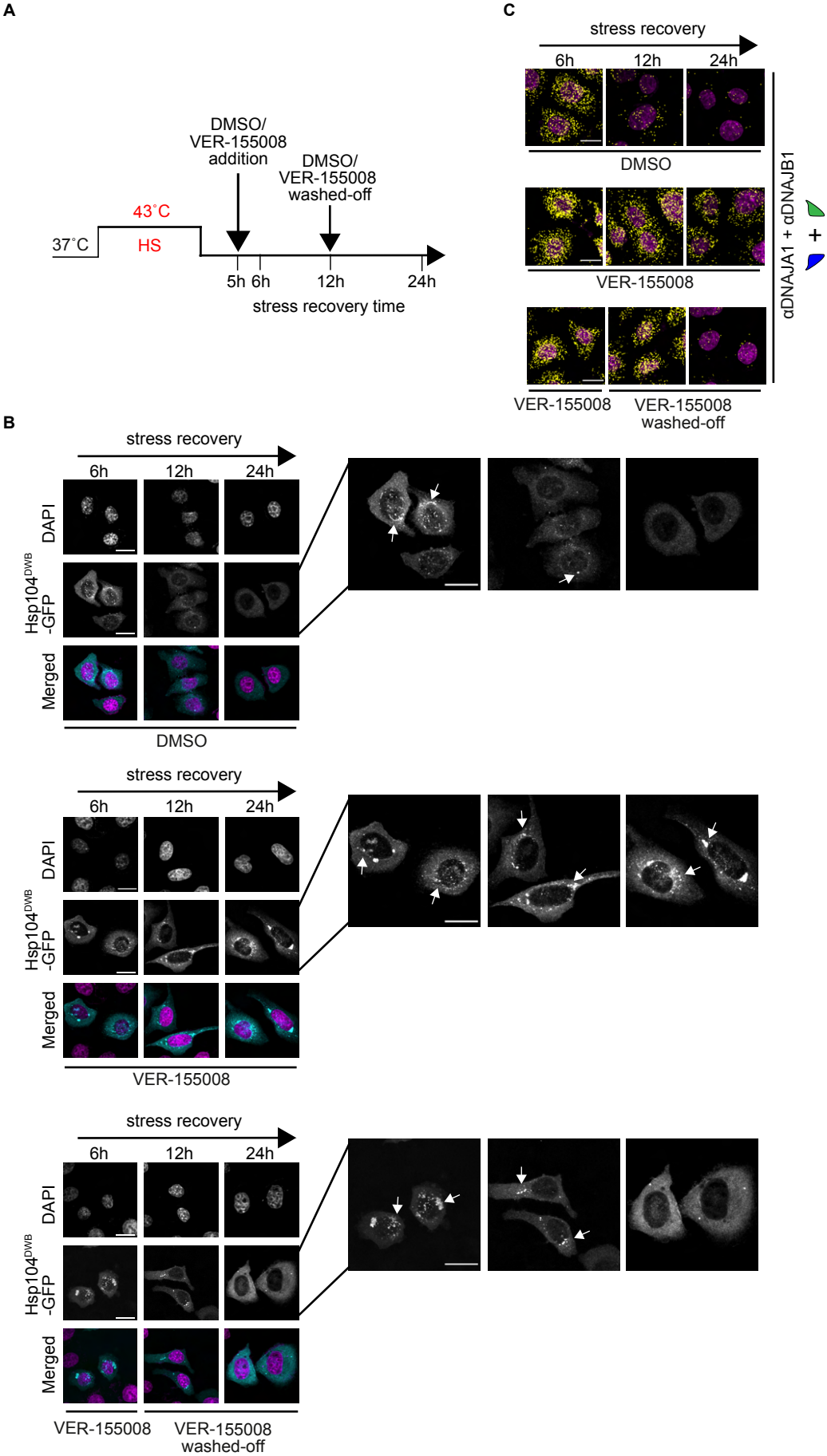
A
DMSO/
VER-155008
addition
DMSO/
VER-155008
washed-off
43˚C
37˚C
HS
5h 6h
12h
24h
stress recovery time
C
stress recovery
6h
12h
24h
DMSO
VER-155008
VER-155008
VER-155008
washed-off
αDNAJA1 + αDNAJB1
B
stress recovery
6h
12h
24h
DAPI
Hsp104DWB
-GFP
Merged
DMSO
VER-155008
VER-155008
VER-155008
washed-off

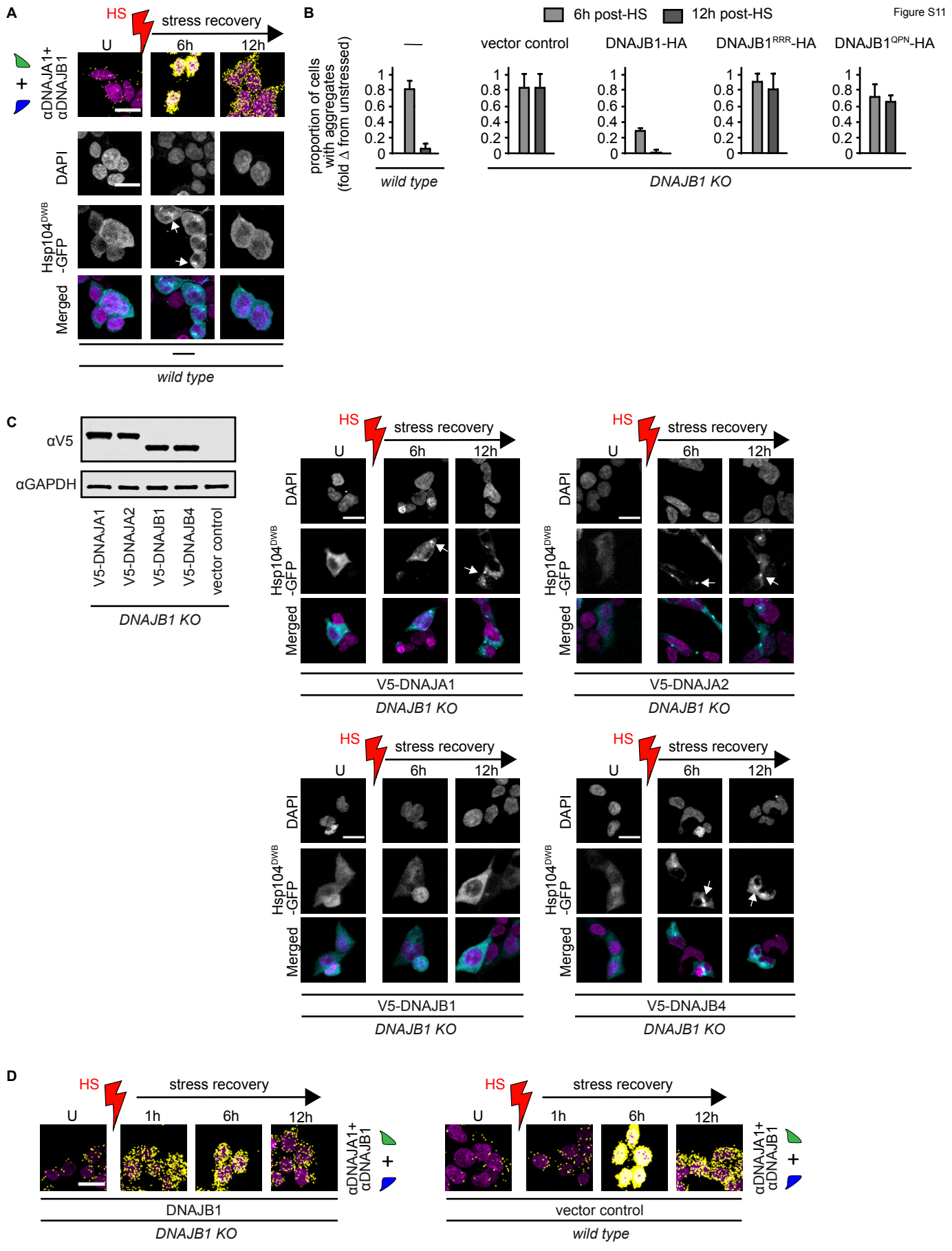
A
HS
stress recovery
U
6h
12h
αDNAJA1+
αDNAJB1
+
DAPI
Hsp104DWB
-GFP
Merged
—
wild type
B
6h post-HS
12h post-HS
proportion of cells
with aggregates
(fold Δ from unstressed)
—
vector control
DNAJB1-HA
DNAJB1RRR-HA
DNAJB1QPN-HA
1
0.8
0.6
0.4
0.2
0
wild type
DNAJB1 KO
C
αV5
αGAPDH
V5-DNAJA1
V5-DNAJA2
V5-DNAJB1
V5-DNAJB4
vector control
DNAJB1 KO
V5-DNAJA1
V5-DNAJA2
V5-DNAJB1
V5-DNAJB4
D
1h
DNAJB1
vector control

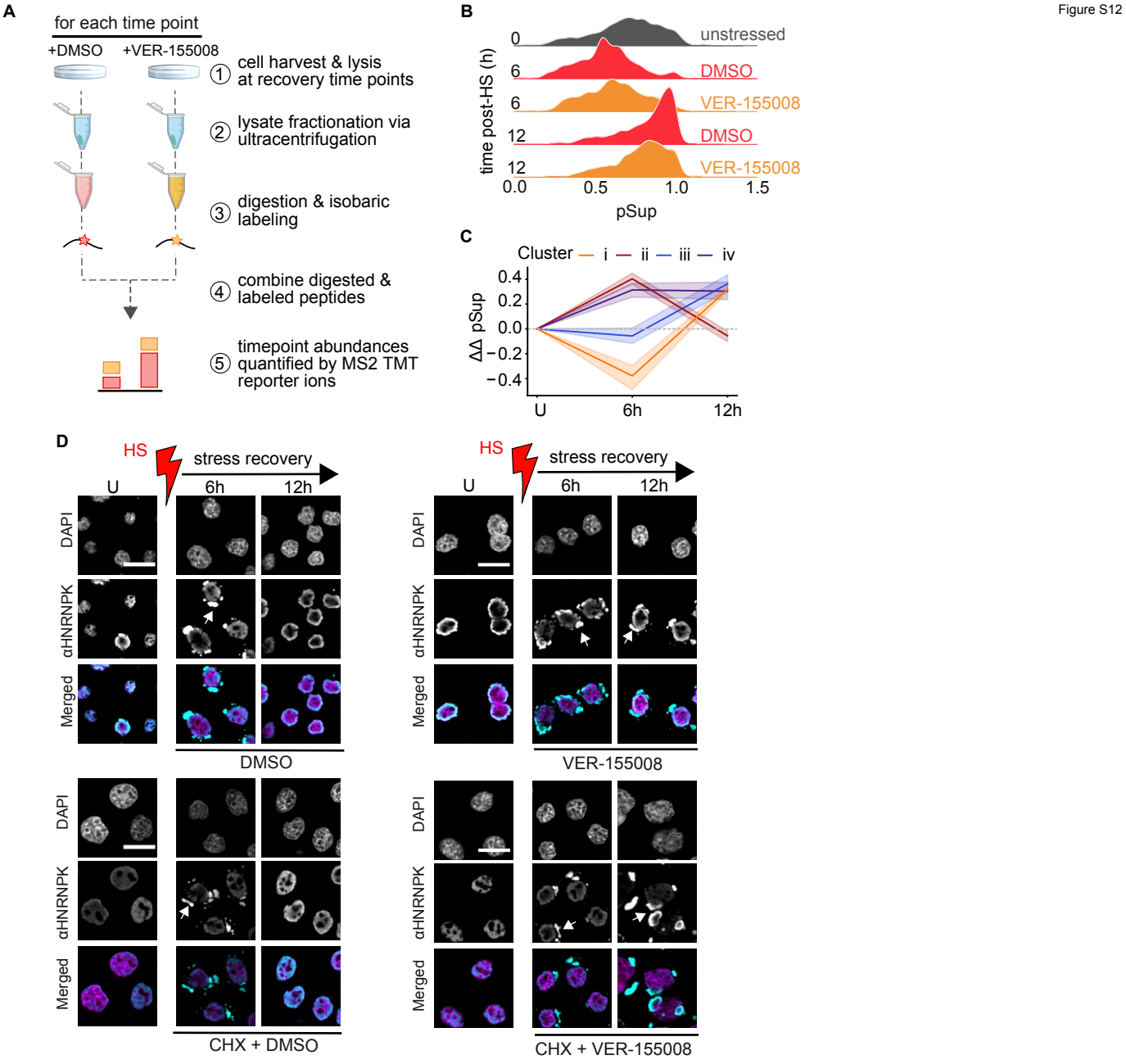
A
for each time point
+DMSO
+VER-155008
① cell harvest & lysis at recovery time points
② lysate fractionation via ultracentrifugation
③ digestion & isobaric labeling
④ combine digested & labeled peptides
⑤ timepoint abundances quantified by MS2 TMT reporter ions
B
time post-HS (h)
0
6
6
12
12
unstressed
DMSO
VER-155008
DMSO
VER-155008
0.0
0.5
1.0
1.5
pSup
C
Cluster i ii iii iv
ΔΔ pSup
0.4
0.2
0.0
−0.2
−0.4
U
6h
12h
D
HS
stress recovery
U
6h
12h
DAPI
αHNRNPK
Merged
DMSO
VER-155008
CHX + DMSO
CHX + VER-155008

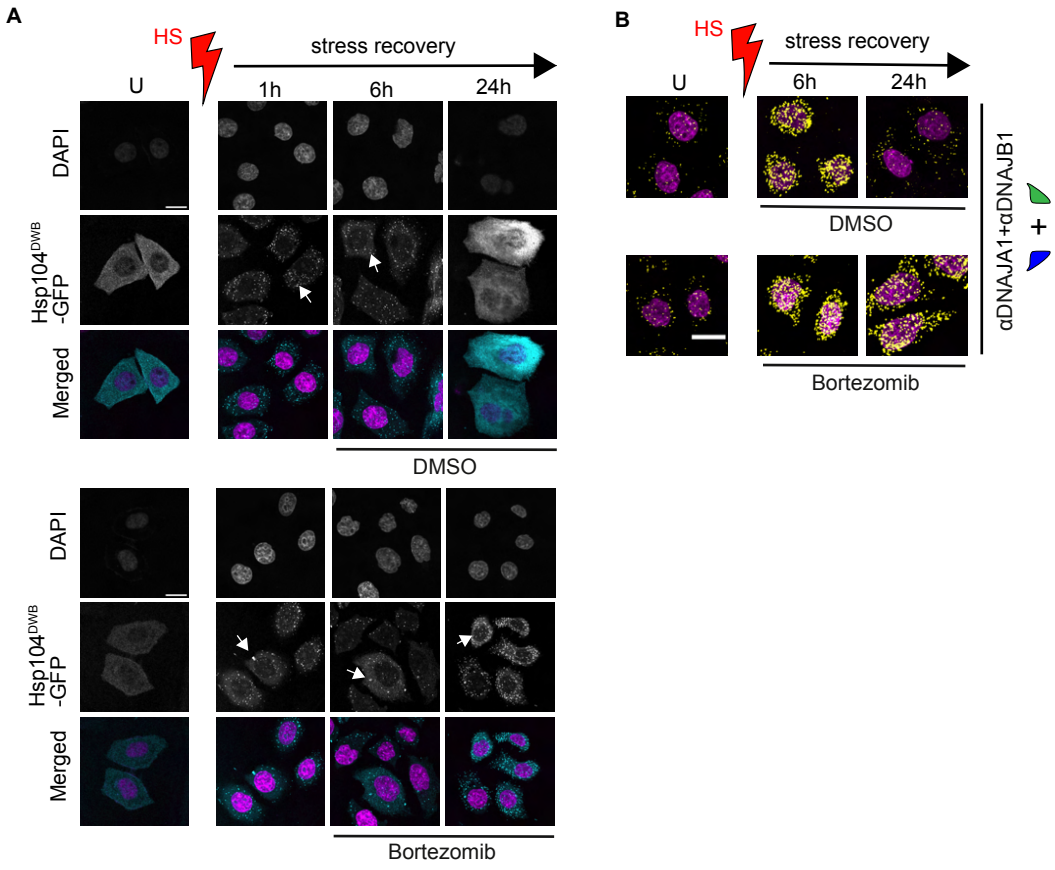
A
HS
stress recovery
U
1h
6h
24h
DAPI
Hsp104DWB -GFP
Merged
DMSO
DAPI
Hsp104DWB -GFP
Merged
Bortezomib
B
HS
stress recovery
U
6h
24h
DMSO
Bortezomib
αDNAJA1+αDNAJB1
+

Figure S14

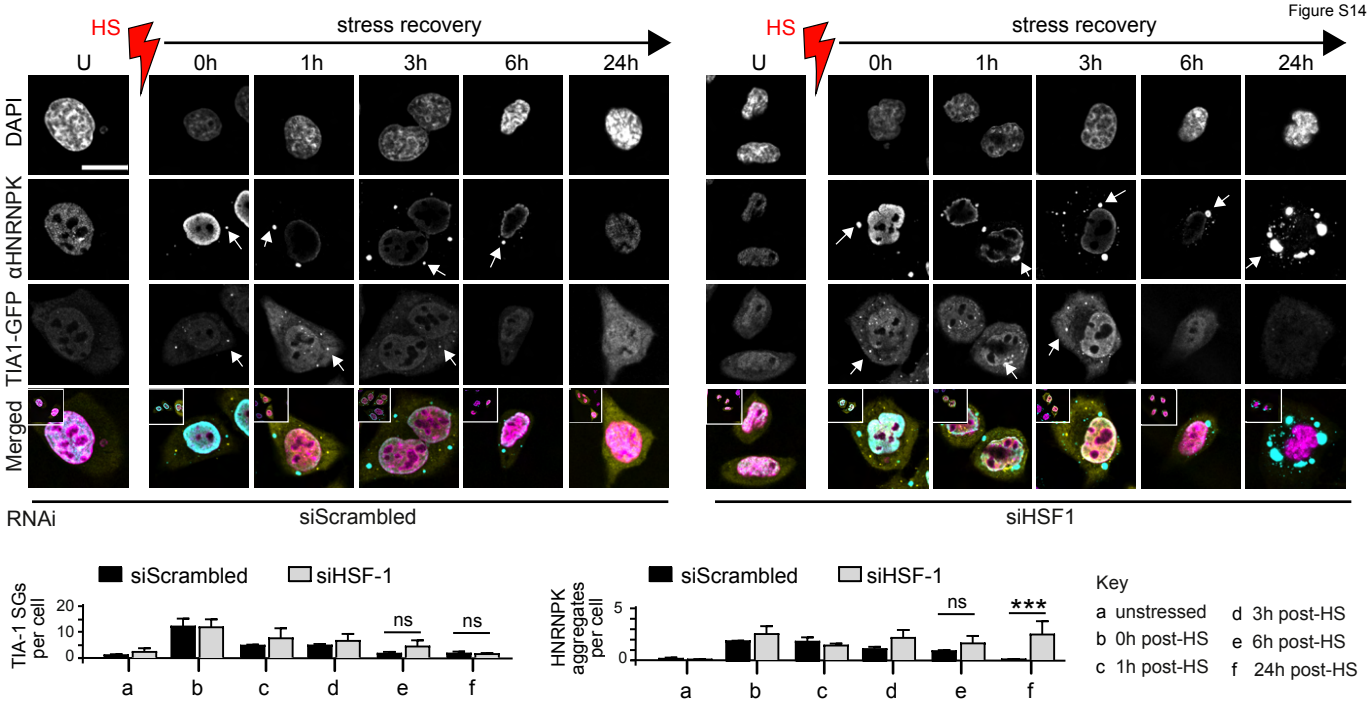
HS
stress recovery
U
0h
1h
3h
6h
24h
DAPI
αHNRNPK
TIA1-GFP
Merged
RNAi
siScrambled
siHSF1
siScrambled
siHSF-1
TIA-1 SGs per cell
20
10
0
ns
ns
a
b
c
d
e
f
HNRNPK aggregates per cell
5
0
ns
***
Key
a unstressed
b 0h post-HS
c 1h post-HS
d 3h post-HS
e 6h post-HS
f 24h post-HS

Figure S15

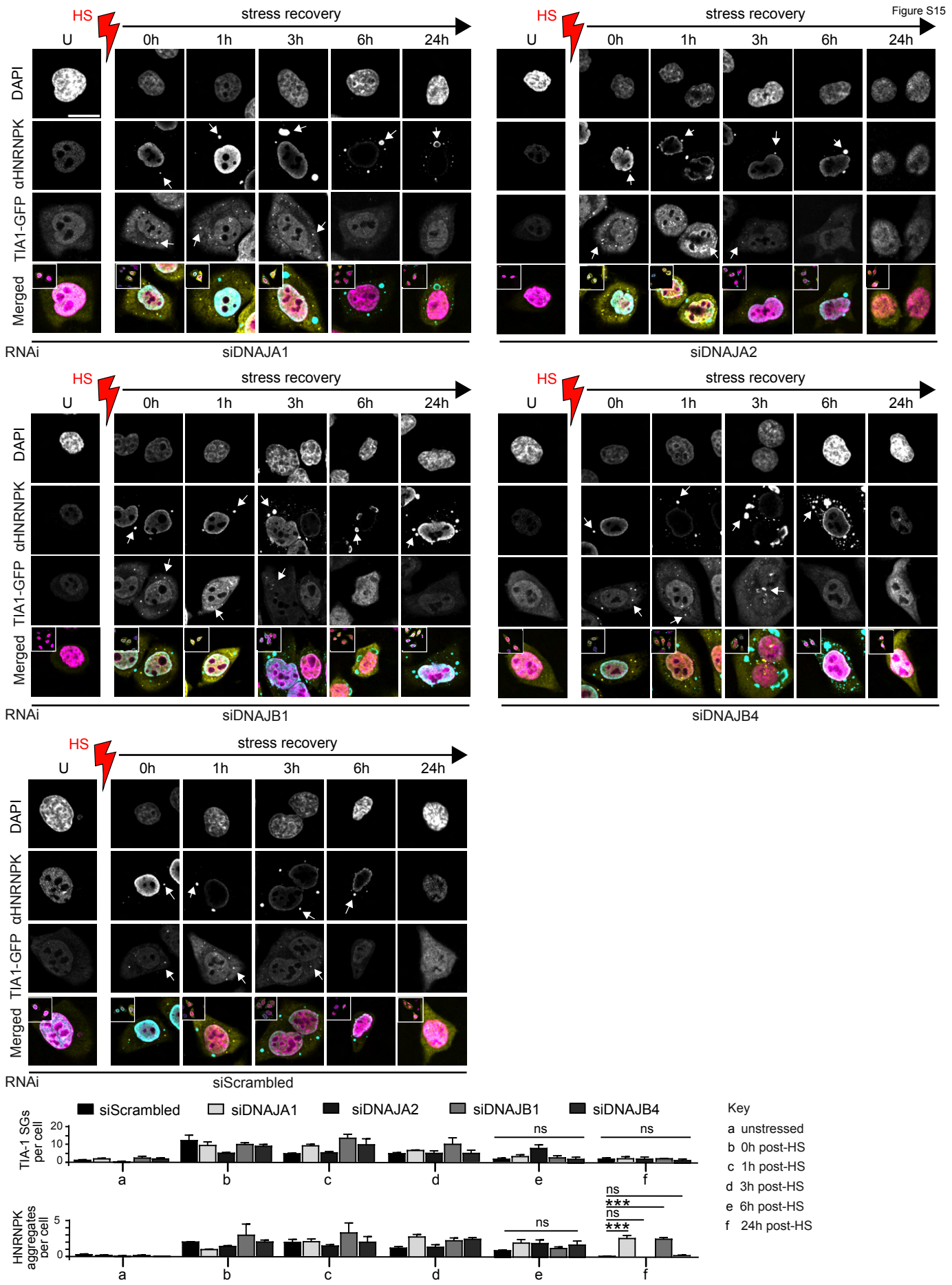
HS
stress recovery
U
0h
1h
3h
6h
24h
DAPI
αHNRNPK
TIA1-GFP
Merged
RNAi
siDNAJA1
siDNAJA2
siDNAJB1
siDNAJB4
siScrambled
siDNAJA1
siDNAJA2
siDNAJB1
siDNAJB4
TIA-1 SGs per cell
HNRNPK aggregates per cell
ns
***
a
b
c
d
e
f
Key
a unstressed
b 0h post-HS
c 1h post-HS
d 3h post-HS
e 6h post-HS
f 24h post-HS

Figure S16

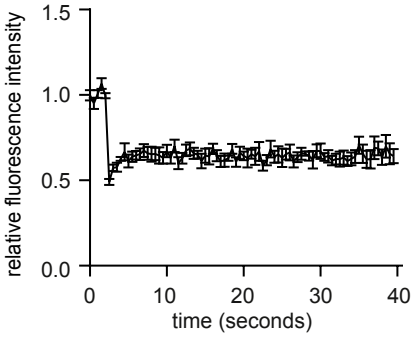
relative fluorescence intensity
1.5
1.0
0.5
0.0
0
10
20
30
40
time (seconds)

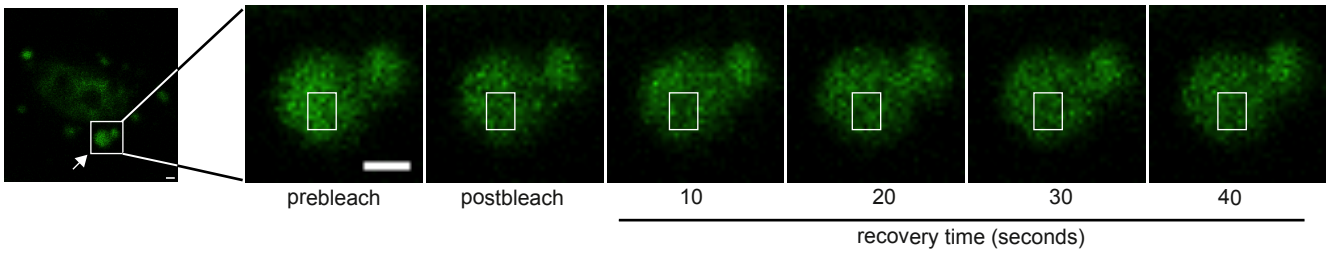
prebleach
postbleach
10
20
30
40
recovery time (seconds)

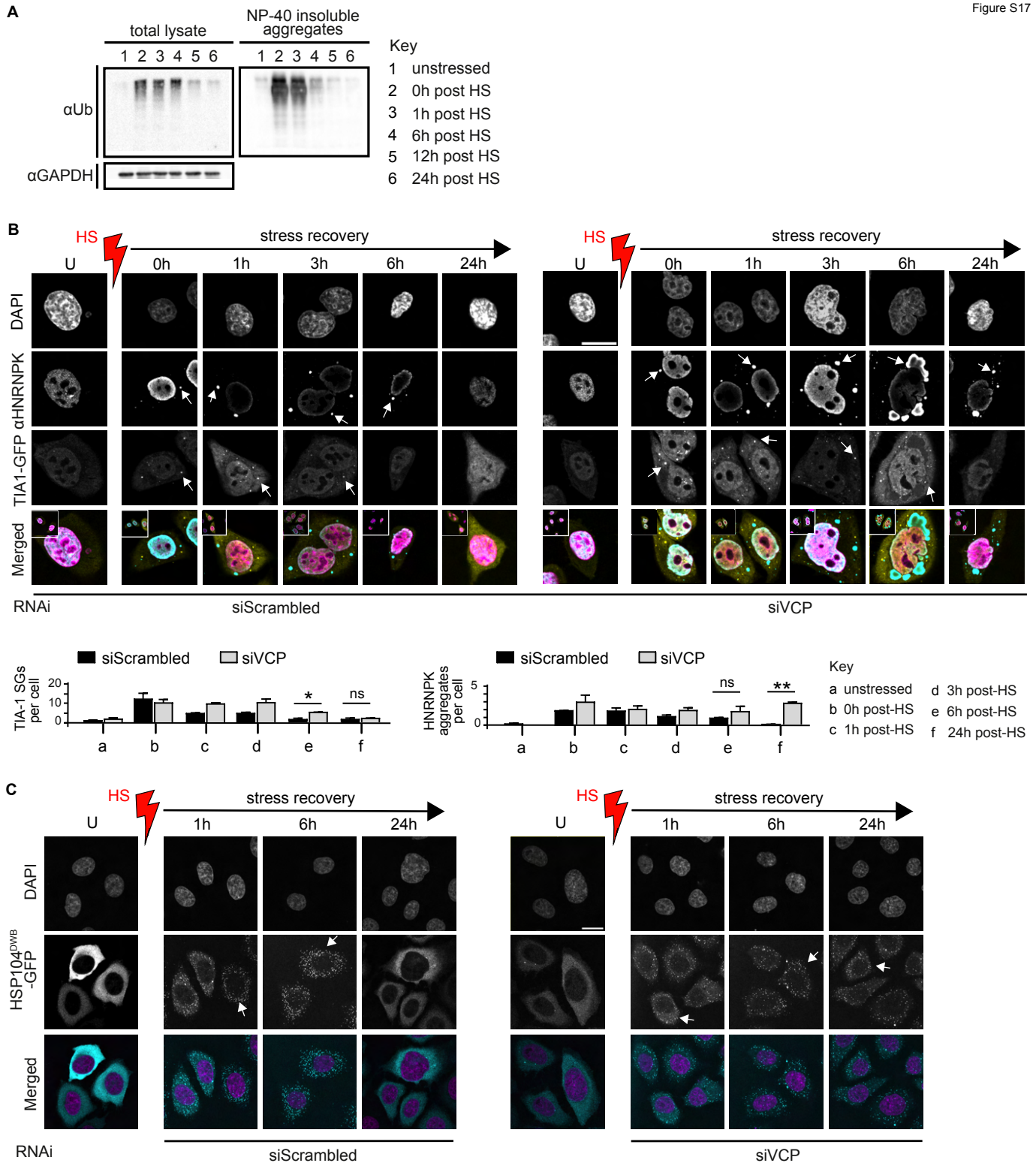
A
total lysate
NP-40 insoluble aggregates
1 2 3 4 5 6
1 2 3 4 5 6
αUb
αGAPDH
Key
1 unstressed
2 0h post HS
3 1h post HS
4 6h post HS
5 12h post HS
6 24h post HS
B
HS
stress recovery
U
0h
1h
3h
6h
24h
DAPI
αHNRNPK
TIA1-GFP
Merged
RNAi
siScrambled
siVCP
siScrambled
siVCP
TIA-1 SGs per cell
20
10
0
*
ns
a
b
c
d
e
f
HNRNPK aggregates per cell
5
0
ns
**
Key
a unstressed
b 0h post-HS
c 1h post-HS
d 3h post-HS
e 6h post-HS
f 24h post-HS
C
HS
stress recovery
U
1h
6h
24h
DAPI
HSP104DWB-GFP
Merged
RNAi
siScrambled
siVCP

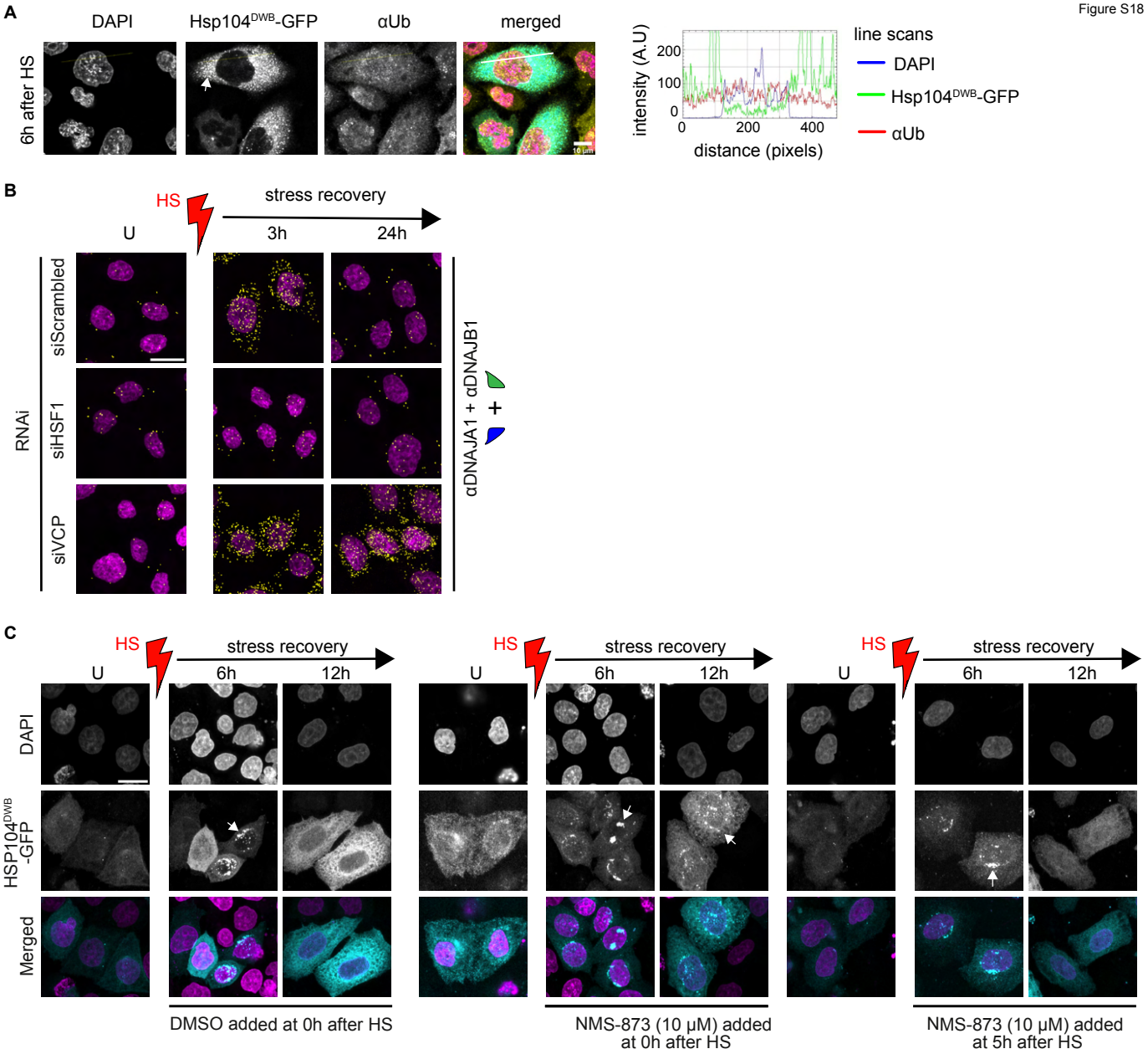
A
DAPI
Hsp104DWB-GFP
αUb
merged
6h after HS
10 µm
intensity (A.U)
200
100
0
0
200
400
distance (pixels)
line scans
DAPI
Hsp104DWB-GFP
αUb
B
HS
stress recovery
U
3h
24h
RNAi
siScrambled
siHSF1
siVCP
αDNAJA1 + αDNAJB1
C
HS
stress recovery
U
6h
12h
DAPI
HSP104DWB-GFP
Merged
DMSO added at 0h after HS
NMS-873 (10 µM) added at 0h after HS
NMS-873 (10 µM) added at 5h after HS

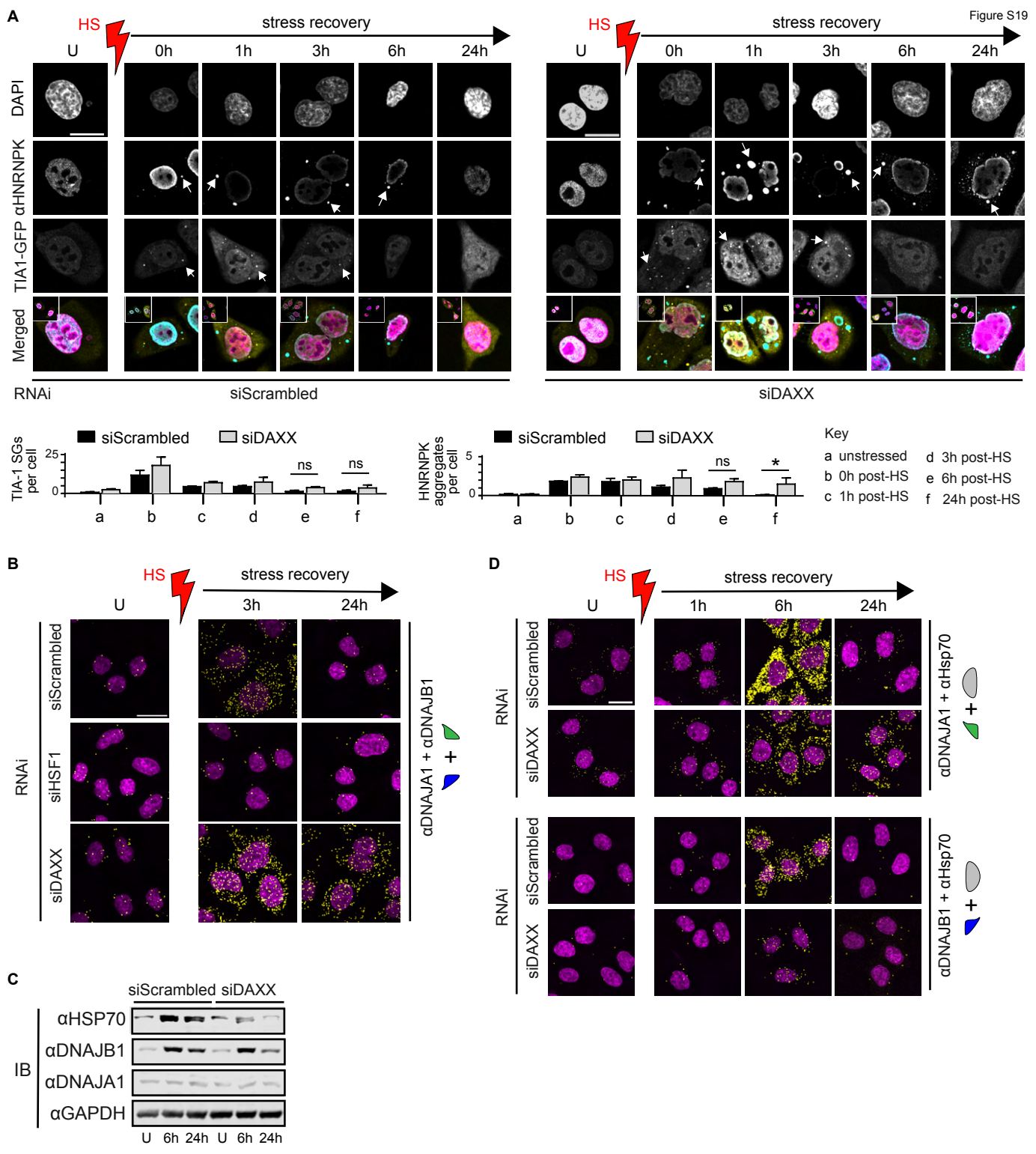
A
HS
stress recovery
U
0h
1h
3h
6h
24h
DAPI
αHNRNPK
TIA1-GFP
Merged
RNAi
siScrambled
siDAXX
siScrambled
siDAXX
TIA-1 SGs per cell
25
0
ns
ns
a
b
c
d
e
f
HNRNPK aggregates per cell
5
0
ns
*
Key
a unstressed
b 0h post-HS
c 1h post-HS
d 3h post-HS
e 6h post-HS
f 24h post-HS
B
HS
stress recovery
U
3h
24h
RNAi
siScrambled
siHSF1
siDAXX
αDNAJA1 + αDNAJB1
+
D
HS
stress recovery
U
1h
6h
24h
RNAi
siScrambled
siDAXX
αDNAJA1 + αHsp70
αDNAJB1 + αHsp70
+
C
siScrambled siDAXX
IB
αHSP70
αDNAJB1
αDNAJA1
αGAPDH
U 6h 24h U 6h 24h

Figure S20

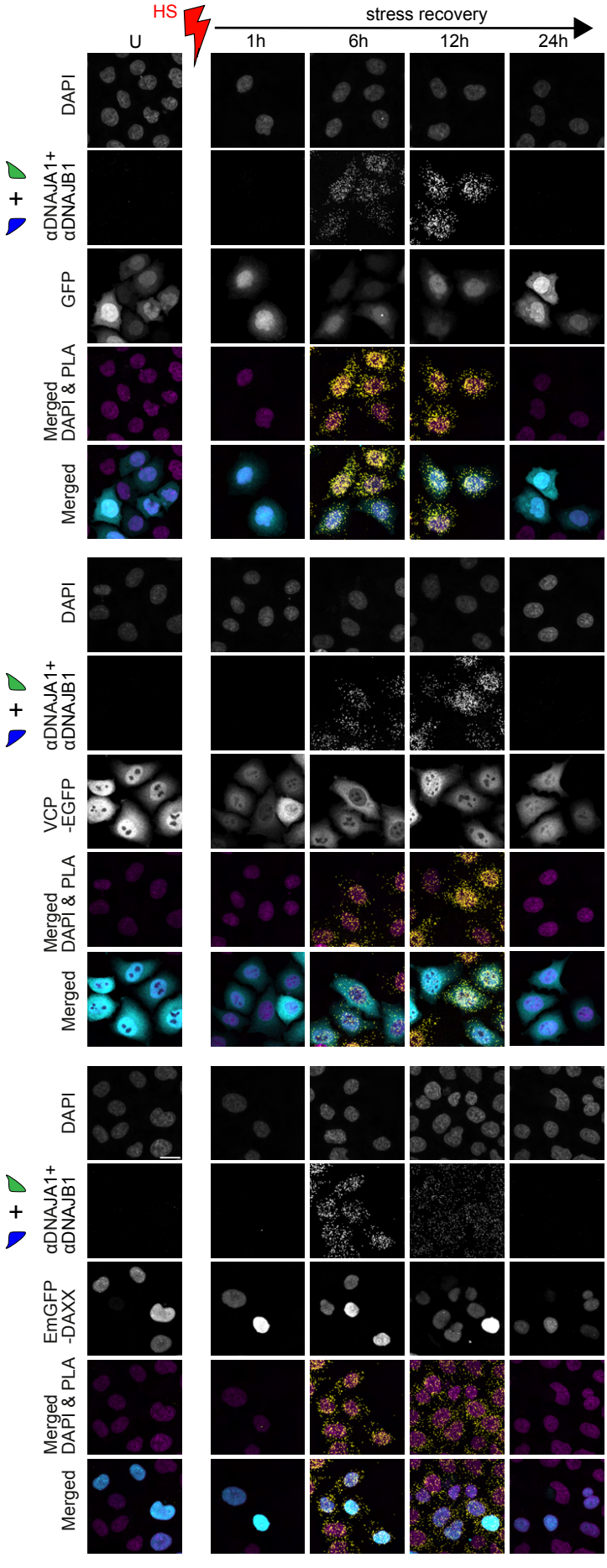
HS
stress recovery
U
1h
6h
12h
24h
DAPI
αDNAJA1+
αDNAJB1
GFP
Merged
DAPI & PLA
Merged
DAPI
αDNAJA1+
αDNAJB1
VCP
-EGFP
Merged
DAPI & PLA
Merged
DAPI
αDNAJA1+
αDNAJB1
EmGFP
-DAXX
Merged
DAPI & PLA
Merged

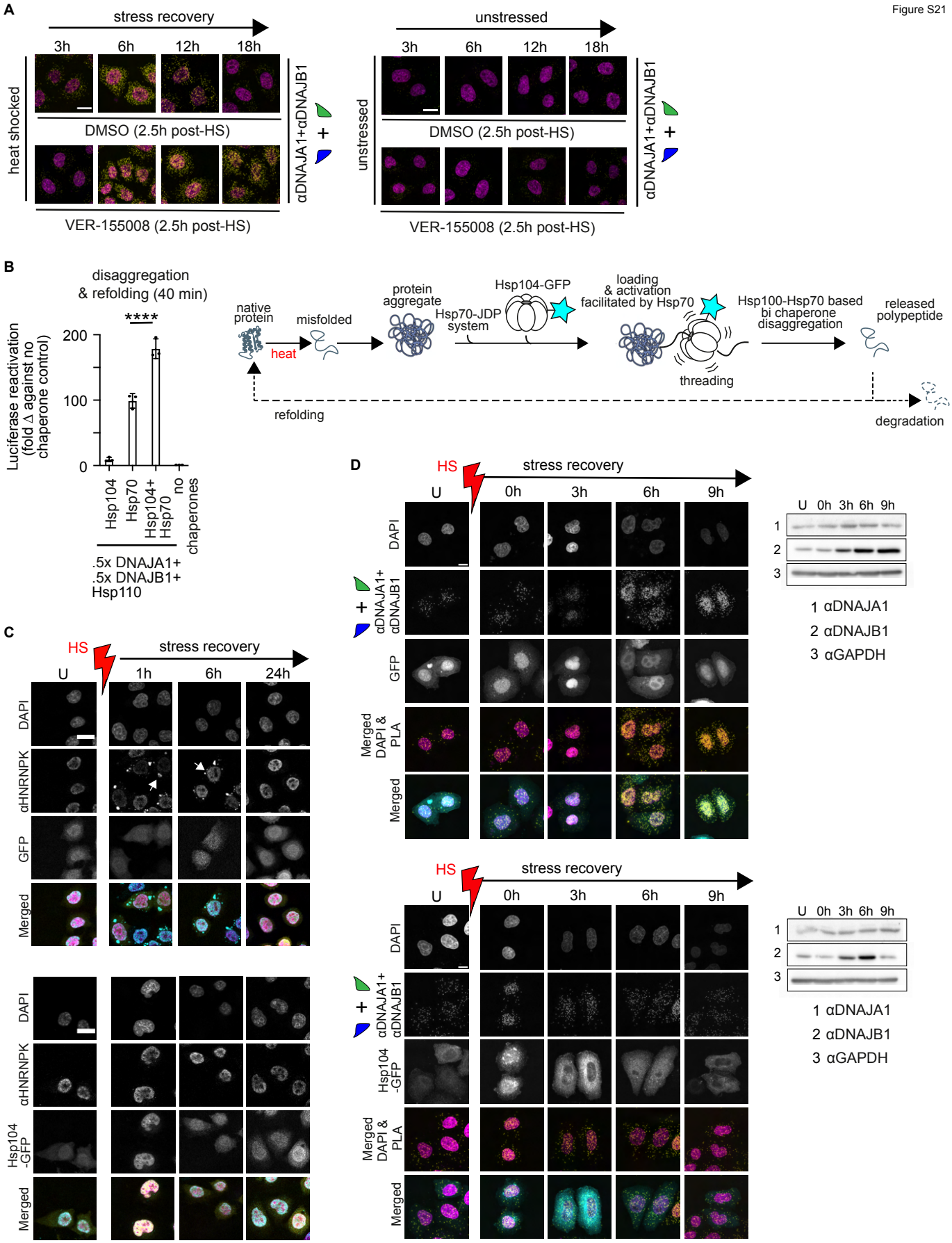
A
stress recovery
3h
6h
12h
18h
heat shocked
DMSO (2.5h post-HS)
VER-155008 (2.5h post-HS)
αDNAJA1+αDNAJB1
unstressed
B
disaggregation
& refolding (40 min)
****
Luciferase reactivation
(fold Δ against no
chaperone control)
200
100
0
Hsp104
Hsp70
Hsp104+
Hsp70
no
chaperones
.5x DNAJA1+
.5x DNAJB1+
Hsp110
native
protein
heat
misfolded
protein
aggregate
Hsp70-JDP
system
Hsp104-GFP
loading
& activation
facilitated by Hsp70
threading
Hsp100-Hsp70 based
bi chaperone
disaggregation
released
polypeptide
refolding
degradation
C
HS
stress recovery
U
1h
6h
24h
DAPI
αHNRNPK
GFP
Merged
Hsp104
-GFP
D
0h
3h
6h
9h
αDNAJA1+
αDNAJB1
Merged
DAPI &
PLA
1 αDNAJA1
2 αDNAJB1
3 αGAPDH

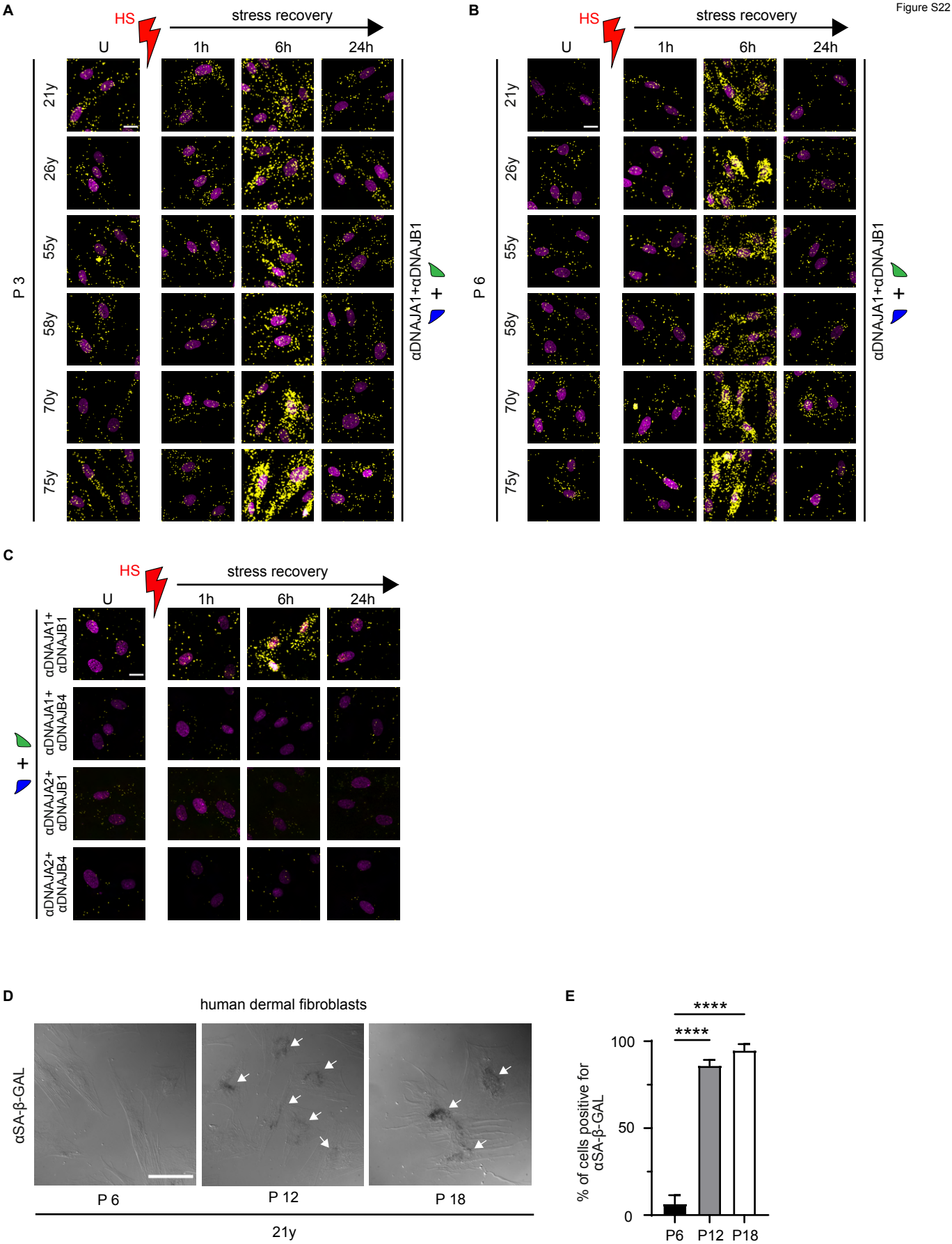
A
HS
stress recovery
U
1h
6h
24h
P 3
21y
26y
55y
58y
70y
75y
αDNAJA1+αDNAJB1
+
B
HS
stress recovery
U
1h
6h
24h
P 6
21y
26y
55y
58y
70y
75y
αDNAJA1+αDNAJB1
+
C
HS
stress recovery
U
1h
6h
24h
αDNAJA1+ αDNAJB1
αDNAJA1+ αDNAJB4
αDNAJA2+ αDNAJB1
αDNAJA2+ αDNAJB4
+
D
human dermal fibroblasts
αSA-β-GAL
P 6
P 12
P 18
21y
E
****
****
100
50
0
% of cells positive for αSA-β-GAL
P6
P12
P18

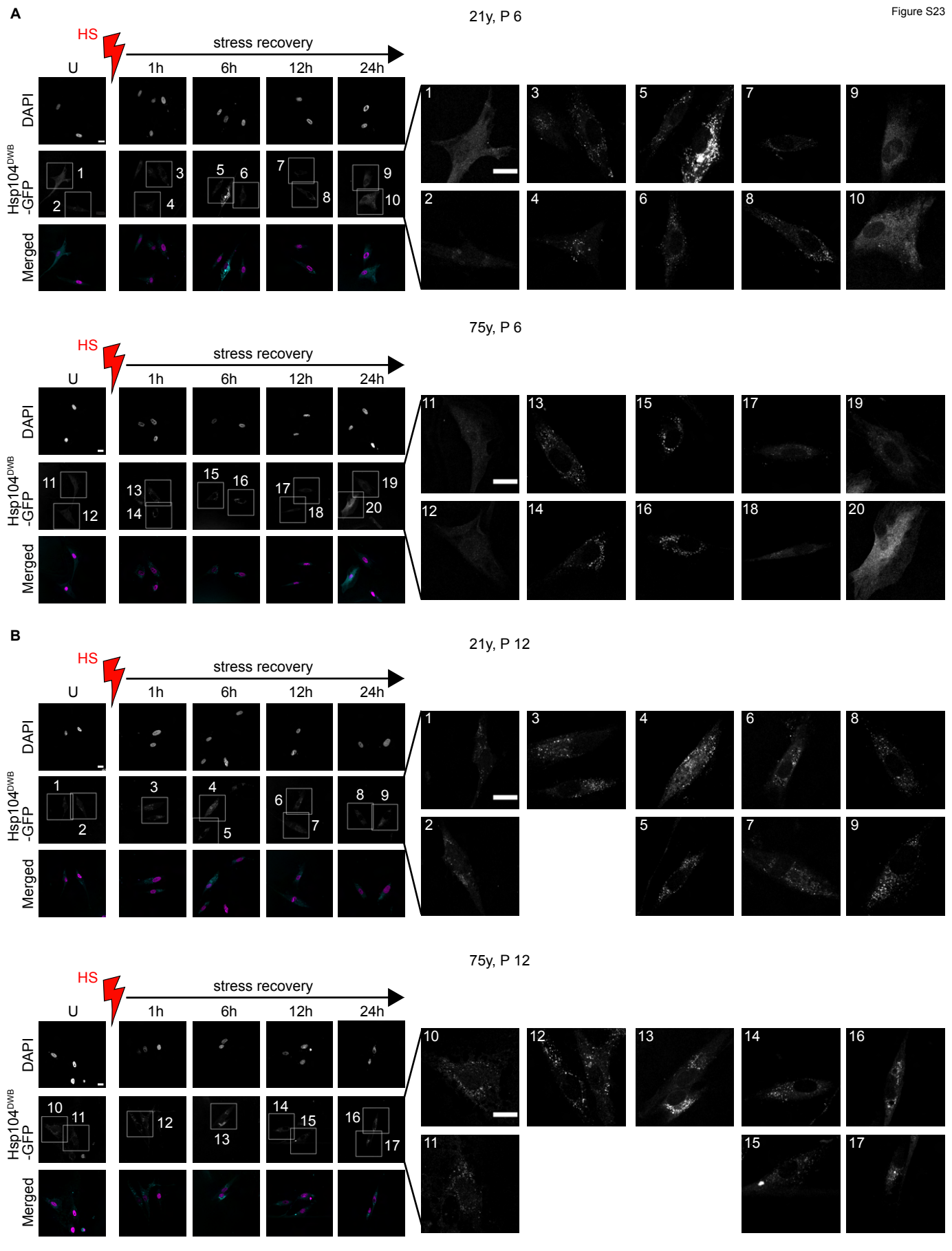
A
21y, P 6
HS
stress recovery
U
1h
6h
12h
24h
DAPI
Hsp104DWB-GFP
Merged
1
2
3
4
5
6
7
8
9
10
75y, P 6
11
12
13
14
15
16
17
18
19
20
B
21y, P 12
75y, P 12

Figure S24

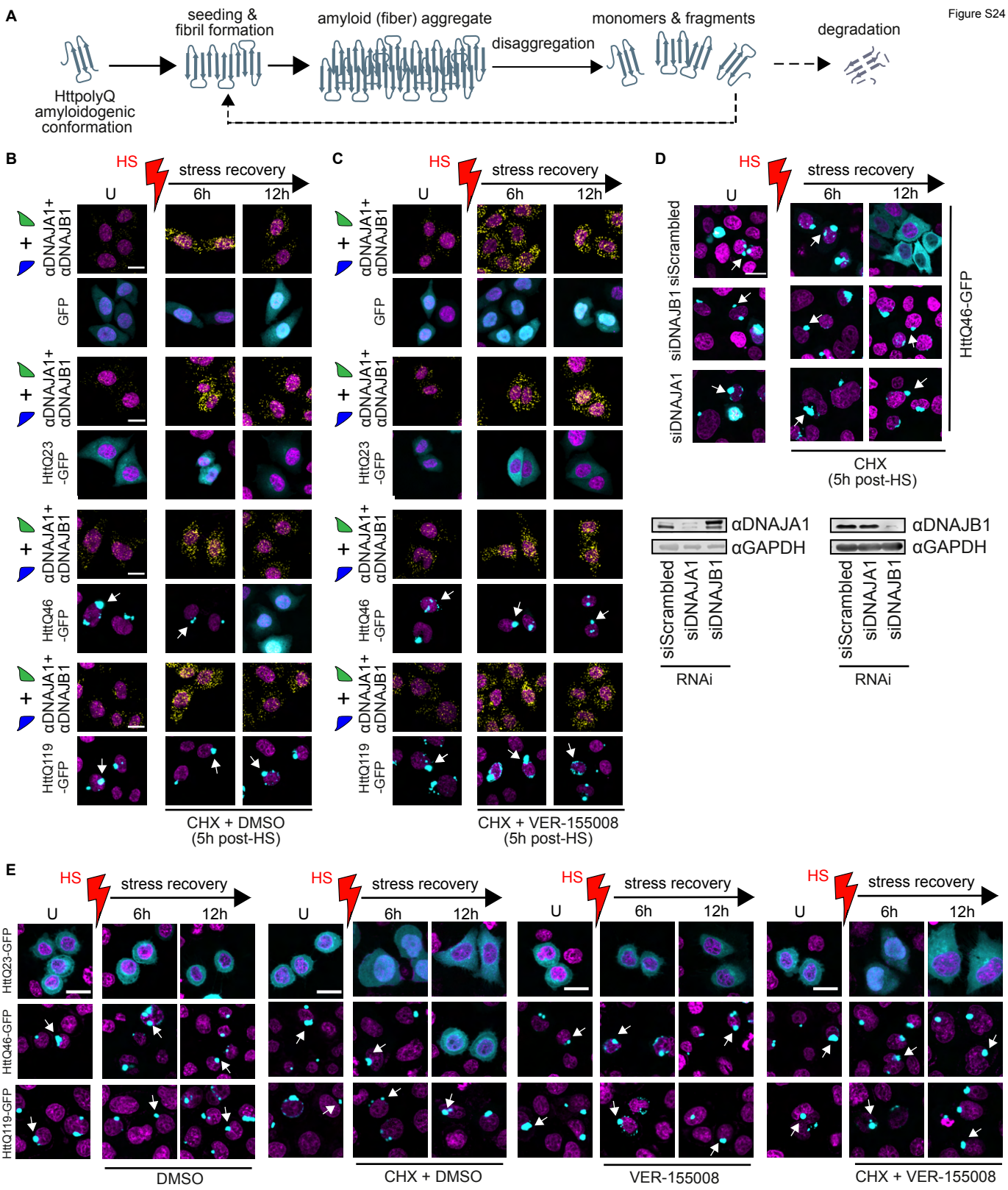
A
seeding & fibril formation
amyloid (fiber) aggregate
disaggregation
monomers & fragments
degradation
HttpolyQ amyloidogenic conformation
B
HS
stress recovery
U
6h
12h
αDNAJA1+ αDNAJB1
GFP
HttQ23 -GFP
HttQ46 -GFP
HttQ119 -GFP
CHX + DMSO (5h post-HS)
C
CHX + VER-155008 (5h post-HS)
D
siScrambled
siDNAJB1
siDNAJA1
HttQ46-GFP
CHX (5h post-HS)
αDNAJA1
αGAPDH
αDNAJB1
RNAi
E
HttQ23-GFP
HttQ46-GFP
HttQ119-GFP
DMSO
CHX + DMSO
VER-155008
CHX + VER-155008